# DISCRETE FRAMES AND TIGHT FRAMES FOR SPARSE IMAGE REPRESENTATION

## YUFEI ZHAO

*(B.Sc., East China Normal University, China)*

A THESIS SUBMITTED

FOR THE DEGREE OF DOCTOR OF PHILOSOPHY

DEPARTMENT OF MATHEMATICS

NATIONAL UNIVERSITY OF SINGAPORE

2016

To my parents

# Declaration

I hereby declare that the thesis is my original work and it has been written by me in its entirety. I have duly acknowledged all the sources of information which have been used in the thesis.

This thesis has also not been submitted for any degree in any university previously.

Yufei Zhao

2016

# Acknowledgements

First, I would like to express my sincere appreciation to my advisor Associate Professor Hui Ji, for his guidance and help. What he taught me is not only the knowledge, but also the way to think when doing research. Our communication and his guidance has greatly inspired me on my research work. And he is very friendly and patient. It is my honor and pleasure to work with him.

I would like to thank Professor Zuowei Shen. Besides the immense knowledge I learned from him during discussion and seminars, his research philosophy of linking things together will also benefit me in my whole life. Also, I would like to thank Associate Professor Qun Mo for inspiring communications.

I am grateful to all members in the wavelet group, Andreas Heinecke, Chenglong Bao, Zhitao Fan, Zheng Gong, Likun Hou, Kai Jiang, Jia Li, Ming Li, Chaoqiang Liu, Yu Luo, Tongyao Pang, Yuhui Quan, Yuping Sun, Kang Wang, Xueshuang Xiang, Peichu Xie, Guodong Xu and Jianbin Yang, for enlighting me in our discussions.

I would like to express my gratitude to my friends in my graduate office, Junrui Chen, Weiqiang Chen, Ying Cui, Han Guo, Liu Hong, Xiaowei Jia, Hengfei Lu, Lei Qiao, Yan Wang, Ran Wei, Chen Yang, Jing Yang, Liuqin Yang, Yu Yang and Jinjiong Yu. They have greatly enriched my graduate life.

Finally, I want to thank my parents for their love and support.

# Contents

# Summary

In recent years, sparse approximation has played a fundamental role in many signal processing areas. The sparsity-induced regularization methods for image recovery are implemented based on the assumption that the underlying images can be sparsely approximated under the given system. Herein, over-complete systems, especially tight frames, possess advantages in sparse image representation and have been widely used in applications.

In the first part of this dissertation, we focus on constructing discrete (tight) frames using Gabor atoms to meet the needs for sparse image modeling. Gabor systems have many advantages in sparse representation, for example accurate local time-frequency analysis and strong orientation selectivity. However, the discretization of continuous Gabor frames is non-trival in the sense that the resulted discrete system may lose the frame property, as well as fast implementation algorithms. Motivated by these, we study the general theory of discrete Gabor frames by developing Gramian and dual Gramian analysis in $\mathbb{C}^N$. Consequently, we derive a necessary and sufficient condition for discrete tight Gabor frames and construct two classes of discrete tight Gabor frames as examples. Further, to remove the non-zero DC (direct current) offset, we revise the tight Gabor frame to Gabor induced frames with closed-form dual frames and the decomposition and recontruction processes can be

implemented via filter bank based fast algorithms. The orientation selectivity of the resulted Gabor induced frame is optimal, i.e. the associated filters provide all the possible directions defined on discrete uniform grid.

A weakness of the Gabor system is that it lacks the multi-scale property since all its atoms are of fixed size. One way to solve this problem is to consider multi-scale Gabor frames composed of several Gabor frames with windows of various lengths. The other way is to construct tight frame with both Gabor and MRA structures. Specifically, we take a set of discrete Gabor atoms as refinement and wavelet masks to define an MRA-based wavelet system. Based on the UEP, a sufficient condition for construcing discrete tight frame with Gabor and MRA structures for $\ell_2(\mathbb{Z})$ is derived, which also promises that the associated continuous MRA-based wavelet system forms a tight frame for $L_2(\mathbb{R})$. Further, it can be shown that systems satisfying such condition must be generated by discrete constant windows. And the experiments of image restoration illustrate the efficiency of both multi-scale Gabor induced frames and tight frames with Gabor and MRA structures in sparse image representation.

The last part of this thesis discusses the theoretical aspect of stability and robustness for image recovery when using $\ell_1$-norm as the sparsity prompting functional. The existing sparsity-based regularization models for image recovery are composed of two parts: regularizers and loss functions. In the dissertation, we focus on $\ell_1$-norm regularized models with either $\ell_1$-norm loss function or square of $\ell_2$-norm loss function. Distinct requirements are imposed on the measurement matrices to ensure the stable and robust recovery of these two models with different loss functions.

# Chapter 1

# Introduction

## 1.1 Overview

In many practical problems, people targeted at reconstructing signals from partial and noisy measurement data. When the information acquisition process is linear, the problem of signal recovery models the measurement data as the output of applying a linear operator $\boldsymbol{A}$ to the signal of interest:

$$\boldsymbol{b} = \boldsymbol{A}\boldsymbol{f} + \boldsymbol{n}, \tag{1.1}$$

where $\boldsymbol{f} \in \mathbb{C}^N$ is the true signal we need to recover, $\boldsymbol{b} \in \mathbb{C}^M$ is the observed data, $\boldsymbol{A} \in \mathbb{C}^{M \times N}$ is the measurement matrix modeling the linear measurement process and $\boldsymbol{n} \in \mathbb{C}^M$ is the measurement noise. In practice, the available information is less than the dimention of true signals, i.e. $M < N$, or the matrix $A$ may be singular. Therefore in most signal recovery tasks, the system (1.1) is under-determined with an infinite number of solutions, some of which could be far away from the truth $\boldsymbol{f}$. That indicates it is impossible to recover $\boldsymbol{f}$ via directly solving the linear system (1.1) without additional information. However, under certain assumptions like sparsity, the goal of recovering signals from underdetermined linear measurements becomes possible.

In recent years, sparse approximation has been an indispensable tool in signal

recovery. A significant amount of research has been devoted to address the problem of sparse recovery from partial and noisy measurements in different contexts, e.g. signal/image reconstruction ([10, 15, 13]), compressed sensing ([19, 33, 59]), nonparametric statistics ([69, 7, 8]) and machine learning ([48, 1, 82]). A signal is said to be sparse if most of its elements are zero or close to zero. By emperical observation, many real-world signals themselves are sparse or their coefficients $\mathcal{W}\boldsymbol{f}$ under some transform $\mathcal{W}$ are sparse. With the assumption of sparsity, one can implement a general constrained regularization model for signal recovery

$$\min_{\boldsymbol{x}} \mathcal{R}(\boldsymbol{x}), \quad \text{subject to} \quad \mathcal{L}(\boldsymbol{x}) \leq \delta, \tag{1.2}$$

or an unconstrained model:

$$\min_{\boldsymbol{x}} \lambda \mathcal{L}(\boldsymbol{x}) + \mathcal{R}(\boldsymbol{x}), \tag{1.3}$$

in both of which, $\mathcal{R}(\boldsymbol{x})$ is a sparsity induced regularizer and $\mathcal{L}(\boldsymbol{x})$ is a loss function measuring how well a signal $\boldsymbol{x}$ fits the observed data $\boldsymbol{b}$. In the unconstrained model (1.3), $\lambda$ is a pre-defined positive parameter balancing the loss function and the regularizer.

For the topic of sparse recovery, we will mainly concentrate on the following two questions in this dissertation:

- Finding proper systems for sparsifying certain types of signals, especially images;

- Choosing suitable sparsity-induced regularization models, by which the truth can be exactly or approximately solved.

Whether theses two problems are solved successfully will influence the result of sparse recovery. And next, we will give a detailed introduction to the background related to these topics.

### 1.1.1 Sparsifying system

In most signal processing tasks, signals of interest are first expanded under some system and then interpreted or processed in terms of their expansion coefficients. More specifically, given a system $\{u_j\}_{j\in I} \subset L_2(\mathbb{R})$, people are seeking the series expansion of signal $f \in L_2(\mathbb{R})$ like

$$f(t) = \sum_{j\in I} \boldsymbol{c}_j u_j(t). \tag{1.4}$$

The process of computing coefficients $\boldsymbol{c}_j$'s is called decomposition and the process of synthesizing $f$ as (1.4) is called reconstruction. If most coefficients of $\{\boldsymbol{c}_j\}_{j\in I}$ are zero, i.e. $f$ can be expressed as a linear combination of very few atoms in $\{u_j\}_{j\in I}$, we say the signal $f$ can be sparsely represented under the system $\{u_j\}_{j\in I}$. The success of the sparsity-driven signal recovery methods largely depends on whether the chosen system can effectively sparsify input signals.

One important class of systems in application are the Gabor systems (or Weyl-Heisenberg systems, [60]). Given a fixed window function $g \in L_2(\mathbb{R})$ with $\|g\|_2 = 1$, a Gabor system $(K, L)_g \subset L_2(\mathbb{R})$ is composed of translations and modulations of $g$ on discrete lattices $K \times L$, i.e. $(K, L)_g = \{g_{k,\ell}(t) = g(t-k)e^{-2\pi i\ell t}, t \in \mathbb{R}\}_{k\in K, \ell\in L}$. In particular, if the uniform time-frequency lattices $K \times L = a\mathbb{Z} \times b\mathbb{Z}$ $(a, b \in \mathbb{R}^+)$ are considered, the corresponding Gabor system can be written as

$$(K, L)_g = \{g_{k,\ell}(t) = g(t-ak)e^{-2\pi ib\ell t}, t \in \mathbb{R}\}_{k,\ell\in\mathbb{Z}}. \tag{1.5}$$

From the definition of Gabor system, the locations of its atoms are shifted across the time-frequency plane, while the support or energy concentration of each atom in a Gabor system is fixed.

Many efforts have been devoted to the study of Gabor theory for function space $L_2(\mathbb{R})$ or $L_2(\mathbb{R}^d)$ (see e.g. [27, 111, 43, 63, 64, 99]). Among the vast literature studying Gabor theory, one noticeable and relevant work is [99]. The authors applies the Gramian and dual Gramian analysis, which is first developed for shift invariant systems in $L_2(\mathbb{R}^d)$ ([96]), to investigating the properties of Gabor systems on the

uniform lattices. In the Gramian and dual Gramian analysis, the frame properties of Gabor systems is converted to the analysis of the eigenvalues of their corresponding Gramian and dual Gramian matrices, i.e. the fiberized matrix representation of frame operators. Consequently, the derivation of duality principle [95, 99] becomes straightforward. For a generalization of Gramian and dual Gramian analysis, as well as the duality principle, to the abstract Hilbert space for one single system ([53]) or bi-systems ([52]), one may refer to related literature.

To seek a series representation of function $f$ in $L_2(\mathbb{R})$ as (1.4) via a Gabor system, the most natural idea is to make the system an orthogonal basis (or a Riesz basis) for $L_2(\mathbb{R})$, under which the decomposition coefficient is determined by taking inner product of $f$ and each atom $g_{k,\ell}$ (or atom in the dual basis). However, the Balian-Low Theorem ([2, 80, 3]) reveals the incompatibility of time-frequency concentration and non-redundancy of Gabor systems in $L_2(\mathbb{R})$ generated on uniform lattices as (1.5). To gain more flexibility in designing a complete and stable Gabor system for the function space $L_2(\mathbb{R})$, it is necessary to introduce redundant Gabor systems and go beyond the orthonormal bases or Riesz bases to the area of Gabor frames. For such redundant frames, there exist non-unique dual frames. And the decomposition and reconstruction processes can be accomplished by using the dual pair. Herein, the construction of tight Gabor frames get people's attention, since the canonical dual frame of a tight frame is just the original system itself. For the existing works about the construction of (tight) Gabor frames for $L_2(\mathbb{R})$, readers may check related references (e.g. [39, 99, 29, 31, 76]). For example, in [39, 99, 29, 31], the authors use the necessary and sufficient conditions imposed on window functions to construct tight Gabor frames or Gabor dual pairs. And in [76], a class of constructible dual Gabor frames is derived relying on the canonical dual.

Another widely used system is the wavelet/affine system. A wavelet is a function $\psi \in L_2(\mathbb{R})$ with a zero average, i.e. $\int_{-\infty}^{+\infty} \psi(t)dt = 0$. For a given set of wavelets $\Psi = \{\psi_1, ..., \psi_r\} \subset L_2(\mathbb{R})$, the *wavelet system* $X(\Psi)$ is composed of dyadic dilations

and translations of $\psi_\ell$'s, i.e.

$$X(\Psi) = \{\psi_{\ell,n,k}(t) = 2^{n/2}\psi_\ell(2^n t - k), t \in \mathbb{R}\}_{\substack{1 \le \ell \le r \\ n,k \in \mathbb{Z}}}. \tag{1.6}$$

According to the definition, the spread of atoms in a wavelet system will be scaled due to dilation. The locations of atoms at the same scaling level are shifted across the time plane, and their location in frequency domain is also adaptively changed with dilation.

Similarly as Gabor systems, people consider to find a complete and stable series expansion by using wavelet systems. The multiresolution analysis (MRA), which is firstly introduced by Mallat and Meyer ([83, 87]), is served as a most widely used design method for the construction of orthonormal wavelet bases, e.g. [86, 38, 40]. However, it has been proved by Daubechies ([40]) that the only symmetric or antisymmetric real orthonormal wavelet basis with compact support is the Haar wavelet, which lacks smoothness.

To obtain the desirable symmetry property, as well as smoothness, one way is to constuct MRA-based biorthogonal wavelet bases, for example [34, 110]. The other way is to consider the overcomplete wavelet system and constructing MRA-based (tight) wavelet frames. A systematic study about frame property of wavelet systems with MRA structure is given in [97]. In [42], the tight frame property of an MRA-based wavelet system in $L_2(\mathbb{R})$ is reduced to conditions on the masks, which is known as the unitary extension principle (UEP). And in [42], the authors give an example of MRA-based tight wavelet frame generated from a class of compactly supported refinable functions, i.e. pseudo-splines, which covers the B-spline refinable function, Daubechies orthogonal refinable function ([38, 40]) and interpolatory refinable function. To raise up the approximation order of spline tight wavelet frames, the oblique extension principle (OEP) is discovered in [32] and [42]. Both UEP and OEP can be generalized to the bi-frame setting, which leads to the mixed extension principle (MEP, [98, 32, 42]). A detailed review about the MRA framework and UEP, will be given in Chapter 2, Section 2.2.

Different structures of Gabor systems and wavelet systems lead to their own characteristics from the viewpoint of signal analysis. A Gabor frame in function space $L_2(\mathbb{R})$, is composed by the translated and modulated copies of a single window function, and a wavelet frame is composed by the scaled and translated copies of a few basic functions (framelets). As the atoms of Gabor frames are essentially the translations of a window function on time-frequency plane, the expansion of signals under a Gabor frame characterizes their local time-frequency properties. Indeed, by Heisenberg Uncertainty Principle, the atoms of Gabor systems with Gaussian window functions have optimal time-frequency concentration. Thus, Gabor frames are considered as a very important tool for local time-frequency analysis of signals. However, when being used for analyzing signals containing multiple local structures with very different sizes, Gabor systems are less effective as the supports of all atoms are fixed, i.e. the support of the window function. Wavelet systems deal with the size variations of signal structures by using the translations and dilations of one or several mother wavelet functions. Although wavelet functions with different scales have close relationship with the translations of wavelet functions in frequency plane, the time-frequency analysis of signals under wavelet systems is less optimal and less accurate than Gabor frames. In other words, both Gabor system and wavelet system have their strengths and weaknesses in terms of signal analysis. Gabor system is a better tool for local time-frequency analysis and wavelet system is better for modeling signal structures with different sizes and particularly local sharp discontinuities.

For practical applications, there is the need to have a suitable scheme that converts frames for $L_2(\mathbb{R})$ to frames for $\ell_2(\mathbb{Z})$, together with an efficient numerical implementation for signal decomposition and reconstruction. The discretization of Gabor frames and wavelet frames, particularly multi-resolution analysis (MRA) based wavelet frames, are done in different manners. Discrete Gabor frames for $\ell_2(\mathbb{Z})$ are usually obtained via directly sampling continuous Gabor frames in a discrete time-frequency grid. Sometimes, the discrete systems obtained by such a

sampling-based discretization may lack desired properties, e.g. tight frame property and efficient signal decomposition and reconstruction algorithms. In contrast, discrete MRA-based wavelet frames for $\ell_2(\mathbb{Z})$ are directly derived from several specific sequences in $\ell_2(\mathbb{Z})$, i.e. the refinement mask of the scaling function of MRA and wavelet masks. As a result, a fast filter bank based algorithm is available for wavelet decomposition and reconstruction, which cascades discrete convolution with masks followed by sub-sampling (up-sampling).

It is worth mentioning that an important property for a system to effectively represent 2D images is the orientation selectivity, as the discontinuities of 2D images often show geometrical regularities along image edges with different orientations. In recent years, many real-valued frames or tight frames have been proposed to improve orientation selectivity, including *curvelets* [20], *bandlets* [73], *shearlets* [71], and many others. Although better orientation selectivity are obtained, the existing implementations of these frame systems are much less efficient than the 1D filter bank based implementation of tensor tight wavelet frames. Another promising approach to gain orientation selectivity without sacrificing computational efficiency is using complex-valued systems. Different from real-valued functions, the real/imaginary part of the tensor product of two 1D complex-valued functions is not separable by itself. Thus, a 2D complex-valued tensor system can have better orientation selectivity using carefully chosen 1D real and imaginary functions. For example, the *dual-tree complex wavelet transform* [101] used two different discrete orthogonal wavelet bases to produce a 2D tensor complex-valued wavelet tight frame whose real part and imaginary part have up to six orientations, which still leaves plenty of rooms for further improvement.

Another characteristic of real-world images is it often contains both cartoon parts and texture parts. Cartoon parts show piecewise smooth content, whose discontinuities (edges) have geometrical regularity along the edge directions. Texture parts are highly non-smooth, but show small elements displaying either random or periodic patterns. Therefore, the design of a good redundant system for sparsity-based

image recovery should be able to effectively characterize both directional regularity of image edges and texture components with local periodicity. Another weakness of the aforementioned tight frames or their extensions is that they cannot model texture regions displaying periodic patterns, which can be sparsely modeled in local frequency domain. The systems containing the sinusoids in local windows are more effective on modelling such a sparsity prior. For example, local *discrete cosine transform* (DCT) has been used in the literature to model such regular textured regions. Thus, the sparsifying frames used in some image restoration methods are composed of two frames: a wavelet frame and a local DCT; see e.g. [105, 11]. Same as real-valued 2D tensor wavelet frames, real-valued 2D local DCT also lacks orientation selectivity such that it cannot effectively express texture regions with varying oriented periodicity.

Owing to the advantage of complex-valued tensor product functions, 2D tensor product Gabor functions

$$g(t_1)g(t_2)e^{2\pi i(\omega_1 t_1 + \omega_2 t_2)}$$

can provide arbitrary orientation selectivity by choosing different frequency pairs $(\omega_1, \omega_2)$. In other words, different modulations gives different orientations of 2D Gabor functions; see Fig. 1.1 for an illustration.
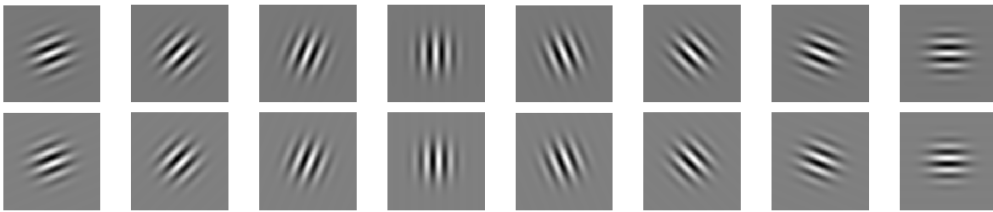


Figure 1.1: Illustration of 2D tensor product Gabor functions with different frequency orientations. The real parts of Gabor functions are shown in the top row and the imaginary parts are shown in the bottom row.

In fact, the Gabor functions can effectively model different image features, for example cartoon components and texture components, by using the window functions with different supports. When using a window function of small support, the imaginary part of a Gabor function (sine function) can be understood as an odd-order

partial differential operator, and its real part (cosine function) can be understood as an even-order partial differential operator. Thus, it can measure local signal gradients of multiple orders for cartoon regions with piecewise smoothness. For texture components with sparse local frequencies, the Gabor function with Gaussian-like window functions of sufficiently large support, is well-known for its optimality on local time-frequency analysis by Heisenberg Uncertainty Principle.

The advantages of 2D Gabor functions on orientation selectivity and local time-frequency analysis make them a very good tool for image analysis. Daugmann [44] showed that simple cells in the visual cortexes of mammalian brains can be modeled by a wavelet system generated by the translations and dilations of Gabor functions with varying frequency orientations. Continuous Gabor wavelet transforms have been widely used in texture analysis and segmentation, whose discrete version is usually done via directly sampling the function on a discrete grid. However, as we have mentioned, the system generated by such a simple discretization lacks some important property needed for sparsity-based image recovery methods, such as the fast numerical algorithm for exact reconstruction process. There is certainly the need to study the general theory of discrete version of Gabor systems from the very beginning.

## 1.1.2   Regularization models for sparse recovery

Next, we will briefly introduce the sparsity-induced regularization models for sparse recovery.

As we have mentioned previously, constrained model (1.2) and unconstrained model (1.3) are widely used for signal recovery based on the sparsity assumption. Herein, the loss function $\mathcal{L}(\cdot)$ is designed according to the statistical property of measurement noise $\boldsymbol{n}$. The popular choices include the square of $\ell_2$-norm based loss function $\mathcal{L}(\boldsymbol{x}) = \|\boldsymbol{A}\boldsymbol{x} - \boldsymbol{b}\|_2^2$ for additive Gaussian noise ( [100, 4, 61, 25]), the $\ell_1$-norm based loss function $\mathcal{L}(\boldsymbol{x}) = \|\boldsymbol{A}\boldsymbol{x} - \boldsymbol{b}\|_1$ for significant amount of outliers

([66, 67, 90]), and the Kullback-Leibler divergence fidelity term for Poisson noise, i.e. $\mathcal{L}(\boldsymbol{x}) = \boldsymbol{1}^\top (\boldsymbol{A}\boldsymbol{x}) - \boldsymbol{b}^\top \log(\boldsymbol{A}\boldsymbol{x})$, where $\boldsymbol{1}$ is the vector with all entries being 1 ([72, 75]).

The regularizer $\mathcal{R}$ is used to enforce a sparsity constraint on the original signals $\boldsymbol{f}$. By assuming the signal $\boldsymbol{f}$ is sparse, we solve the system (1.1) by penalizing $\boldsymbol{f}$ against its $\ell_0$-norm. The $\ell_0$-norm of a signal $\boldsymbol{x}$ is defined as the number of its nonzero components, i.e.

$$\|\boldsymbol{x}\|_0 = |\text{supp}(\boldsymbol{x})|,$$

where $|S|$ represents the cardinality of a set $S$. Under certain conditions, the $\ell_0$-norm regularized minimization provides good reconstruction. For example, in the noise-free case, the model

$$\min \|\boldsymbol{x}\|_0 \quad \text{subject to} \quad \boldsymbol{A}\boldsymbol{x} = \boldsymbol{b}$$

will exactly recover the $s$ sparse signal $\boldsymbol{f}$ satisfying $\boldsymbol{A}\boldsymbol{f} = \boldsymbol{b}$, if any $2s$ columns of $\boldsymbol{A}$ are linearly independent ([59]). Such result shows the theoretical effectiveness of sparsity-induced model. However, it may be challenging to implement a feasible algorithm for the $\ell_0$-norm related model. For instance, it has been proved that for any $\delta \geq 0$, the $\ell_0$-norm regularized model with $\ell_2$-norm based constraint

$$\min_{\boldsymbol{x} \in \mathbb{C}^N} \|\boldsymbol{x}\|_0 \quad \text{subject to} \quad \|\boldsymbol{A}\boldsymbol{x} - \boldsymbol{f}\|_2 \leq \delta$$

is an NP hard problem ([89]). Consequently, people have tried to set other regularizers, which both induce sparsity and possess the properties like being convex and smooth, such that the corresponding minimization problems are easy to solve in practice.

Partially owing to the breakthrough in compressed sensing ([24, 23, 46], $\ell_1$-norm has been widely used as the convex relaxation of $\ell_0$-norm for sparse signal recovery. Typical $\ell_1$-norm regularizer based optimization models for sparse recovery can be either a constrained model:

$$\min_{\boldsymbol{x}} \|\boldsymbol{x}\|_1, \quad \text{subject to} \quad \mathcal{L}(\boldsymbol{x}) \leq \delta, \tag{1.7}$$

or an unconstrained model:

$$\min_{\boldsymbol{x}} \lambda \mathcal{L}(\boldsymbol{x}) + \|\boldsymbol{x}\|_1, \tag{1.8}$$

where $\delta$ and $\lambda$ are both pre-defined parameters. There exists an abundant literature on studying sparse recovery using the constrained model (1.7); see e.g. [24, 23, 19, 58, 56, 17, 18, 59, 57, 107, 21]. The study of robust and stable sparse recovery using unconstrained model (1.8) has been scant in the literature. A detailed review of these exsisting results will be given in Chapter 6. Considering the fact that the unconstrained model (1.8) is also common to use in practice as it is easier to solve, there is a need to study the robustness and stability when using (1.8) for sparse recovery.

Besides, many other regularizers have also been proposed in sparse signal recovery. For example, people consider a generalization of the above $\ell_0$-norm and $\ell_1$-norm based regularizers: the $\ell_q$-norm based regularizer $\mathcal{R}(\boldsymbol{x}) = \|\boldsymbol{x}\|_q^q$ with $0 < q \leq 1$ (e.g. [58, 107, 108]), which is continuous but nonconvex except the case $q = 1$. And in [117], the author considers the Capped-$\ell_1$ regularizer defined as $\mathcal{R}(\boldsymbol{x}) = \sum_{j=1}^{N} \min(|\boldsymbol{x}_j|, \alpha)$, which is a good approximation to $\ell_0$-norm. A smoother but still nonconvex regularizer SACD is introduced in [51]. Interested readers may refer to related literature for more details. And in this dissertation, we just focus on the most widely used, convex and continuous $\ell_1$-norm based regularizer $\mathcal{R}(\boldsymbol{x}) = \|\boldsymbol{x}\|_1$.

## 1.2   What is this dissertation about

The redundancy of (tight) frames gives more flexibilities on filter design and better sparse approximation. The first goal of this dissertation is to construct discrete (tight) frames meeting the needs from sparsity-induced signal recovery, especially image recovery. To make the constructed system more effective and powerful for sparsifying real-world images, it is hoped to have the following properties: 1) the system may provide accurate local time-frequency analysis; 2) the corresponding

two dimentional system possesses the directional selectivity; 3) the system can characterize different signal features of multi-scales; and 4) there exists a fast algorithm for the implementation of decomposition and reconstruction processes.

As we have mentioned in the last section, the atoms of a Gabor system inherently have the local time-frequency analysis. And the 2D Gabor system defined from tensor product of 1D ones provides strong directional selectivity. However, the discretization of Gabor systems is non-trival in the sense that the resulted discrete system may lose the frame property. Motivated by these, we study the general theory of discrete Gabor systems, and develop the Gramian and dual Gramian analysis for the discrete Gabor systems in $\mathbb{C}^N$. Further, based on the duality principle derived from the Gramian and dual Gramian analysis, we get a necessary and sufficient condition for discrete tight Gabor frames, and use them to construct two classes of discrete tight Gabor frames. However, the proposed tight frames cannot be directly used in sparsity-based image recovery methods, as the associated high-pass filters have non-zero DC offsets. Therefore, a new class of discrete Gabor induced frames with closed-form dual frames are constructed which remove the non-zero DC offsets of all high-pass filters of tight Gabor frames.

By varying the size of window sequences, Gabor systems can provide powerful expressions on both cartoon image regions and texture image regions. However, a single Gabor system cannot characterize image features of multi-scales simultaneously, since all the atom sizes are fixed to be the window size.

To solve this problem, we consider to study discrete tight frames with both Gabor and MRA structures. Such discrete tight frames will have the same multi-scale structures as discrete MRA-based wavelet tight frames for $\ell_2(\mathbb{Z})$, and their 2D tensor products have strong orientation selectivity and good performance on local time-frequency analysis. Our construction is based on the standard framework of MRA, and particularly we use a set of discrete Gabor filters with frequency parameter $b$

$$\{g_\ell(m) = g(m)e^{-2\pi ib\ell m}\}_{0 \le \ell \le \frac{1}{b}-1}. \tag{1.9}$$

as the refinement and wavelet masks, which consequently define the refinable function $\phi$ and wavelet functions $\{\psi_\ell\}_{\ell=1}^{\frac{1}{b}-1}$. Based on the unitary extension principle (UEP) [97, 42], we presented a sufficient condition for constructing discrete tight frames with Gabor and MRA structures for $\ell_2(\mathbb{Z})$, and showed that the associated systems generated by $\{\psi_\ell\}_{\ell=1}^{\frac{1}{b}-1}$ in the continuum domain indeed form MRA-based tight wavelet frames for $L_2(\mathbb{R})$. Clearly, the discrete tight frames constructed by such an approach have all the properties mentioned at the begining of this section. Furthermore, we showed that only those discrete systems generated by a constant discrete window function, i.e.

$$\boldsymbol{g} = \frac{1}{p}(1, 1, \ldots, 1)$$

for some positive even integer $p$, can form compactly supported discrete tight frame with Gabor and MRA structures for $\ell_2(\mathbb{Z})$. Clearly, when $p = 2$, it corresponds to Haar orthonormal wavelet basis with the discrete window function $(1/2, 1/2)$. It is noted that when $p > 2$, it is not necessarily corresponding to Haar basis, whose refinable function is an indicator function. Indeed, we showed that the refinable function $\phi$ is a continuous piece-wise spline function when $p = 2^m, m > 1$. In addition, we also gave a construction of Gabor frames for $L_2(\mathbb{R})$ whose window function is the refinable function of an MRA, and tight Gabor frames for $L_2(\mathbb{R})$ whose window function is the square root of the scaling function of an MRA.

Totally, we construct two types of discrete systems to meet our needs for sparse recovery. One is the discrete Gabor induced frame and the other is MRA-based discrete tight wavelet frame with Gabor structure. In fact, it's hard to tell which system is overwhelmingly better than the other. For the discrete Gabor induced frames we have constructed, one has more flexibility to choose the window sequence, while to deal with the scaling challenge, the multi-scale Gabor induced frame is necessary to be considered. For the tight wavelet frame with Gabor structure, the multi-scale property is automatically embedded in the MRA framework. As a result, the window is restricted to have uniform values and lacks the smoothness, although the corresponding continuous refinable functions can be arbitrarily smooth.

To demonstrate the benefits of the discrete Gabor induced frames and MRA-based tight wavelet frames with Gabor structure, we develop an $\ell_1$-norm regularized method for solving ill-posed linear inverse problem in image recovery. For the multi-scale Gabor induced frame, our regularization model follows the idea proposed in [16] for image inpainting, i.e., the image is read as the composite of multiple layers, and each layer represents image parts that can be sparsely modeled by the discrete Gabor induced frame with a particular scale. For the single frame system, i.e. the tight frame with Gabor and MRA stuctures, this model is reduced to the usual analysis model. The experimental results indicate the advantages of these two types of discrete frames over other tight wavelet frames in sparsity-based image recovery.

The last part in this dissertation is about the sparsity-induced regularization models. As aforementioned, the unconstrained $\ell_1$-norm relating model for sparse recovery has been seen its wide applications in practice. However, the analysis on the robustness and stability of such unconstrained models is scant in the literature. In this dissertation, we investigate the sufficient conditions for stable and robust recovery of sparse signals when using unconstrained models. Both the $\ell_1$-norm loss function and the square of $\ell_2$-norm loss function are considered. It is shown that these two models with different loss functions have different requirements on $\boldsymbol{A}$ for guaranteeing stable and robust sparse recovery. When using $\ell_1$-norm as the loss function, only null space property is sufficient for a good recovery while it is not sufficient when using square of $\ell_2$-norm as the loss function. How to set optimal value of regularization parameter in the unconstrained model is also provided in the analysis, which is helpful to the applications.

## 1.3   Organization of the dissertation

The remaining chapters of this dissertation is organized as follows.

- In Chapter 2, we introduce some mathematical preliminaries related to our discussion.

- In Chapter 3, firstly we develop the Gramian and dual Gramian analysis for studying the general theory of discrete Gabor systems, from which we derive the duality principle. Based on the duality principle, we investigate the construction of tight Gabor frames and Gabor induced frames suitable for image recovery.

- In Chapter 4, we are devoted to the construction of discrete tight frames with Gabor and MRA structures, as well as MRA-based tight wavelet frame for $L_2(\mathbb{R})$. Additionally, we also give a construction of (tight) Gabor frames for $L_2(\mathbb{R})$ using the scaling function of an MRA.

- In Chapter 5, we apply the constructed Gabor induced frames and tight frames with Gabor and MRA structures in the $\ell_1$-norm relating regularization for image recovery problems.

- In Chapter 6, we study the sufficient conditions on measurement matrix $\boldsymbol{A}$ for guaranteeing a robust and stable recovery of sparse signals via solving (1.8), as well as how to set optimal value of the regularization parameter $\lambda$.

# Mathematical preliminary

In this chapter, we will introduce some mathematical preliminaries related to this dissertation, for example the general frame theory and MRA-based wavelet frames, as well as two widely used conditions on measurement matrices in sparse recovery. These concepts introduced in this chapter will be employed throughout this dissertation.

And in this dissertation, we use $\mathbb{Z}, \mathbb{Z}^+, \mathbb{N}, \mathbb{R}$ to denote the set of integers, positive integers, natural numbers and real numbers, respectively.

## 2.1  Hilbert space and systems

Let $H$ be a Hilbert space, for example $L_2(\mathbb{R})$, $\ell_2(\mathbb{Z})$ or $\mathbb{C}^N$, with the usual inner product $\langle \cdot, \cdot \rangle$ and 2-norm $\| \cdot \|$. $\{v_j\}_{j \in I} \subset H$ is called a *Bessel sequence* if there exists a positive constant $B$ such that

$$\sum_{j \in I} |\langle f, v_j \rangle|^2 \leq B\|f\|^2, \quad \forall f \in H.$$

And it is called a *frame sequence* if there exist two positive constants $A, B$ such that

$$A\|f\|^2 \leq \sum_{j \in I} |\langle f, v_j \rangle|^2 \leq B\|f\|^2, \quad \forall f \in \overline{\mathrm{span}(\{v_j\}_{j \in I})}.$$

A Bessel sequence becomes a *frame* for $H$ if there also exists a positive constant $A$ such that

$$A\|f\|^2 \leq \sum_{j \in I} |\langle f, v_j \rangle|^2 \leq B\|f\|^2, \quad \forall f \in H.$$

$A/B$ is called the lower/upper frame bound. The notion of frame was first introduced by Duffin and Schaeffer ([47]). A frame $\{v_j\}_{j \in I}$ is called *tight frame* when $A = B = 1$. Clearly, a (tight) frame sequence of $H$ becomes a (tight) frame for $H$ if its linear span is dense in $H$.

A sequence $\{v_j\}_{j \in I}$ is called a *Riesz sequence* if there exist two positive constants $C_1, C_2$ such that

$$C_1 \sum_{j \in I} |\boldsymbol{c}(j)|^2 \leq \| \sum_{j \in I} \boldsymbol{c}(j)v_j \|_2^2 \leq C_2 \sum_{j \in I} |\boldsymbol{c}(j)|^2, \quad \forall \boldsymbol{c} \in \ell_2(I),$$

where $\ell_2(I)$ denotes the space of square summable sequences with index $I$. When $C_1 = C_2 = 1$, the Riesz sequence $\{v_j\}_{j \in I}$ becomes an *orthonormal sequence*. The Riesz (orthonormal) sequence $\{v_j\}_{j \in I}$ is a *Riesz (orthonormal) basis* for $H$ if its linear span is dense in $H$.

For a Bessel sequence $\{v_j\}_{j \in I}$ for $H$, its *synthesis* operator, $\mathcal{T} : \ell_2(I) \to H$ is defined by

$$\mathcal{T}\boldsymbol{c} = \sum_{j \in I} \boldsymbol{c}(j)v_j \quad \forall \boldsymbol{c} \in \ell_2(I) \tag{2.1}$$

and its adjoint operator, called *analysis* operator $\mathcal{T}^* : H \to \ell_2(I)$ is defined by

$$\mathcal{T}^* f(j) = \langle f, v_j \rangle, \quad j \in I. \tag{2.2}$$

The *frame* operator $\mathcal{S} : H \to H$ is then defined by $\mathcal{S} = \mathcal{T}\mathcal{T}^*$. Given a frame $U = \{u_j\}_{j \in I}$ for $H$, the sequence $V = \{v_j\}_{j \in I}$ is called its dual frame if

$$f = \mathcal{T}_V \mathcal{T}_U^* f = \mathcal{T}_U \mathcal{T}_V^* f, \quad \forall f \in H. \tag{2.3}$$

A frame $\{u_j\}_{j \in I}$ and its dual $\{v_j\}_{j \in I}$ are called *bi-frames* for $H$. Given a frame $\{v_j\}_{j \in I}$ for $H$, its dual frame is not unique and the so-called *canonical* dual frame

is given by $\{(\mathcal{T}\mathcal{T}^*)^{-1}v_j\}_{j \in I}$. Two sequences $\{u_j\}_{j \in I}$ and $\{v_j\}_{j \in I}$ are called *bi-orthogonal* sequences if

$$\langle u_j, v_k \rangle = \delta_{j-k,0}, \quad \forall\, j,k \in I,$$

with $\delta_{0,0} = 1$ and $\delta_{j-k,0} = 0$ otherwise.

## 2.2   Gabor frames and MRA-based wavelet frames

For any function $f \in L_2(\mathbb{R})$, its Fourier transform is defined by

$$\widehat{f}(\omega) = \int_{\mathbb{R}} f(t)e^{-i\omega t}dt, \quad \omega \in \mathbb{R}.$$

For any sequence $\boldsymbol{h} \in \ell_2(\mathbb{Z})$, its Fourier series is defined by

$$\widehat{\boldsymbol{h}}(\omega) = \sum_{m \in \mathbb{Z}} \boldsymbol{h}(m)e^{-im\omega}, \quad \omega \in \mathbb{R}.$$

The construction of tight wavelet frames often starts with the construction of MRA, which is built on refinable functions. A function $\phi \in L_2(\mathbb{R})$ is called *refinable* if

$$\phi(t) = 2\sum_{k \in \mathbb{Z}} \boldsymbol{a}_0(k)\phi(2t - k), \quad t \in \mathbb{R}, \tag{2.4}$$

for some $\boldsymbol{a}_0 \in \ell_2(\mathbb{Z})$, or equivalently $\widehat{\phi}(2\omega) = \widehat{\boldsymbol{a}_0}(\omega)\widehat{\phi}(\omega), \omega \in \mathbb{R}$. The sequence $\boldsymbol{a}_0$ is called the *refinement mask* of $\phi$. Given a refinable function $\phi \in L_2(\mathbb{R})$ with $\widehat{\phi}(0) \neq 0$, the sequence of sub-spaces $\{V_n\}_{n \in \mathbb{Z}}$ defined by

$$V_n = \overline{\mathrm{span}\{\phi(2^n \cdot - k)\}}_{k \in \mathbb{Z}}. \tag{2.5}$$

forms an MRA for $L_2(\mathbb{R})$ if it satisfies

(i) $V_n \subset V_{n+1},\ n \in \mathbb{Z}$,   (ii) $\overline{\cup_n V_n} = L_2(\mathbb{R})$,   (iii) $\cap_n V_n = \{0\}$.

Given an MRA generated by the refinable function $\phi$, we can define a set of framelets $\Psi = \{\psi_\ell\}_{\ell=1}^r$ by

$$\psi_\ell(t) = 2\sum_{k \in \mathbb{Z}} \boldsymbol{a}_\ell(k)\phi(2t - k), \quad t \in \mathbb{R}, \tag{2.6}$$

or equivalently $\widehat{\psi_\ell}(2\omega) = \widehat{\boldsymbol{a}_\ell}(\omega)\widehat{\phi}(\omega), \omega \in \mathbb{R}$, for some sequences $\{\boldsymbol{a}_\ell\}_{\ell=1}^r \subset \ell_2(\mathbb{Z})$. The sequences $\{\boldsymbol{a}_\ell\}_{\ell=1}^r$ are called *wavelet masks* of the framelets $\{\psi_\ell\}_{\ell=1}^r$.

The so-called *unitary extension principle* (UEP) ([42]) provides a sufficient condition on refinement mask $\boldsymbol{a}_0$ and wavelet mask $\{\boldsymbol{a}_\ell\}_{\ell=1}^r$ such that the affine system $X(\Psi)$ defined by

$$X(\Psi) = \{2^{n/2}\psi_\ell(2^n \cdot -k)\}_{1\le\ell\le r, n,k\in\mathbb{Z}} \tag{2.7}$$

forms a tight frame for $L_2(\mathbb{R})$. For simplicity, we assume that the refinement mask $\boldsymbol{a}_0$ is finitely supported.

**Theorem 2.1** (UEP [97]). *Let $\phi$ be a refinable function with $\widehat{\phi}(0) \neq 0$ and with finitely supported mask $\boldsymbol{a}_0$. For a given $\Psi = \{\psi_\ell, \ell = 1, \ldots, r\}$ defined by (2.6) with wavelet masks $\{\boldsymbol{a}_\ell\}_{\ell=1}^r$, the affine system $X(\Psi)$ defined by (2.7) forms a tight frame of $L_2(\mathbb{R})$, if the masks $\{\boldsymbol{a}_0, \boldsymbol{a}_1, \ldots, \boldsymbol{a}_r\}$ satisfy*

$$\sum_{\ell=0}^r |\widehat{\boldsymbol{a}_\ell}(\omega)|^2 = 1 \quad and \quad \sum_{\ell=0}^r \widehat{\boldsymbol{a}_\ell}(\omega)\overline{\widehat{\boldsymbol{a}_\ell}(\omega+\pi)} = 0, \tag{2.8}$$

*for almost all $\omega \in [-\pi, \pi]$.*

It is noted that in Theorem 2.1, the mask $\boldsymbol{a}_0$ is assumed to be the refinement mask of a function in $L_2(\mathbb{R})$, which might not hold true for arbitrary sequences. Nevertheless, it is shown in [52, Section 5.4] that a finitely supported mask $\boldsymbol{a}_0$ with $\widehat{\boldsymbol{a}_0}(0) = 1$ will admit a refinable function in $L_2(\mathbb{R})$ if the mask $\boldsymbol{a}_0$, together with other masks $\{\boldsymbol{a}_\ell\}_{\ell=1}^r$, satisfies the condition (2.8). The condition (2.8) can be expressed as

$$\sum_{\ell=0}^r \sum_{n\in\Omega_j} \overline{\boldsymbol{a}_\ell(n)}\boldsymbol{a}_\ell(n+m) = \frac{1}{2}\delta_{m,0} \tag{2.9}$$

for all $m \in \mathbb{Z}$, $j \in \mathbb{Z}/2\mathbb{Z}$, where $\Omega_j = (2\mathbb{Z} + j) \cap \operatorname{supp}(\boldsymbol{a}_0)$. In short, once a set of finitely supported masks $\{\boldsymbol{a}_\ell\}_{\ell=0}^r$ satisfying (2.9) is constructed, we have an MRA-based wavelet tight frame for $L_2(\mathbb{R})$, and a filter bank based efficient numerical implementation is available for the decomposition and reconstruction of signals in $\ell_2(\mathbb{Z})$.

Before ending this section, we introduce a sufficient condition for the construction of tight Gabor frames for $L_2(\mathbb{R})$.

**Theorem 2.2.** ([99]) Consider a compactly supported non-negative function $g \in L_2(\mathbb{R})$. Suppose that the support of $g$ is $[0, \gamma]$ and $g > 0$ on $(0, \gamma)$. Then $\{g(t - ak)e^{-2\pi i b\ell t}\}_{k,\ell \in \mathbb{Z}}$ forms a tight frame for $L_2(\mathbb{R})$ if and only if the following two conditions hold:

(a) $\gamma b \leq 1$;

(b) $\sum_{k \in \mathbb{Z}} |g(\cdot - ak)|^2$ is constant.

## 2.3 Conditions for sparse recovery

For an index set $T \subset \{1, ..., N\}$, let $|T|$ denote the cardinality of $T$ and let $T^c$ denote the complement of $T$ in $\{1, ..., N\}$. For a vector $\boldsymbol{x} \in \mathbb{C}^N$, let $|\boldsymbol{x}|$ denote the absolute values of $\boldsymbol{x}$, i.e. $|\boldsymbol{x}|(j) = |\boldsymbol{x}(j)|$, $j \in \{1, \ldots, N\}$. Given a vector $\boldsymbol{x} \in \mathbb{C}^N$ and an index set $T$, $\boldsymbol{x}_T \in \mathbb{C}^N$ is defined as

$$\boldsymbol{x}_T(j) = \begin{cases} \boldsymbol{x}(j) & j \in T \\ 0 & j \notin T. \end{cases}$$

Consider the problem of recovering signals from the underdetermined linear system (1.1). In the literature of compressed sensing, various conditions have been imposed on $\boldsymbol{A}$ to ensure the exact recovery of signals in the noise-free case or to ensure a stable recovery in the noisy case, when the constrained model

$$\min_{\boldsymbol{g}} \|\boldsymbol{g}\|_1, \quad \text{subject to} \quad \mathcal{L}(\boldsymbol{b} - \boldsymbol{A}\boldsymbol{g}) \leq \delta,$$

is used. One of such conditions is the so-called *null-space property* ([33, 59]) for exact recovery in the noise-free case.

**Definition 2.1** (Null-space Property)**.** The matrix $\boldsymbol{A}$ is said to satisfy the null space property of order $s$, if there exists a constant $0 \leq \beta < 1$ such that for any

$\boldsymbol{h} \in \ker(\boldsymbol{A})$ and any index set $T \subset \{1, ..., N\}$ of size $|T| \leq s$,

$$\|\boldsymbol{h}_T\|_1 \leq \beta \|\boldsymbol{h}_{T^c}\|_1. \tag{2.10}$$

The other is the so-called *robust null-space property* [59, 57]) or *sparse approximation property* ([107]) which considers the noise-robustness and approximation-stability of sparse recovery in the presence of noise.

**Definition 2.2** (Robust Null-space Property)**.** The matrix $\boldsymbol{A}$ is said to satisfy the robust null space property of order $s$ if there exist two constants $D_1 > 0$ and $0 \leq \beta_1 < 1$ such that for any $\boldsymbol{h} \in \mathbb{C}^N$ and any index set $T \subset \{1, ..., N\}$ with $|T| \leq s$, we have

$$\|\boldsymbol{h}_T\|_2 \leq D_1 \|\boldsymbol{A}\boldsymbol{h}\|_2 + \beta_1 s^{-1/2} \|\boldsymbol{h}_{T^c}\|_1. \tag{2.11}$$

It can be seen that for any matrix $\boldsymbol{A}$ satisfying the robust null-space property will satisfy the null space property by restricting $\boldsymbol{h} \in \ker(\boldsymbol{A})$. These two conditions will be used in our discussion of the robust and stable sparse recovery by the unconstrained $\ell_1$ regularized models.

# Chapter 3

# Discrete Gabor frames

## 3.1 Introduction

As we have introduced in Chapter 1, a Gabor system has the advantages of accurate local time-frequency analysis and the orientation selectivity, which make it a promising tool in signal analysis and signal processing. Since D. Gabor introduced the Gabor system ([60]) in 1946, most efforts have been devoted to the study of Gabor theory for the function space $L_2(\mathbb{R}^d)$ (see e.g. [40, 63, 27, 99]) and for the infinite dimensional discrete space $\ell_2(\mathbb{Z})$ or $\ell_2(\mathbb{Z}^d)$ (see e.g. [88, 36, 79]).

The goal of this chapter is to construct discrete Gabor frames in $\mathbb{C}^N$ that meet the needs from sparsity-based image recovery methods. The discrete Gabor system we considered is clarified as follows. Let $\boldsymbol{g} \in \mathbb{R}^N$ denote a window function with the length of support $p \leq N$, and let $(a, b)$ denote two shift parameters in finite time-frequency plane with both $a$ and $b^{-1}$ being positive integers. A discrete Gabor system in $\mathbb{C}^N$ generated from $\boldsymbol{g}$ is defined by

$$X = (K, L)_{\boldsymbol{g}} = \{\boldsymbol{g}_{k,\ell}(m) = \boldsymbol{g}((m - ak) \bmod N)\mathrm{e}^{-2\pi i \ell b m}, m = 0, 1, \ldots, N-1\}_{k \in K, \ell \in L},$$

(3.1)

where $K, L \subset \mathbb{Z}$ are the pair of integer lattices of finite time-frequency plane. The density of $X$ is defined as $\mathrm{den} X = \frac{|K||L|}{N}$ where $|\cdot|$ denotes the cardinality of a set.

While the Gabor theory in $\ell_2(\mathbb{Z})$ are applicable to discrete Gabor systems in $\mathbb{C}^N$ by viewing finite signals as the sequences in $\ell_2(\mathbb{Z})$, there are also studies of Gabor systems for the space of finite signals $\mathbb{R}^N$ or $\mathbb{C}^N$. In the next, we give a brief review on the existing results of Gabor theory for $\mathbb{C}^N$ and outline our contributions in this chapter.

### 3.1.1 Literature review

For discrete Gabor systems in $\mathbb{C}^N$ defined by (3.1), there have been various characterizations presented in the past for Gabor frames and tight Gabor frames. A necessary condition on the frame property of a discrete Gabor system for $\mathbb{C}^N$ or $\ell_2(\mathbb{Z})$ is $ab \leq 1$ to ensure the cardinality of the system is no less than $N$. The so-called Wexler-Raz duality condition for $\mathbb{C}^N$ ([113, 81]) gives a necessary and sufficient condition on Gabor bi-frames on specific finite time-frequency lattices. Many fundamental facts of tight Gabor frames and Gabor frames for $\mathbb{C}^N$ are provided in Feichtinger et al. [54], which uses twisted group algebras as the main tool. Feichtinger et al. [54] studies Gabor frames for finite signals over a finite Abelian group generated by an arbitrary lattice in finite time-frequency plane, and it covers many existing results on Gabor analysis for both product lattices and non-product lattices, including the duality principle [95, 99] which relates frame properties of a Gabor system to that of its adjoint system. In [53], the duality principle is generalized to the abstract Hilbert space for one single system, and further in [52], the conclusion was extended to bi-systems. The studies for Gabor systems in $\ell_2(\mathbb{Z})$ and $\mathbb{C}^N$ can be seen as their specialization.

For the construction of discrete Gabor frames, many existing schemes are done via sampling a Gabor frame for $L_2(\mathbb{R})$, see e.g [91, 65, 103]. The main difference among these methods lies in the conditions used in the discrete sampling to generate a frame. For example, it is shown in [65] that the certain regularization condition should be imposed on the window function in order to form a frame for $\ell_2(\mathbb{Z})$ by

sampling a Gabor frame for $L_2(\mathbb{R})$ with integer shift parameters. Moreover, it is shown in [65] that if the inner product of window function and its time-frequency shift has some decay, the minimal energy dual window can be sampled as well, preserving the duality and minimality.

Other exisiting approaches to construct the discrete Gabor bi-frames is either implicitly using the duality principle for bi-frames, i.e. the bi-orthogonality condition of the adjoint frame and its dual, or using the definition of canonical dual frame which is done either by solving a linear system or by using unitary matrix factorization of frame operator. Interested readers are referred to [92, 113, 88, 77, 93] for more details. The discrete Gabor frames constructed by these methods usually do not have closed-form dual frames. Thus a linear system needs to be solved to find its dual which could be troublesome when the dimension of signals is very high. Using the fact that the Zak transform diagonalizes the analysis operator of a Gabor system when $ab$ is 1 or reciprocal of an integer, an effective computation scheme is proposed in [6] for calculating a dual frame of a Gabor frame by using the Zak transform and the inverse Zak transform. There have been few approaches for constructing discrete tight Gabor frame. In [36], a discrete Gabor tight frame is expressed from the viewpoint of a filter bank and thus the construction of tight Gabor frames is equivalent to the construction of paraunitary polyphase matrices, whose involved computation is non-trivial.

In [30], the authors study a general theory of Fourier-like frames on locally compact abelian groups, which can be applied to obtain explicit constructions of discrete Gabor frames and dual Gabor frames for $\mathbb{C}^N$.

### 3.1.2 Our works

In this chapter, we use the Gramian and dual Gramian analysis first developed in [99] for function spaces as the main tools to relate all frame properties of discrete Gabor systems to the analysis of the eigenvalues of their corresponding Gramian

and dual Gramian matrices. Once the Gramian and dual Gramian analysis are established, the derivations of many existing results on discrete Gabor frames become straightforward, including the duality principle. The simplicity of such an approach comes from the fiberization technique introduced in [99]. While the frame properties of Gabor frames for function space require almost all fibers have such frame properties, the frame properties of discrete Gabor frames only require a given set of fibers have such frame properties.

Using the duality principle, we first derive a necessary and sufficient condition for Gabor systems with non-negative window function to form tight frames for $\mathbb{C}^N$, followed by the constructions of two classes of tight Gabor frames generated by sampling two types of window functions satisfying the property of *partition of unity*: the square root of B-splines and the Fourier transform of refinable functions of Meyer wavelets. It is noted that partition of unity has also been used for constructing Gabor frames of function spaces; see e.g. [28]. However, the constructed tight Gabor frames are not suitable for image recovery, as the associated high-pass filter bank has non-zero DC offsets, i.e., the mean value of each atom is not zero. Therefore, a new class of Gabor induced frames is proposed by removing the DC offsets of all high-pass filters. Although the new discrete Gabor induced frames are not tight, their associated decomposition and reconstruction processes remain as simple as tight Gabor frames. And it can be observed that the constructed (tight) frames have the optimal orientation selectivity.

## 3.2 (Dual) Gramian analysis, fiberization and duality principle

In this section, we develop the Gramian and dual Gramian analysis for Gabor systems in $\mathbb{C}^N$, from which some useful corollaries including the duality principle are derived.

Before the discussion, we first introduce some notations and definitions related to the Gramian and dual Gramian analysis for Gabor systems. For a Gabor system $X$ defined as (3.1), it is clearly a Bessel sequence of $\mathbb{C}^N$, as well as a frame sequence of $\mathbb{C}^N$. The *pre-Gramian matrix* of $X$, denoted by $\boldsymbol{J}_X$, is an $N$-by-$|K||L|$ matrix defined by

$$\boldsymbol{J}_X[m, j(k, \ell)] = \boldsymbol{g}_{k,\ell}(m), \quad 0 \le m < N, 0 \le j(k, \ell) < |K||L|, \qquad (3.2)$$

which collects all elements of $X$ column-wise. It is consistent with the definition of pre-Gramian defined in [53] using canonical orthonormal basis of $\mathbb{C}^N$. After defining the pre-Gramian, we define the *Gramian matrix* of $X$ by $\boldsymbol{G}_X = \boldsymbol{J}_X^* \boldsymbol{J}_X$ and the *dual Gramian matrix* by $\widetilde{\boldsymbol{G}}_X = \boldsymbol{J}_X \boldsymbol{J}_X^*$. For two Gabor systems $X, Y$, we define their *mixed Gramian matrix* by $\boldsymbol{G}_{X,Y} = \boldsymbol{J}_X^* \boldsymbol{J}_Y$, and their *mixed dual Gramian matrix* by $\widetilde{\boldsymbol{G}}_{X,Y} = \boldsymbol{J}_Y \boldsymbol{J}_X^*$.

For a system $X$, its frame properties are closely related to the eigenvalues of its Gramian $\boldsymbol{G}_X$ and dual Gramian $\widetilde{\boldsymbol{G}}_X$. Indeed, from the definition of pre-Gramian given in (3.2), it can be seen that $\boldsymbol{J}_X$ is exactly the synthesis operator $\mathcal{T}_X$ defined as (2.1) and the analysis operator $\mathcal{T}_X^*$ is the conjugate transpose of $\boldsymbol{J}_X$. Thus, the frame properties of $X$ can be described by the eigenvalues of $\boldsymbol{G}_X$ and $\widetilde{\boldsymbol{G}}_X$. Let $\lambda(\boldsymbol{G})$ denote the set of all eigenvalues of a matrix $\boldsymbol{G}$. Then,

(i) The frame sequence $X$ has lower frame bound

$$A = \min_{\lambda \ne 0}\{\lambda(\boldsymbol{G}_X)\} = \min_{\lambda \ne 0}\{\lambda(\widetilde{\boldsymbol{G}}_X)\}$$

and upper frame bound

$$B = \max_{\lambda}\{\lambda(\boldsymbol{G}_X)\} = \max_{\lambda}\{\lambda(\widetilde{\boldsymbol{G}}_X)\}.$$

(ii) $X$ is a tight frame sequence of $\mathbb{C}^N$ if and only if all non-zero eigenvalues of $\boldsymbol{G}_X$ (or $\widetilde{\boldsymbol{G}}_X$) are 1.

(iii) $X$ is a frame for $\mathbb{C}^N$ if and only if all eigenvalues of $\widetilde{\boldsymbol{G}}_X$ are non-zero.

(iv) $X$ is a tight frame for $\mathbb{C}^N$ if and only if all eigenvalues of $\widetilde{\boldsymbol{G}}_X$ equal to 1.

(v) $X$ is a Riesz sequence of $\mathbb{C}^N$ if and only if all eigenvalues of $\boldsymbol{G}_X$ are non-zero.

(vi) $X$ and $Y$ are bi-frames for $\mathbb{C}^N$ if and only if $\widetilde{\boldsymbol{G}}_{X,Y} = \widetilde{\boldsymbol{G}}_{Y,X} = I$.

(vii) $X$ and $Y$ are bi-orthogonal sequences of $\mathbb{C}^N$ if and only if $\boldsymbol{G}_{X,Y} = \boldsymbol{G}_{Y,X} = I$.

Clearly, the frame properties of a system $X$ can be completely characterized from the eigenvalues of $\boldsymbol{G}_X$ and $\widetilde{\boldsymbol{G}}_X$.

Recall that the columns of $\boldsymbol{J}_X$ are the elements of $X$. Consider another system $X^*$ defined by all rows of $\boldsymbol{J}_X$ up to unitary equivalence, i.e. $\boldsymbol{J}_{X^*} = \boldsymbol{V}_1 \boldsymbol{J}_X^* \boldsymbol{V}_2$ where $\boldsymbol{V}_1$ and $\boldsymbol{V}_2$ are two unitary matrices. Such a system $X^*$ is called an *adjoint system* of $X$ in [53], as the dual Gramian matrix $\widetilde{\boldsymbol{G}}_X$ of $X$ is the Gramian matrix $\boldsymbol{G}_{X^*}$ of $X^*$ up to unitary equivalence. In other words, all frame properties of a system $X$ (e.g. frame property, frame bound and tight frame property) determined by its dual Gramian matrix $\widetilde{\boldsymbol{G}}_X$ now can be also derived from the Gramian matrix $\boldsymbol{G}_{X^*}$ of $X^*$. Such a connection is the essential ingredient of the so-called *duality principle* ([95, 99, 53, 52]). In general, for a Gabor system, the adjoint system defined as above is not a Gabor system. Later, we will consider another type of adjoint systems which are Gabor systems themselves.

For the simplicity of discussion, we consider that the length of signal $N$ can be divided exactly by two shift parameters $a$ and $b^{-1}$. Then an often seen lattice set $\{K, L\}$ of a Gabor system $X = (K, L)_{\boldsymbol{g}}$ is given as follows,

$$K := \mathbb{N}_{N/a} = \{0, 1, \ldots, N/a - 1\}, \quad \text{and } L := \mathbb{N}_{\frac{1}{b}} = \{0, 1, \ldots, b^{-1} - 1\}. \quad (3.3)$$

Before discussing its adjoint Gabor system and the duality principle, we introduce a fiberization technique which can greatly simplify the analysis of the Gramian matrix and dual Gramian matrix of a Gabor system. The fiberization matrices of the pre-Gramian $\boldsymbol{J}_X$, denoted by $\boldsymbol{J}_X(m) \in \mathbb{C}^{bN \times \frac{N}{a}}$, is defined by

$$\boldsymbol{J}_X(m)[\ell^*, k] = b^{-\frac{1}{2}} \boldsymbol{g}((m - b^{-1}\ell^* - ak) \bmod N), \quad 0 \le \ell^* \le bN - 1, 0 \le k \le N/a - 1,$$
$$(3.4)$$

for $m = 0, 1, \ldots, N-1$. Then, the fiberization matrices for the Gramians $\boldsymbol{G}_X$, $\widetilde{\boldsymbol{G}}_X$, $\boldsymbol{G}_{X,Y}$, $\widetilde{\boldsymbol{G}}_{X,Y}$ is defined by

$$
\begin{cases}
\boldsymbol{G}_X(m) = \boldsymbol{J}_X(m)^*\boldsymbol{J}_X(m), & \widetilde{\boldsymbol{G}}_X(m) = \boldsymbol{J}_X(m)\boldsymbol{J}_X(m)^*; \\
\boldsymbol{G}_{X,Y}(m) = \boldsymbol{J}_X(m)^*\boldsymbol{J}_Y(m), & \widetilde{\boldsymbol{G}}_{X,Y}(m) = \boldsymbol{J}_Y(m)\boldsymbol{J}_X(m)^*,
\end{cases}
\quad \text{for } 0 \le m < N.
$$

$$(3.5)$$

Then, a direct extension of the fiberization technique introduced in [99] for continuous setting to the discrete setting leads to the following proposition.

**Proposition 3.1.** *Let $X = (K, L)_{\boldsymbol{g}}$ denote a Gabor system defined on the lattices $(K, L)$ given by (3.3). Then there exist two unitary matrices $\boldsymbol{V}_1 \in \mathbb{C}^{\frac{N}{ab} \times \frac{N}{ab}}$ and $\boldsymbol{V}_2 \in \mathbb{C}^{N \times N}$ such that*

$$
\begin{cases}
\boldsymbol{V}_1 \boldsymbol{G}_X \boldsymbol{V}_1^* = \mathrm{diag}(\boldsymbol{G}_X(0), \boldsymbol{G}_X(1), \ldots, \boldsymbol{G}_X(b^{-1}-1)); \\
\boldsymbol{V}_2 \widetilde{\boldsymbol{G}}_X \boldsymbol{V}_2^* = \mathrm{diag}(\widetilde{\boldsymbol{G}}_X(0), \widetilde{\boldsymbol{G}}_X(1), \ldots, \widetilde{\boldsymbol{G}}_X(b^{-1}-1)).
\end{cases}
$$

$$(3.6)$$

*where $\boldsymbol{G}_X(m), \widetilde{\boldsymbol{G}}_X(m), m = 0, \ldots, b^{-1}-1$ are fiberization matrices given by (3.5).*

*Proof.* For a Gabor system $X = (K, L)_{\boldsymbol{g}}$, $\boldsymbol{J}_X^* \in \mathbb{C}^{|K||L| \times N}$ has its rows indexed by $k \in K$ and $\ell \in L$ and its columns indexed by $\mathbb{N}_N$. One may also index $\mathbb{N}_N$ via two indices $(L, L^*)$ such that $\mathbb{N}_N = \{m\ell^*\}_{m \in L, \ell^* \in L^*}$, where $L = \mathbb{N}_{\frac{1}{b}}$ and $L^* = \mathbb{N}_{Nb}$. Using the double indices $(K, L) \times (L, L^*)$, $\boldsymbol{J}_X^*$ can be re-written in the block-wise form:

$$
\boldsymbol{J}_X^* = \left( \boldsymbol{J}_{k,\ell^*} \right)_{K \times L^*},
$$

where $\boldsymbol{J}_{k,\ell^*} \in \mathbb{C}^{\frac{1}{b} \times \frac{1}{b}}$ is given by

$$
\boldsymbol{J}_{k,\ell^*}[\ell, m] = \boldsymbol{J}_X^*[j(k,\ell), l(m, \ell^*)] = \overline{\boldsymbol{g}_{k,\ell}(m - b^{-1}\ell^*)}, \quad 0 \le \ell, m \le b^{-1}-1.
$$

Consider a square matrix $\boldsymbol{U}_1 \in \mathbb{C}^{|L| \times |L|}$ defined by $\boldsymbol{U}_1[m, \ell] = e^{-2\pi i b\ell m}$. Clearly, $\boldsymbol{U}_1^*\boldsymbol{U}_1 = \boldsymbol{U}_1\boldsymbol{U}_1^* = b^{-1}I_{\frac{1}{b}}$. Let $\boldsymbol{U} \in \mathbb{C}^{|K||L| \times |K||L|}$ denote the block-wise diagonal matrix defined by $\boldsymbol{U} = \mathrm{diag}(\boldsymbol{U}_1, \ldots, \boldsymbol{U}_1)$. Then, we have $\boldsymbol{U}^*\boldsymbol{U} = \boldsymbol{U}\boldsymbol{U}^* = b^{-1}I_{\frac{|K|}{b}}$ and $\boldsymbol{U}\boldsymbol{J}_X^* = \left( \boldsymbol{U}_1\boldsymbol{J}_{k,\ell^*} \right)_{K \times L^*}$. Indeed, each block matrix $\boldsymbol{U}_1\boldsymbol{J}_{k,\ell^*} \in \mathbb{C}^{|L| \times |L|}$ is a diagonal matrix whose diagonal entries are given by

$$
\boldsymbol{U}_1\boldsymbol{J}_{k,\ell^*}[m, m] = b^{-1}\overline{\boldsymbol{g}((m - ak - b^{-1}\ell^*) \bmod N)}, \quad 0 \le m \le b^{-1}-1.
$$

Recall that the definition (3.4) of the fiberization matrix $\boldsymbol{J}_X(m)$ is given by

$$\boldsymbol{J}_X(m)[\ell^*, k] = b^{-\frac{1}{2}}\boldsymbol{g}((m - b^{-1}\ell^* - ak) \bmod N), \quad 0 \leq \ell^* \leq bN - 1, 0 \leq k \leq N/a - 1,$$

By re-shuffling its row indices and column indices, we can rewrite the matrix $\boldsymbol{U}\boldsymbol{J}_X^*$ as a diagonal block-wise matrix with diagonal entries being the fiberization matrices:

$$b^{\frac{1}{2}}\boldsymbol{P}_1\boldsymbol{U}\boldsymbol{J}_X^*\boldsymbol{P}_2 = \mathrm{diag}(\boldsymbol{J}_X(0)^*, \boldsymbol{J}_X(1)^*, \dots, \boldsymbol{J}_X(1/b - 1)^*) \in \mathbb{C}^{|L||K| \times N}, \qquad (3.7)$$

where $\boldsymbol{P}_1, \boldsymbol{P}_2$ are two permutation matrices and $\boldsymbol{J}_X(m)$ is the fiberization matrix defined by (3.4). Then, by definition, the Gramian matrix $\boldsymbol{G}_X$ and dual Gramian matrix $\widetilde{\boldsymbol{G}}_X$ satisfy

$$\boldsymbol{V}_1\boldsymbol{G}_X\boldsymbol{V}_1^* = \mathrm{diag}(\boldsymbol{G}_X(0), \boldsymbol{G}_X(1), \dots, \boldsymbol{G}_X(b^{-1} - 1))$$

and

$$\boldsymbol{V}_2\widetilde{\boldsymbol{G}}_X\boldsymbol{V}_2^* = \mathrm{diag}(\widetilde{\boldsymbol{G}}_X(0), \widetilde{\boldsymbol{G}}_X(1), \dots, \widetilde{\boldsymbol{G}}_X(b^{-1} - 1)),$$

here $\boldsymbol{V}_1 = b^{\frac{1}{2}}\boldsymbol{P}_1\boldsymbol{U}$ and $\boldsymbol{V}_2 = \boldsymbol{P}_2^*$ are unitary matrices. $\qquad\square$

Proposition 3.1 shows that up to unitary equivalence, the Gramian matrix $\boldsymbol{G}_X$ and dual Gramian matrix $\widetilde{\boldsymbol{G}}_X$ can be rewritten as block diagonal matrices of fiberization matrices. Thus, all frame properties of $X$ now can be determined by analyzing the union of the eigenvalues of $\frac{1}{b}$ fiberization matrices of small size: $\boldsymbol{G}_X(m) \in \mathbb{C}^{\frac{N}{a} \times \frac{N}{a}}, \widetilde{\boldsymbol{G}}_X(m) \in \mathbb{C}^{Nb \times Nb}, m = 0, \dots, \frac{1}{b} - 1$, which is easier to analyze than the big matrices $\boldsymbol{G}_X$ and $\widetilde{\boldsymbol{G}}_X$.

Moreover, by a direct calculation, it can be seen that the transpose of fiberization matrices $\boldsymbol{J}_X(m)$ defined by (3.4) is indeed the fiberization matrices of another Gabor system $X^*$ (up to a constant), i.e.,

$$\boldsymbol{J}_{X^*}(m) = (ab)^{\frac{1}{2}}\overline{\boldsymbol{J}_X(m)^*}, \quad m = 1, 2, \dots, N - 1, \qquad (3.8)$$

where $X^* = (L^*, K^*)_{\boldsymbol{g}}$ is the Gabor system defined by the same window function $\boldsymbol{g}$ but with different shift parameters and different lattices:

$$L^* = \mathbb{N}_{Nb} = \{0, 1, \dots, Nb - 1\}, \quad and \quad K^* = \mathbb{N}_a = \{0, 1, \dots, a - 1\}. \qquad (3.9)$$

Thus, by the definition (3.5) of fiberization for Gramian and dual Gramian, there exists a connection between the dual Gramian $\widetilde{\boldsymbol{G}}_X$ of $X = (K, L)_{\boldsymbol{g}}$ and the Gramian $\boldsymbol{G}_{X^*}$ of $X^* = (L^*, K^*)_{\boldsymbol{g}}$ given by (3.9). In other words, the Gabor system $X^* = (L^*, K^*)_{\boldsymbol{g}}$ is an adjoint system of $X$, which is connected to $X$ via duality principle as stated in the following proposition.

**Proposition 3.2.** *Let $X = (K, L)_{\boldsymbol{g}}$ and $Y = (K, L)_{\widetilde{\boldsymbol{g}}}$ be two Gabor systems for $\mathbb{C}^N$ defined on the lattices given by (3.3). Let $X^* = (L^*, K^*)_{\boldsymbol{g}}$ and $Y^* = (L^*, K^*)_{\widetilde{\boldsymbol{g}}}$ be the corresponding adjoint systems defined on the lattices given by (3.9). Then we have*

(a) *The frame bounds of two frame sequences $X$ and $X^*$ are related by $B^* = (ab)B$, $A^* = (ab)A$.*

(b) *$X$ is a tight frame sequence of $\mathbb{C}^N$ if and only if $(ab)^{-\frac{1}{2}} X^*$ is a tight frame sequence of $\mathbb{C}^N$.*

(c) *$X$ is a frame for $\mathbb{C}^N$ if and only if $(ab)^{-\frac{1}{2}} X^*$ is a Riesz sequence of $\mathbb{C}^N$.*

(d) *$X$ is a tight frame for $\mathbb{C}^N$ if and only if $(ab)^{-\frac{1}{2}} X^*$ is an orthonormal sequence of $\mathbb{C}^N$.*

(e) *$X$ and $Y$ are bi-frames for $\mathbb{C}^N$ if and only if $(ab)^{-\frac{1}{2}} X^*$ and $(ab)^{-\frac{1}{2}} Y^*$ are bi-orthogonal sequences of $\mathbb{C}^N$.*

*Proof.* Let $X = (K, L)_{\boldsymbol{g}}$ denote the Gabor system defined on the lattices $(K, L)$ given by (3.3). By Proposition 3.1, the eigenvalues of $\boldsymbol{G}_X$ (or $\widetilde{\boldsymbol{G}}_X$) are the union of the eigenvalues of $\boldsymbol{G}_X(m)$ (or $\widetilde{\boldsymbol{G}}_X(m)$) for $0 \leq m \leq b^{-1} - 1$. Then, the frame properties of $X$ are determined by the eigenvalues $\cup_{m \in L} \lambda(\boldsymbol{G}_X(m))$, and $\cup_{m \in L} \lambda(\widetilde{\boldsymbol{G}}_X(m))$ and the statements about frame properties of $X$ can be rewritten as:

(i) $X$ is a frame for $\overline{\operatorname{span}(X)}$, with its lower and upper frame bounds given by

$$\begin{cases} A = \min_{m \in L}\{\min_{\lambda \neq 0} \lambda(\boldsymbol{G}_X(m))\} = \min_{m \in L}\{\min_{\lambda \neq 0} \lambda(\widetilde{\boldsymbol{G}}_X(m))\}, \\ B = \max_{m \in L}\{\max_{\lambda} \lambda(\boldsymbol{G}_X(m))\} = \max_{m \in L}\{\max_{\lambda} \lambda(\widetilde{\boldsymbol{G}}_X(m))\}; \end{cases}$$

(ii) $X$ is a tight frame for $\overline{\mathrm{span}(X)}$ if and only if for each $m \in L$, all non-zero eigenvalues of $\boldsymbol{G}_X(m)$ (or $\widetilde{\boldsymbol{G}}_X(m)$) equal to 1;

(iii) $X$ is a frame for $\mathbb{C}^N$ if and only if all eigenvalues of $\widetilde{\boldsymbol{G}}_X(m)$ are non-zero for each $m \in L$;

(iv) $X$ is a tight frame for $\mathbb{C}^N$ if and only if all eigenvalues of $\widetilde{\boldsymbol{G}}_X(m)$ equal to 1 for each $m \in L$;

(v) $X$ is a Riesz sequence of $\mathbb{C}^N$ if and only if all eigenvalues of $\boldsymbol{G}_X(m)$ are non-zero for each $m \in L$.

Similarly, the frame properties of system $X^*$ are determined by the eigenvalues $\cup_{m \in K^*} \lambda(\boldsymbol{G}_{X^*}(m))$ and $\cup_{m \in K^*} \lambda(\widetilde{\boldsymbol{G}}_{X^*}(m))$.

By checking the entries of $\boldsymbol{G}_X$, we have for any $m \in L$,

$$\boldsymbol{G}_X(m)[k', k] = \boldsymbol{G}_X(m + b^{-1})[[k', k], \quad 0 \le k', k \le \frac{N}{a} - 1,$$

and

$$\widetilde{\boldsymbol{G}}_X(m)[\ell^{*\prime}, \ell^*] = \widetilde{\boldsymbol{G}}_X(m + b^{-1})[(\ell^{*\prime} + 1) \bmod bN, (\ell^* + 1) \bmod bN], \quad 0 \le \ell^{*\prime}, \ell^* \le bN - 1.$$

Thus, for each $m \in L$, $\boldsymbol{G}_X(m)$ and $\boldsymbol{G}_X(m + b^{-1})$ are exactly the same, and $\widetilde{\boldsymbol{G}}_X(m)$ and $\widetilde{\boldsymbol{G}}_X(m + b^{-1})$ are also the same, up to the multiplication of some permutation matrix. Therefore,

$$\begin{cases} \cup_{m \in L} \lambda(\boldsymbol{G}_X(m)) = \cup_{m \in \mathbb{N}_N} \lambda(\boldsymbol{G}_X(m)), \\ \cup_{m \in L} \lambda(\widetilde{\boldsymbol{G}}_X(m)) = \cup_{m \in \mathbb{N}_N} \lambda(\widetilde{\boldsymbol{G}}_X(m)). \end{cases} \tag{3.10}$$

The same conclusion holds true for $X^*$. Notice that $\widetilde{\boldsymbol{G}}_{X^*}(m) = ab\overline{\boldsymbol{G}_X(m)}$ and $\boldsymbol{G}_{X^*} = ab\overline{\widetilde{\boldsymbol{G}}_X(m)}$ for $m \in \mathbb{N}_N$. Thus, we have

$$\begin{cases} \cup_{m \in K^*} \lambda(\widetilde{\boldsymbol{G}}_{X^*}(m)) = ab \cup_{m \in L} \lambda(\boldsymbol{G}_X(m)), \\ \cup_{m \in K^*} \lambda(\boldsymbol{G}_{X^*}(m)) = ab \cup_{m \in L} \lambda(\widetilde{\boldsymbol{G}}_X(m)). \end{cases} \tag{3.11}$$

Together with the statements (i)–(v), the relationships between the union of the eigenvalues of $\boldsymbol{G}_X(m), \widetilde{\boldsymbol{G}}_X(m), \boldsymbol{G}_{X^*}(m), \widetilde{\boldsymbol{G}}_{X^*}(m)$ over different lattice sets, as shown in (3.10) and (3.11), allow us to come to the conclusions (a)–(d) in Proposition 3.2.

The proof of (e) in the proposition is essentially the same. We consider two systems $X$ and $Y$ defined on the same lattices $K$ and $L$. By (3.7), the mixed Gramian and mixed dual Gramian matrices are also equivalent to block-wise diagonal matrices up to unitary operators:

$$b\boldsymbol{P}_1 \boldsymbol{U}\boldsymbol{G}_{X,Y}\boldsymbol{U}^*\boldsymbol{P}_1^* = \mathrm{diag}(\boldsymbol{G}_{X,Y}(0), \ldots, \boldsymbol{G}_{X,Y}(b^{-1} - 1))$$

and

$$\boldsymbol{P}_2^*\widetilde{\boldsymbol{G}}_{X,Y}\boldsymbol{P}_2 = \mathrm{diag}(\widetilde{\boldsymbol{G}}_{X,Y}(0), \ldots, \widetilde{\boldsymbol{G}}_{X,Y}(b^{-1} - 1)),$$

where $b^{\frac{1}{2}}\boldsymbol{U}, \boldsymbol{P}_1, \boldsymbol{P}_2$ are all unitary matrices. Thus, we get

(vi) $X$ and $Y$ are bi-frames for $\mathbb{C}^N$ if and only if $\widetilde{\boldsymbol{G}}_{X,Y}(m) = \widetilde{\boldsymbol{G}}_{Y,X}(m) = \boldsymbol{I}$ for each $m \in L$;

(vii) $X$ and $Y$ are bi-orthogonal sequences of $\mathbb{C}^N$ if and only if $\boldsymbol{G}_{X,Y}(m) = \boldsymbol{G}_{Y,X}(m) = \boldsymbol{I}$ for each $m \in L$.

Also, $\boldsymbol{G}_{X,Y}(m) = \boldsymbol{I}$ or $\widetilde{\boldsymbol{G}}_{X,Y}(m) = \boldsymbol{I}$ for $m \in L$ if and only if the same equality is true for all $m \in \mathbb{N}_N$. Then by the fact that $\widetilde{\boldsymbol{G}}_{Y^*,X^*}(m) = ab\overline{\boldsymbol{G}_{X,Y}(m)}$, one can obtain the bi-frame property (e) in Proposition 3.2. $\square$

The connection between $X$ and its adjoint Gabor system $X^*$ stated in Proposition 3.2 shows that the construction of a tight Gabor frame $X$ can be done via constructing a Gabor system $X^*$ which is an orthonormal sequence. Often, the construction and the analysis of orthonormal sequences are easier and simpler than that of tight frames. The advantages by working on the adjoint system $X^*$ are exploited when deriving frame bounds of discrete Gabor frames, as well as a sufficient and necessary condition for Gabor tight frames with non-negative window functions.

**Remark 3.3.** Fiberization matrices for Gabor systems can also be defined in frequency domain. Similar to the case of functional space [99], we define

$$\widehat{\boldsymbol{J}}_X(\omega)[k^*, \ell] = a^{-\frac{1}{2}} \widehat{\boldsymbol{g}}(\omega/N + \frac{k^*}{a} + b\ell), \quad k^* \in K^*, \ell \in L,$$

for $\omega \in \mathbb{N}_N$. Then, $X$ and $X^*$ have the same relationship as (3.8) via $\widehat{\boldsymbol{J}}_X(\omega)$ and $\widehat{\boldsymbol{J}}_{X^*}(\omega)$:

$$\widehat{\boldsymbol{J}}_{X^*}(\omega) = (ab)^{\frac{1}{2}} \, \overline{\widehat{\boldsymbol{J}}_X(\omega)^*}, \qquad \omega \in \mathbb{N}_N.$$

Let $\boldsymbol{F}$ denote the discrete Fourier transform given by $\boldsymbol{F}[\omega, m] = e^{-2\pi i \frac{m\omega}{N}}, \omega, m \in \mathbb{N}_N$. Define a block-wise diagonal matrix $\widehat{\boldsymbol{U}} = \mathrm{diag}(\widehat{\boldsymbol{U}}_\ell)_{\ell \in L}$ with the $\ell$-th block given by

$$\widehat{\boldsymbol{U}}_\ell[\omega, k] = e^{-2\pi i a k(\frac{\omega}{N} + b\ell)}, \quad \omega, k \in K.$$

Then, $\frac{\sqrt{a}}{N} \widehat{\boldsymbol{U}} \boldsymbol{J}_X^* \boldsymbol{F}^*$ is the same as the block diagonal matrix $\widehat{\boldsymbol{J}}_X^* = \mathrm{diag}(\widehat{\boldsymbol{J}}_X(\omega)^*)_{0 \le \omega < N/a}$, up to permutations. As $\sqrt{\frac{a}{N}} \widehat{\boldsymbol{U}}$ and $\frac{1}{\sqrt{N}} \boldsymbol{F}$ are both unitary matrices, the duality principle is established.

## 3.3  Construction of discrete tight Gabor frames

Many fundamental results of discrete Gabor frames can be easily obtained using the duality principle stated in Proposition 3.2. For example, a direct application of (a) and (c) in Proposition 3.2 leads to the relationship between frame bounds and the frame density.

**Corollary 3.4.** *Let $X$ be a Gabor frame for $\mathbb{C}^N$. Then the frame bounds $A, B$ of $X$ satisfy*

$$\frac{A}{\|\boldsymbol{g}\|_2^2} \le \mathrm{den}X \le \frac{B}{\|\boldsymbol{g}\|_2^2}.$$

*In particular, the windows function of a Gabor tight frame for $\mathbb{C}^N$ satisfies $\|\boldsymbol{g}\|_2^2 = (\mathrm{den}X)^{-1} = ab$.*

*Proof.* Given a Gabor frame $X$ for $\mathbb{C}^N$, its adjoint system $X^*$ is then a Riesz sequence by Proposition 3.2. Let $A^*$ and $B^*$ denote its frame bounds. Then we have

$\mathcal{T}_{X^*} e_0 = g$ where $e_0$ denote the unit vector with first entry being 1. Therefore, $A^* \leq \|\mathcal{T}_{X^*} e_0\|_2^2 \leq B^*$ which gives $A^* \leq \|g\|_2^2 \leq B^*$. By Proposition 3.2 (a), we have then

$$\frac{A}{\mathrm{den}X} = A^* \leq \|g\|_2^2 \leq B^* = \frac{B}{\mathrm{den}X}.$$

Thus, $A \leq \mathrm{den}X \|g\|_2^2 \leq B$. $\qquad\square$

Suppose that the window function $g$ is non-negative with its support on a finite interval, which usually holds true in practice. Then, using the statement (d) in Proposition 3.2, we have the following sufficient and necessary condition for $X$ to form a tight frame for $\mathbb{C}^N$.

**Corollary 3.5.** *Suppose that $g \in \mathbb{R}^N$ is a non-negative vector with support $[0, p-1]$. Then, the Gabor system $X = (K, L)_g$ is a tight frame for $\mathbb{C}^N$ if and only if the following two conditions hold true:*

$$(i) \quad b \leq p^{-1}; \quad and \quad (ii) \quad \sum_{k=0}^{N/a-1} g^2((\cdot - ak) \bmod N) \equiv b.$$

*Proof.* Suppose that $X$ is a tight frame for $\mathbb{C}^N$. Then, $X^*$ is an orthogonal sequence by the duality principle (Proposition 3.2). By contradiction, suppose that $b > p^{-1}$, then consider the following two elements in $X^*$: $\{g(m)\}$ and $\{g((m - \frac{1}{b}) \bmod N)\}$. Then their inner product

$$\sum_{m=0}^{N-1} g(m)g((m - \frac{1}{b}) \bmod N) \geq \sum_{m=1/b}^{p-1} g(m)g(m - \frac{1}{b}) > 0,$$

since $g$ is non-negative and $g(m) > 0$ for $0 \leq m \leq p - 1$, which contradicts the assumption that $X^*$ is an orthogonal sequence. Thus, we have $b \leq p^{-1}$. Moreover, by the definition of tight frame, we have $I = \mathcal{T}_X \mathcal{T}_X^*$. Notice that for $0 \leq m, n \leq N - 1$,

$$
\begin{aligned}
(\mathcal{T}_X \mathcal{T}_X^*)[m, n] &= \sum_{k \in K, \ell \in L} g((m - ak) \bmod N)g((n - ak) \bmod N)e^{2\pi i \ell(n-m)b} \\
&= \begin{cases} 1/b \sum_{k \in K} g^2((m - ak) \bmod N), & m = n; \\ 0, & m \neq n. \end{cases}
\end{aligned}
$$

Recall that $(\mathcal{T}_X\mathcal{T}_X^*)[m,m] = \boldsymbol{I}[m,m] = 1$, which gives $\sum_{k\in K} \boldsymbol{g}^2((\cdot - ak) \bmod N) \equiv b$.

Conversely, suppose that both conditions hold true. It can be seen that

$$(\mathcal{T}_X\mathcal{T}_X^*)[m,n] = \begin{cases} 1, & \text{if } m = n; \\ 0, & \text{otherwise.} \end{cases}$$

Therefore, $X$ is a tight frame for $\mathbb{C}^N$. $\hfill\square$

It can be seen from Corollary 3.5 that the construction of tight Gabor frames for $\mathbb{C}^N$ is simplified to finding a non-negative window $\boldsymbol{g}$ which satisfies the so-called *partition of unity* property, provided that $b$ is set to be no larger than $1/p$. There are actually many such window functions with good regularity.

**Example 3.6.** *Let $B_n^a$ denote the B-spline of order $n$ with the knots $\{0, a, \ldots, an\}$. Then, it is known ([45]) that the function $B_n^a$ is a non-negative function with support $[0, an]$ and satisfies*

$$\sum_{k\in\mathbb{Z}} B_n^a(t - ak) = 1, \qquad \forall t \in \mathbb{R},$$

*which leads to $\sum_{k\in\mathbb{Z}} B_n^a(j - ak) = 1$ for any integer $j$. Define the vector $\boldsymbol{g}$ by $\boldsymbol{g}(m) = \sqrt{bB_n^a(m)}$ for $m = 1, 2, \ldots, an-1$. Then it can be seen that $\sum_{k=0}^{N/a-1} |\boldsymbol{g}((\cdot - ak) \bmod N)|^2 = b$. Thus, the Gabor system $(K, L)_{\boldsymbol{g}}$ generated by $\boldsymbol{g}$ with $b \leq \frac{1}{an-1}$ is a tight frame for $\mathbb{C}^N$.*

**Example 3.7.** *Let $\phi$ denote the scaling function of Meyer wavelets defined by*

$$\hat{\phi}(\omega) = \begin{cases} 1, & |\omega| \leq \frac{2\pi}{3}; \\ \cos\left[\frac{\pi}{2}\beta\left(\frac{3}{2\pi}|\omega| - 1\right)\right], & \frac{2\pi}{3} \leq |\omega| \leq \frac{4\pi}{3}; \\ 0, & \text{otherwise,} \end{cases}$$

*where $\beta$ is a function satisfying $\beta(x) + \beta(1-x) = 1$ for $x \in [0,1]$. For example, the one used in [40] is given by $\beta(x) = x^4(35 - 84x + 70x^2 - 20x^3)$. It can be seen that*

$$\sum_{k\in\mathbb{Z}} |\widehat{\phi}(\omega - 2k\pi)|^2 = 1, \quad \forall \omega \in \mathbb{R}.$$

*Let $\widehat{\phi_a}(\omega) = \widehat{\phi}(\frac{2\pi\omega}{a})$. Then, $\sum_{k\in\mathbb{Z}} |\widehat{\phi_a}(\cdot - ak)|^2 = 1$. Define the window function $\boldsymbol{g}$ by $\boldsymbol{g}(m) = \sqrt{b}|\widehat{\phi_a}(m)|$. Then, a non-negative window function with partition of unity property is obtained, which leads to a tight frame $(K,L)_{\boldsymbol{g}}$ for $\mathbb{C}^N$ if setting $b \le \frac{1}{p}$. For example, when $a = 4$, the vector $\boldsymbol{g}$ is given by $\boldsymbol{g} = [1/\sqrt{2}, 1, 1, 1, 1/\sqrt{2}]$.*

# 3.4 Construction of discrete Gabor induced frames for image recovery

The discrete tight frames constructed in the aforementioned section are not suitable for image recovery, as the associated filter banks have non-zero DC offsets. Thus, in this section, we derive a class of Gabor induced frames with zero DC offset and with closed-form dual frames.

## 3.4.1 Decomposition and reconstruction by filter banks

Discrete Gabor systems $X = (K,L)_{\boldsymbol{g}}$ are closely connected to filter banks; see e.g. [6, 36]). For a signal $\boldsymbol{f} \in \mathbb{C}^N$, let $\downarrow_a$ denote the down-sampling operator and $\uparrow_a$ denote the up-sampling operator defined by

$$\boldsymbol{f}_{\downarrow_a}(n) = \boldsymbol{f}(an), \quad n = 0, 1, \ldots, \tfrac{N}{a} - 1;$$

$$\boldsymbol{f}_{\uparrow_a}(an) = \begin{cases} \boldsymbol{f}(n), & n = 0, 1, \ldots \tfrac{N}{a} - 1, \\ 0 & \text{otherwise.} \end{cases}$$

For a filter $\boldsymbol{h} \in \mathbb{C}^N$, there are two essential operators: one is the *analysis* operator $\boldsymbol{W_h} : \mathbb{C}^N \to \mathbb{C}^{N/a}$ defined in the matrix form by

$$(\boldsymbol{W_h f})[j] = (\overline{\boldsymbol{h}(-\cdot)} * \boldsymbol{f})_{\downarrow_a}(j) = \sum_{k=0}^{N-1} \boldsymbol{f}(k)\overline{\boldsymbol{h}((k - aj) \bmod N)}.$$

and the other is the *synthesis* operator $\boldsymbol{W_h^*} : \mathbb{C}^{N/a} \to \mathbb{C}^N$ defined by

$$(\boldsymbol{W_h^* c})(j) = (\boldsymbol{h} * \boldsymbol{c}_{\uparrow_a})(j) = \sum_{k=0}^{\frac{N}{a}-1} \boldsymbol{c}(k)\boldsymbol{h}[(j - ak) \bmod N].$$

The analysis operator $\mathcal{T}_X$ and the synthesis operator $\mathcal{T}_X^*$ of a Gabor system $X = (K, L)_{\boldsymbol{g}}$ given by (3.1) can be expressed in terms of the set of analysis operators $\{\boldsymbol{W}_{\boldsymbol{g}_\ell}\}_{\boldsymbol{g}_\ell \in G}$ and the set of synthesis operators $\{\boldsymbol{W}_{\boldsymbol{g}_\ell}^*\}_{\boldsymbol{g}_\ell \in G}$, where $G$ is a filter bank defined by

$$G = \{\boldsymbol{g}_\ell(m) = \boldsymbol{g}(m)e^{-2\pi imb\ell}\}_{0 \le \ell \le 1/b-1}.$$

More specifically, let $\boldsymbol{D} \in \mathbb{C}^{\frac{N}{ab}}$ denote the diagonal unitary matrix defined by

$$\boldsymbol{D} = \text{diag}(\boldsymbol{D}_0, \boldsymbol{D}_1, \dots, \boldsymbol{D}_{b^{-1}-1}), \tag{3.12}$$

where $\boldsymbol{D}_\ell = \text{diag}(1, e^{i\omega_0\ell}, \dots, e^{i\omega_0\ell(\frac{N}{a}-1)})$ with $\omega_0 = 2\pi ab$. Then a direct calculation shows that the analysis operator $\mathcal{T}_X^*$ and the synthesis operator $\mathcal{T}_X$ can be rewritten as

$$\mathcal{T}_X^* = \boldsymbol{D}\boldsymbol{W}_X; \quad \mathcal{T}_X = \boldsymbol{W}_X^*\boldsymbol{D}^*, \tag{3.13}$$

where $\boldsymbol{W}_X : \mathbb{C}^N \to \mathbb{C}^{\frac{N}{ab}}$ denotes the analysis operator defined by the filter bank $G$:

$$\boldsymbol{W}_X\boldsymbol{f} = \{\boldsymbol{c}_0 = \boldsymbol{W}_{\boldsymbol{g}_0}\boldsymbol{f}, \boldsymbol{c}_1 = \boldsymbol{W}_{\boldsymbol{g}_1}\boldsymbol{f}, \dots, \boldsymbol{c}_{\frac{1}{b}-1} = \boldsymbol{W}_{\boldsymbol{g}_{\frac{1}{b}-1}}\boldsymbol{f}\}, \quad \forall \boldsymbol{f} \in \mathbb{C}^N, \tag{3.14}$$

and $\boldsymbol{W}_X^* : \mathbb{C}^{\frac{N}{ab}} \to \mathbb{C}^N$ denotes the synthesis operator defined by $G$:

$$\boldsymbol{W}_X^*\boldsymbol{c} = \sum_{\ell=0}^{1/b-1} \boldsymbol{W}_{\boldsymbol{g}_\ell}^*\boldsymbol{c}_\ell, \quad \forall \boldsymbol{c} \in \mathbb{C}^{N/ab}. \tag{3.15}$$

It can be seen from (3.13) that the operator $\mathcal{T}_X$ ($\mathcal{T}_X^*$) defined by $X$ is the same as the operator $\boldsymbol{W}_X$ ($\boldsymbol{W}_X^*$) defined from the filter bank $G$, up to a diagonal matrix $\boldsymbol{D}$ with phase factors which does not have any impact in image recovery. Thus, in the remaining of this section, we focus on the analysis operator $\boldsymbol{W}_X$ and synthesis operator $\boldsymbol{W}_X^*$.

The analysis operator $\boldsymbol{W}$ decomposes a signal $\boldsymbol{f}$ into multiple frequency sub-band channels, where $\boldsymbol{W}_{\boldsymbol{g}_0}f$ represents the low-frequency sub-band component and all other components $\{\boldsymbol{W}_{\boldsymbol{g}_\ell}\boldsymbol{f}\}_{\ell=1}^{\frac{1}{b}-1}$ are high-frequency sub-band components. The filters $\{\boldsymbol{g}_\ell\}_{\ell\neq0}$ are windowed sinusoids that are only the approximation to high-pass filters, as none of their DC offsets (the mean value of filter) are zero. As a result,

the sub-band component decomposed by $\boldsymbol{g}_\ell$ ($\ell \neq 0$) contains a small percentage of low-frequency sub-band component, whose magnitude may be significant as image intensities are always non-negative. As images have sparse coefficients in high-frequency sub-bands but not in low-frequency sub-band, the effectiveness of sparse approximation under $X$ could be noticeably degraded owing to non-zero DC offsets of these high-pass filters $\{\boldsymbol{g}_\ell\}_{\ell \neq 0} \subset G$.

Take the tight Gabor frames constructed in Example 3.6 for instance. Consider the tight Gabor frames constructed from cubic B-spline with nodes $\{0, 1, 2, 3, 4\}$ and $a = 1, b = 1/3$. Then, we have three filters with support 3:

$$
\begin{aligned}
\boldsymbol{g}_0 &= \tfrac{\sqrt{2}}{6}(1, 2, 1); \\
\boldsymbol{g}_1 &= \tfrac{\sqrt{2}}{12}(2, -2, -1) + i\tfrac{\sqrt{6}}{12}(0, -2, 1); \\
\boldsymbol{g}_2 &= \tfrac{\sqrt{2}}{12}(2, -2, -1) + i\tfrac{\sqrt{6}}{12}(0, 2, -1).
\end{aligned}
\tag{3.16}
$$

It can be seen that the two high-pass filters $\boldsymbol{g}_1$ and $\boldsymbol{g}_2$ have non-zero DC offsets. The same holds true for other tight frames in Example 3.6 and Example 3.7. It is observed in the experiments that when using these high-pass filters with non-zero DC offset in sparsity-based image recovery, the results often show strong artifacts, especially in those smooth regions.

## 3.4.2 Gabor induced frames with filters of zero DC offsets

Motivated by the needs from sparsity-based image recovery, we proposed a modified version of tight Gabor frames to remove the DC offsets of the corresponding high-pass filters. Although the resulting frames are not tight anymore, there exist closed-form dual frames with simple structures. The modification is done by keeping the low-pass filter $\boldsymbol{g}_0$ and modifying high-pass filters $\{\boldsymbol{g}_\ell\}_{\ell \neq 0}$ as the following:

$$
\mathring{\boldsymbol{g}}_\ell = e^{i\theta_\ell}\boldsymbol{g}_\ell - \mu_\ell \boldsymbol{g}_0, \quad \text{for } \ell = 1, 2, \ldots, b^{-1} - 1,
$$

where $e^{i\theta_\ell}$ and $\mu_\ell$ are chosen such that $\sum_m \mathring{\boldsymbol{g}}_\ell(m) = 0$. Denote $\theta_0 = \mu_0 = 0$. In our implementation, $\{e^{i\theta_\ell}\}_{\ell \neq 0}$ and $\{\mu_\ell\}_{\ell \neq 0}$ are given by

$$e^{i\theta_\ell} = \overline{\sum_m \boldsymbol{g}_\ell(m)}/|\sum_m \boldsymbol{g}_\ell(m)|; \quad \text{and} \quad \mu_\ell = |\overline{\sum_m \boldsymbol{g}_\ell(m)}|/\sum_m \boldsymbol{g}_0(m). \tag{3.17}$$

(In the event that $\sum_m \boldsymbol{g}_\ell(m) = 0$, we adopt the convention that $\theta_\ell = 0$ and $\mu_\ell = 0$.) It can be seen that the system $Y$ corresponding to these modified high-pass filters are

$$Y = \{\mathring{\boldsymbol{g}}_{k,\ell}\}_{k \in K, \ell \in L} = \{e^{i\theta_\ell}\boldsymbol{g}_{k,\ell} - \mu_\ell e^{-2\pi i akb\ell}\boldsymbol{g}_{k,0}\}_{k \in K, \ell \in L}. \tag{3.18}$$

Strictly speaking, the new frame $Y$ is not a Gabor system. Therefore, we call it a *Gabor induced frame*. Although the system $Y$ derived from $X$ is no longer a tight frame, it has a closed-form dual frame with well-posed frame bounds. By the definition of $\{\mathring{\boldsymbol{g}}_\ell\}_{\ell \in L}$,

$$\boldsymbol{W}_Y = \boldsymbol{M}\boldsymbol{W}_X. \tag{3.19}$$

and the analysis operator $\mathcal{T}_Y^*$ of $Y$ is then

$$\mathcal{T}_Y^* = \boldsymbol{D}\boldsymbol{M}\boldsymbol{W}_X, \tag{3.20}$$

where $\boldsymbol{M} \in \mathbb{C}^{N \times \frac{N}{ab}}$ is given by

$$\boldsymbol{M} = \begin{pmatrix} \boldsymbol{I}_{\frac{N}{a}} & \boldsymbol{0} & \dots & \boldsymbol{0} \\ -\mu_1 \boldsymbol{I}_{\frac{N}{a}} & e^{-i\theta_1}\boldsymbol{I}_{\frac{N}{a}} & & \\ \vdots & & \ddots & \\ -\mu_{\frac{1}{b}-1}\boldsymbol{I}_{\frac{N}{a}} & & & e^{-i\theta_{\frac{1}{b}-1}}\boldsymbol{I}_{\frac{N}{a}} \end{pmatrix},$$

and here $\boldsymbol{I}_{\frac{N}{a}}$ denotes the $\frac{N}{a} \times \frac{N}{a}$ identity matrix. The matrix $\boldsymbol{M}$ is a sparse matrix with a sparse inverse:

$$\boldsymbol{M}^{-1} = \begin{pmatrix} \boldsymbol{I}_{\frac{N}{a}} & \boldsymbol{0} & \dots & \boldsymbol{0} \\ e^{i\theta_1}\mu_1 \boldsymbol{I}_{\frac{N}{a}} & e^{i\theta_1}\boldsymbol{I}_{\frac{N}{a}} & & \\ \vdots & & \ddots & \\ e^{i\theta_{\frac{1}{b}-1}}\mu_{\frac{1}{b}-1}\boldsymbol{I}_{\frac{N}{a}} & & & e^{i\theta_{\frac{1}{b}-1}}\boldsymbol{I}_{\frac{N}{a}} \end{pmatrix}$$

Define the system $\widetilde{Y} = \{\widetilde{\boldsymbol{g}}_{k,\ell}\}_{k\in K, \ell\in L}$ by

$$
\begin{aligned}
\widetilde{\boldsymbol{g}}_{k,0} &= \boldsymbol{g}_{k,0} + \sum_{\ell\neq 0, \ell\in L} \mu_l e^{2\pi i a k b\ell + i\theta_\ell} \boldsymbol{g}_{k,\ell}, \quad k \in K; \\
\widetilde{\boldsymbol{g}}_{k,\ell} &= e^{i\theta_\ell} \boldsymbol{g}_{k,\ell}, \quad k \in K, \ell \in L\backslash\{0\}.
\end{aligned}
\tag{3.21}
$$

Then, the systhesis operator defined by $\widetilde{Y}$ which leads to $\mathcal{T}_{\widetilde{Y}} = \boldsymbol{W}_X^* \boldsymbol{M}^{-1} \boldsymbol{D}^*$ and gives

$$
\mathcal{T}_{\widetilde{Y}} \mathcal{T}_Y^* = \boldsymbol{W}_X^* \boldsymbol{M}^{-1} \boldsymbol{D}^* \boldsymbol{D} \boldsymbol{M} \boldsymbol{W}_X = \boldsymbol{I}.
$$

Thus, $Y$ and $\widetilde{Y}$ form dual frames for $\mathbb{C}^N$. It can be seen that the computational cost of the analysis operator $\mathcal{T}_Y^*$ and the synthesis operator $\mathcal{T}_{\widetilde{Y}}$ is nearly the same as $\mathcal{T}_X^*$ and $\mathcal{T}_X$.

**Proposition 3.8.** *Suppose that $X$ is a discrete Gabor tight frame for $\mathbb{C}^N$ defined as (3.1). Then, $Y$ and $\widetilde{Y}$ derived from $X$ by (3.18) and (3.21) are dual frames for $\mathbb{C}^N$.*

Note that the approach provided by Proposition 3.8 can also be applied to a pair of non-tight Gabor dual frames to remove the DC offsets of high-pass filters.

**Example 3.9.** *Consider the tight Gabor frame constructed from B-spline of order $3$ whose three filters are listed in (3.16). The corresponding filters of the Gabor induced frame $Y$ and its dual $\widetilde{Y}$ are now*

$$
\begin{cases}
\boldsymbol{g}_0 = \frac{\sqrt{2}}{6}(1, 2, 1); \\
\boldsymbol{g}_1 = \frac{\sqrt{2}}{8}(-1, 2, -1) + i\frac{\sqrt{6}}{12}(1, 0, -1); \\
\boldsymbol{g}_2 = \frac{\sqrt{2}}{8}(-1, 2, -1) + i\frac{\sqrt{6}}{12}(-1, 0, 1),
\end{cases}
\tag{3.22}
$$

*and*

$$
\begin{cases}
\widetilde{\boldsymbol{g}}_0 = \frac{\sqrt{2}}{8}(1, 4, 1); \\
\widetilde{\boldsymbol{g}}_1 = \frac{\sqrt{2}}{12}(-1, 4, -1) + i\frac{\sqrt{6}}{12}(1, 0, -1); \\
\widetilde{\boldsymbol{g}}_2 = \frac{\sqrt{2}}{8}(-1, 4, -1) + i\frac{\sqrt{6}}{12}(-1, 0, 1).
\end{cases}
\tag{3.23}
$$

*It can be seen that the filters $\boldsymbol{g}_1$ and $\boldsymbol{g}_2$ are both high-pass filters with zero DC offset. The frame bounds are $A = 0.8000$ and $B = 1.0000$. And the redundancy is $3N/N = 3$.*
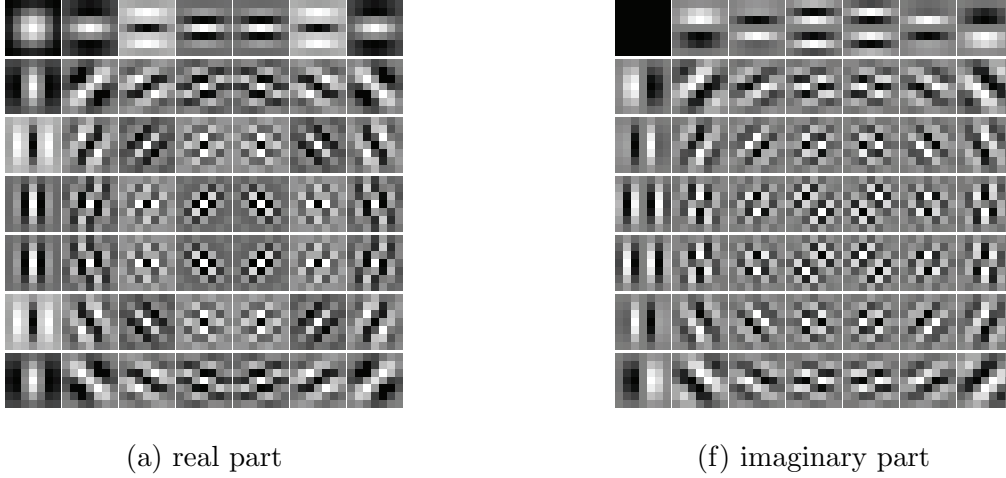
<div align="center">

(a) real part                                      (f) imaginary part

</div>

Figure 3.1: Complex-valued filter bank with support $7 \times 7$ of a 2D tensor product Gabor induced frame constructed in Example 3.6.

**Example 3.10.** *2D discrete Gabor induced frames can be generated by the tensor product of two 1D discrete Gabor induced frames along two axes. Consider the 1D tight Gabor frame constructed in Example 3.6 by using the B-spline of order 4 and setting $a = 2, b = 1/7$. Let $Y$ denote the corresponding 1D Gabor induced frame after removing non-zero DC offsets in all high-pass filters. Then, the frame bounds of the resulting 2D discrete Gabor induced frames $Y \otimes Y$ are $A = 0.5443$ and $B = 1.0069$. The redundancy is $(\frac{7N}{2})^2/N^2 = 12.25$. The support of all associated filters is $7 \times 7$. The concentrations of the atoms associated with low-pass filters are illustrated in Fig. 3.2 for both frame and dual frame. The associated high-pass filters have good orientation selectivity as shown in Fig. 3.1.*

### 3.4.3   Orientation selectivity

Next we will discuss the orientation selectivity of the constructed frames. And we start with functions defined on $\mathbb{R}^2$. Consider a continuous function $f(x, y) \in L^2(\mathbb{R}^2)$ of particular orientation $\theta$ that is expressed as

$$f(x, y) = h(x \cos \theta - y \sin \theta)\kappa(x, y),$$

(a) Gabor atom of frame
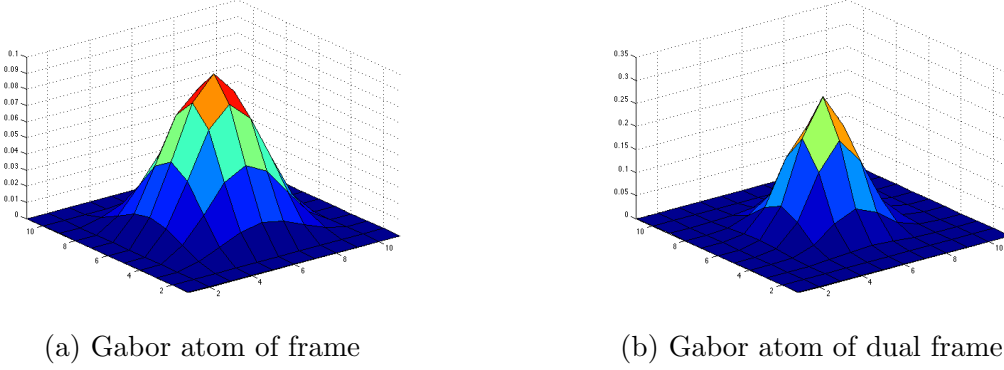


(b) Gabor atom of dual frame

Figure 3.2: Gabor atoms of discrete Gabor induced frame constructed in Example 3.10 with respect to low-pass filters

where $h \in L^2(\mathbb{R})$ and $\kappa \in L^2(\mathbb{R}^2)$ is the isotrophic separable regularizer for $f \in L^2(\mathbb{R}^2)$ satisfying $\kappa(x, y) = g(x)g(y)$, e.g. Gaussian function $g(t) = \sqrt{2\pi\sigma} e^{-\frac{t^2}{2\sigma^2}}$. Then, we have

$$
\begin{aligned}
& \widehat{f}(\omega_x, \omega_y) \\
&= \int_{\mathbb{R}} \int_{\mathbb{R}} h(x \cos\theta - y \sin\theta)\kappa(x, y) e^{-i(\omega_x x + \omega_y y)} dx dy \\
&= \int_{\mathbb{R}} \int_{\mathbb{R}} h(x)\kappa(x, y) e^{-i(\omega_x(x\cos\theta + y\sin\theta) + \omega_y(-x\sin\theta + y\cos\theta))} dx dy \quad \text{(isotrophy)} \\
&= \int_{\mathbb{R}} \int_{\mathbb{R}} h(x)\kappa(x)\kappa(y) e^{-i(\omega_x(x\cos\theta + y\sin\theta) + \omega_y(-x\sin\theta + y\cos\theta))} dx dy \quad \text{(separability)} \\
&= (\widehat{h} * \widehat{\kappa})(\omega_x \cos\theta - \omega_y \sin\theta)\widehat{\kappa}(\omega_x \sin\theta + \omega_y \cos\theta).
\end{aligned}
$$

Suppose that $\widehat{g}$ decays fast when going away from origin, e.g. $\sigma \to \infty$ for Gaussian function. It can be seen that magnitude of $\widehat{f}(\omega_x, \omega_y)$ also decays fast when $(\omega_x, \omega_y)$ is away from the line $\omega_x \sin\theta + \omega_y \cos\theta = 0$. Thus, the orientation of a function $f$ is closely related to the peaks of its Fourier transform. To be specific, the peaks of the Fourier transform of an oriented function forms a line in frequency domain and its orientation is complementary to that of the function.

Discrete filters can be regarded as samplings of continuous functions. Therefore by the intuition from continuous case, we consider to define the orientation of discrete 2D filters from the support of their Fourier spectrum. Suppose $\boldsymbol{h} \in \mathbb{C}^{p \times p}$ is a discrete 2D filter of size $p \times p$. Let $p$ be an odd positive integer and $\mathbb{Z}_p \times \mathbb{Z}_p =$

$\{-\frac{p-1}{2}, -\frac{p-1}{2}+1, ..., 0, ..., \frac{p-1}{2}\} \times \{-\frac{p-1}{2}, -\frac{p-1}{2}+1, ..., 0, ..., \frac{p-1}{2}\}$ denote the discrete 2D uniform grid. Let $\widehat{\boldsymbol{h}} \in \mathbb{C}^{p \times p}$ denote the 2D discrete Fourier transform of $\boldsymbol{h}$. Then filter $\boldsymbol{h}$ is defined to have orientation $\theta$ if both the following conditions hold:

(1) all maximum points of $|\widehat{\boldsymbol{h}}|$ are on the line $\omega_x \cos\theta + \omega_y \sin\theta = 0$ in frequency domain;

(2) the values of the points away from the line $\omega_x \cos\theta + \omega_y \sin\theta = 0$ are zero (perfect) or negligible (strong).

Clearly, the high-pass filters derived from both real part and imaginary part of 2D DFT have perfect orientation selectivity as the non-maximum points of their DFTs vanish outside the line. See Fig. 3.3 for an illustration. Similar to that from DFT, the high-pass filters derived from the proposed Gabor induced frames also have very strong orientation selectivity as the values of non-maximum points of their DFTs are much smaller than the maximum; see Fig. 3.4 for a comparison.



(a) $\mathrm{Real}(\boldsymbol{f}_{j_1,j_2})$  (b) $|\widehat{\mathrm{Real}(\boldsymbol{f}_{j_1,j_2})}|$
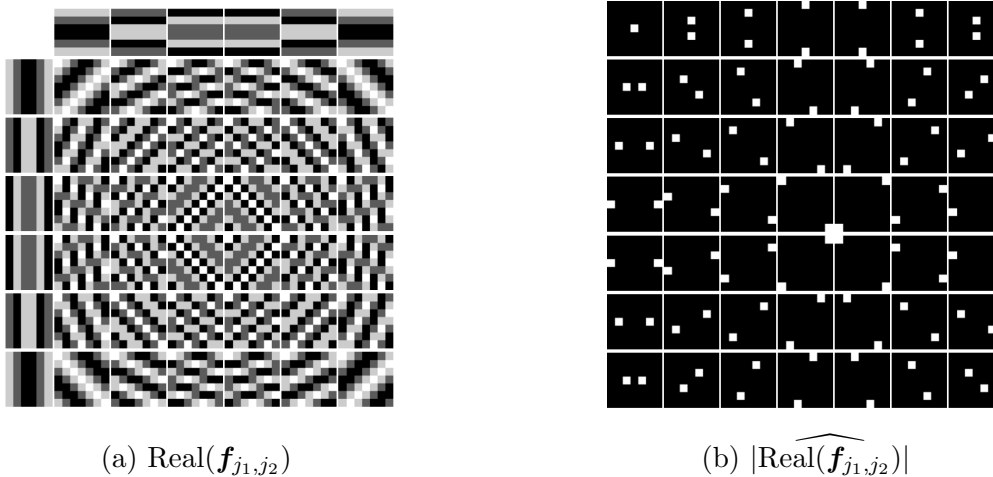
Figure 3.3: Real part of 2D discrete Fourier basis $\{\boldsymbol{f}_{j_1,j_2}\}_{0 \le j_1, j_2 \le 6}$ of size $7 \times 7$ and their Fourier spectrum (zero frequency is moved to the center of the image).

In addition, the orientation selectivity of the high-pass filters from 2D DFT or from the proposed Gabor induced frames is optimal in the sense that they cover all possible orientations in finite discrete grid. One orientation is feasible for a finite discrete grid only if the line with such orientation can intersect the grid $\mathbb{Z}_p \times \mathbb{Z}_p$,

(a) $\mathrm{Real}(\boldsymbol{g}_{\ell_1,\ell_2})$

(b) $|\widehat{\mathrm{Real}(\boldsymbol{g}_{\ell_1,\ell_2})}|$
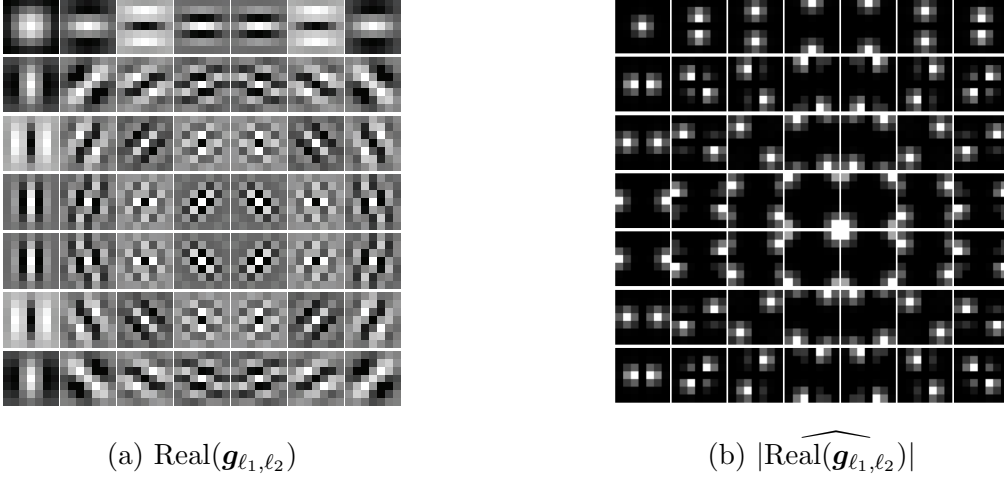
Figure 3.4: Real part of filters $\{\boldsymbol{g}_{\ell_1,\ell_2}\}_{0\leq\ell_1,\ell_2\leq 6}$ for 2D discrete revised Gabor frame with $p = 7$ and their Fourier spectrum (zero frequency is moved to the center of the image).

which makes the number of all feasible orientations limited. It can be seen that for 2D filters of size $5 \times 5$, the total number of possible orientations is 8, and for 2D filters of size $7 \times 7$, the total number is 16; see Fig. 3.5 for an illustration. Indeed, by induction, the total number of feasible orientations for 2D filters of odd size $p \times p$ is $4\Phi(\frac{p-1}{2})$, where the function $\Phi(\cdot)$ is the summation function of the Euler's totient function $\varphi(\cdot)$ which counts the positive integer up to $k$ that are relatively prime to $k$, i.e. $\Phi(n) = \sum_{k=1}^{n} \varphi(k)$. The derivation is quite straightforward. It can be seen that the number of all feasible orientations doubles that of the first quadrant of the grid with length $\frac{p-1}{2}$. The possible candidates of additional feasible orientations in the first quadrant from $k = p-1$ to $k = p$ are those come from the boundary points the grid. For such a point, if its x-coordinate or $y$-coordinate is relatively prime to $\frac{p-1}{2}$, then it induces a new orientation. Thus, the number of new feasible orientations induced from $k = p - 1$ to $k = p$ in the first quadrant is $2\phi(\frac{p-1}{2}))$, and the total number is then $4\phi(\frac{p-1}{2})$. By induction, the proof is done.

(a) Filter size is 5                        (b) Filter size is 7
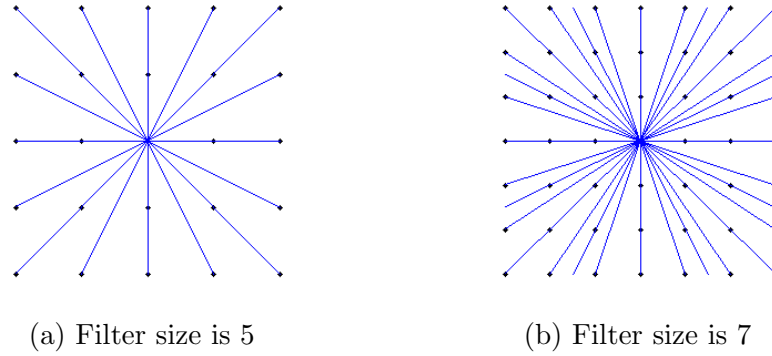
Figure 3.5: All the possible directions of 2D filters of size $5 \times 5$ or $7 \times 7$.

## 3.5   Conclusion

In this chapter, we have studied the theory of discrete Gabor systems in $\mathbb{C}^N$. We have developed the Gramian and dual Gramian analysis for $\mathbb{C}^N$, which relates the frame properties of a discrete Gabor system to the eigenvalues of their Gramian and dual Gramian matrices. One important corollary of these conclusions is the duality principle, based on which a necessary and sufficient condition for the construction of discrete tight Gabor frames has been derived. To sum up, the resulted tight Gabor frame has the following advantages. Firstly, it possesses accurate local time-frequency analysis. Secondly, it can be implemented by a fast filter bank algorithm of both decomposition and reconstruction processes. Thirdly, 2D tight Gabor frames generated from tensor product of 1D ones have the optimal orientation selectivity. Fourthly, the Gabor frames of different sizes have the flexibilities of modelling both image edges and local textures. Further, we revise the constructed tight Gabor frames to discrete Gabor induced frames whose high-pass filters have zero DC offsets in the 1D filter bank. Meanwhile, the dual frames of these systems have a closed-form. Therefore, the newly derived frames also possess the above advantages as tight Gabor frames and they are more suitable for sparsity-based image recovery. And note that the orientation selectivity of such discrete Gabor induced frames is also optimal.

One example of Gabor induced frames we illustrated is generated from the square

root of B-spline sequences. By changing the order of B-spline, one may obtain a series of Gabor systems in unified form but with different levels of scale. This inspires us to utilize multi-scale Gabor induced frames in application to overcome the weakness of a Gabor system that it lacks multi-scale structure. We will discuss more about this in Chapter 5.

In the next chapter, we will solve the scaling challenge of Gabor systems from the viewpoint of MRA-based wavelet system.

# Chapter 4

# Discrete tight frames with Gabor and MRA structures

## 4.1  Introduction

For years, orthonormal wavelet bases [39] has been an indispensable tool in signal processing. Its wide usages in signal processing are mainly motivated by two advantages: effective multi-scale representation of point-wise discontinuities, and efficient numerical implementations of signal decomposition and reconstruction. In recent years, tight wavelet frames are more often seen in many applications, as the redundancy of tight frames gives more flexibilities on filter design and better sparse approximation of signals while having the same numerical implementation as orthogonal wavelet bases. Such tight wavelet frames include undecimated Daubechies' wavelet systems [35], spline framelets [97, 42] and many others. For processing 2D signals like images, the most popular tight wavelet frames are tensor product wavelet systems. As most natural images exhibit line-like edges, i.e. discontinuities across local edges, with different orientations, one main disadvantage of tensor real-valued wavelet systems is the lack of orientation selectivity. As we have introduced in

Chapter 1, one approach to gain orientation selectivity is considering tensor product of complex-valued wavelet systems. For example, the dual-tree complex wavelet transform [101] uses two different discrete orthogonal wavelet bases to produce a 2D tensor complex-valued tight wavelet frame whose real part and imaginary part each have up to six orientations.

Motivated by the strong orientation selectivity of tensor product of Gabor functions, a class of discrete tight Gabor frames and Gabor induced frames is constructed in Chapter 3. With the same efficient numerical implementation of signal decompositon/reconstruction, they have better orientation selectivity than tensor tight wavelet frames (including complex-valued ones) and have better performance on local time-frequency analysis. The performance gain of such discrete Gabor induced frames is illustrated in various image recovery applications; more details will be given in Chapter 5. However, the discrete Gabor induced frames constructed in Chapter 3 lack the multi-scale structure of MRA-based tight wavelet frames. As a result, it cannot be used for modeling local signal structures with different sizes. An ad-hoc approach is used in Chapter 5 to gain multi-scale structures by combining (tight) Gabor frames generated by the window functions with different sizes. Nevertheless, such discrete Gabor frames still do not have the multi-resolution analysis (MRA) structure that many existing MRA-based tight wavelet frames have.

In this chapter, we are interested in studying discrete tight frames for $\ell_2(\mathbb{Z})$ combining both Gabor and MRA structures. Such discrete tight frames will have the same multi-scale structures as discrete MRA-based tight wavelet frames for $\ell_2(\mathbb{Z})$, and their 2D tensor products have strong orientation selectivity and good performance on local time-frequency analysis.

### 4.1.1   Literature review

Given a fixed window function $g \in L_2(\mathbb{R})$ and a uniform time-frequency lattice set $K \times L = a\mathbb{Z} \times b\mathbb{Z}$ $(a, b \in \mathbb{R}^+)$, the Gabor system is defined as (1.5) in Chapter 1,

i.e.

$$(K, L)_g = \{g(x - ak)e^{-2\pi i b\ell x}, x \in \mathbb{R}\}_{k,\ell \in \mathbb{Z}}. \tag{4.1}$$

Interested readers are referred to [39, 99, 76, 29, 31] for more details on the characterizations of frame and tight frame properties of the system (4.1).

Discrete Gabor frames for $\ell_2(\mathbb{Z})$ are usually obtained by directly sampling continuous Gabor frames for $L_2(\mathbb{R})$ using shift parameters $a, b$ with $a, \frac{1}{b} \in \mathbb{N}^+$:

$$\{\boldsymbol{g}(m - ak)e^{-2\pi i b\ell m}, m \in \mathbb{Z}\}_{k \in \mathbb{Z}, \ell \in \{0,\dots,\frac{1}{b}-1\}}. \tag{4.2}$$

Many different conditions have been proposed for guaranteeing the (tight) frame properties of discrete Gabor systems of the form (4.2). In [113, 92], the Wexler-Raz biorthogonal condition is applied for the construction of dual discrete Gabor frames. It is shown in [36] that discrete tight Gabor frames for $\ell_2(\mathbb{Z})$ can be obtained once the polyphase matrix of the filters bank associated with Gabor system is para-unitary. In Chapter 3, based on duality principle for discrete Gabor systems, a necessary and sufficient condition for a system (4.2) to form a discrete tight Gabor frame is presented, under the assumption that $g$ is a sequence with non-negative entries. All these discrete Gabor frames have no so-called MRA structure, which is closely related to tight wavelet frames.

For a given set of wavelet functions $\Psi = \{\psi_1, ..., \psi_r\} \subset L_2(\mathbb{R})$, the wavelet system $X(\Psi)$ is composed of dilations and translations of these wavelet functions:

$$X(\Psi) = \{\psi_{\ell,n,k}\}_{\substack{1 \le \ell \le r \\ n,k \in \mathbb{Z}}} = \{2^{n/2}\psi_\ell(2^n \cdot -k)\}_{\substack{1 \le \ell \le r \\ n,k \in \mathbb{Z}}}. \tag{4.3}$$

The key framework for constructing wavelet (bi)-orthonormal bases ([40, 34]) and tight frames ([97, 42]) is the multiresolution analysis (MRA) introduced by Mallat and Meyer ([83, 87]). The construction of MRA-based tight wavelet frame for $L_2(\mathbb{R})$ is presented in [97, 42]. The key ingredient in their construction is the so-called unitary extension principle (UEP) [42], which simplified the construction of MRA-based tight wavelet frames to the construction of a set of filters with certain properties. Different from the discretization of Gabor systems, discrete tight wavelet

frames for $\ell_2(\mathbb{Z})$ can be directly derived from a set of filters (i.e., refinement mask and wavelet masks) associated with tight wavelet frames in the continuum domain constructed via UEP. As a result, a fast filter bank based algorithm is available for efficient signal decomposition and reconstruction.

The studies on the systems with both wavelet and Gabor structures have been scant in the literature. A continuous Gabor wavelet transform for $L_2(\mathbb{R}^2)$ is introduced in [74], which extends continuous wavelet transform by using the set of Gabor functions as mother wavelets. The system for $L_2(\mathbb{R}^2)$ is defined by the discretization of the transform in the phase space. Numerical simulation done in [74] indicates that the systems obtained via such a discretization form frames for $L_2(\mathbb{R}^2)$, provided that the sampling in phase space is sufficiently dense. In the context of image in-painting, a class of MRA-based discrete tight frames is developed in [78] for vector space $\mathbb{R}^N$. In [78], the first column of a local discrete cosine transform in $\mathbb{R}^{d \times d}$ is viewed as the refinement mask of the MRA for Haar wavelets with respect to dilation factor $d$ and the other columns are viewed as wavelet masks. Then, by the orthogonality of local discrete cosine transform, an MRA-based tight wavelet frames can be obtained for $\mathbb{R}^N$ via the standard discretization of the undecimated Haar wavelet frames with dilation factor $d$.

### 4.1.2   Our works

This chapter aims at studying discrete tight frames for $\ell_2(\mathbb{Z})$ with both Gabor and MRA structures. In other words, we are interested in tight frames for $\ell_2(\mathbb{Z})$ that have the following properties: (1) local time-frequency analysis of discrete Gabor frames, (2) multi-scale structures induced by the MRA, and (3) fast numerical implementation of signal decomposition/reconstruction.

The basic idea is to connect the discrete Gabor frames of the form (4.2) to the UEP. Consider a discrete Gabor system with $a = 2$ and $\frac{1}{b} > 1$:

$$\{\boldsymbol{g}(m - 2k)e^{-2\pi i b \ell m}\}_{k \in \mathbb{Z}, 0 \leq \ell \leq \frac{1}{b} - 1}. \tag{4.4}$$

Clearly, such a system is generated by the even translations of the following $\frac{1}{b} - 1$ sequences

$$\{\boldsymbol{g}_\ell(m) = \boldsymbol{g}(m)e^{-2\pi ib\ell m}\}_{0 \le \ell \le \frac{1}{b}-1}. \tag{4.5}$$

We use the sequences above to define a wavelet system $X(\Psi)$ with MRA structure:

$$\phi(t) = 2\sum_{m \in \mathbb{Z}} \boldsymbol{g}_0(m)\phi(2t - m), \quad t \in \mathbb{R}, \tag{4.6}$$

$$\psi_\ell(t) = 2\sum_{m \in \mathbb{Z}} \boldsymbol{g}_\ell(m)\phi(2t - m), \quad t \in \mathbb{R}, \tag{4.7}$$

for $\ell = 1, \ldots, \frac{1}{b} - 1$. Suppose that these masks satisfy the UEP so that the system $X(\Psi)$ forms an MRA-based tight wavelet frame for $L_2(\mathbb{R})$. Then, a discrete wavelet tight frames for $\ell_2(\mathbb{Z})$ can be constructed using these masks, and the Gabor system (4.4) is exactly the part of tight frames that corresponds to the sub-space $V_0$ of the MRA. Thus, such a tight frame system can be viewed as a discrete tight frame for $\ell_2(\mathbb{Z})$ with Gabor and MRA structures.

In this chapter, we first present a UEP-based sufficient condition for the wavelet system generated by compactly supported functions $\{\psi_1, \ldots, \psi_{\frac{1}{b}-1}\}$ defined by (4.7) to form an MRA-based tight wavelet frame for $L_2(\mathbb{R})$. Then, by further examining the conditions imposed on the masks $\{\boldsymbol{g}_\ell\}_{\ell=0}^{\frac{1}{b}-1}$ of the form (4.5), we present a sufficient and necessary condition for the finitely supported masks $\{\boldsymbol{g}_\ell\}_{\ell=0}^{\frac{1}{b}-1}$ to satisfy the UEP. Such a sufficient and necessary condition implies that any set of compactly supported masks $\{\boldsymbol{g}_\ell\}_{\ell=0}^{\frac{1}{b}-1}$ satisfying UEP is of the following form (up to a translation): for $\ell = 0, \ldots, p - 1$,

$$\boldsymbol{g}_\ell(m) = \begin{cases} p^{-1}e^{-\frac{2\pi}{p}i\ell m}, & 0 \le m \le p - 1 \\ 0, & \text{otherwise}, \end{cases}$$

where $p$ is an even positive integer. Clearly, when $p = 2$, it corresponds to Haar orthonormal wavelet basis. It is noted that when $p > 2$, it is not necessarily corresponding to Haar basis. Instead, the refinable functions $\phi$ is a continuous piecewise spline function when $p = 2^m, m > 1$.

In addition, we also investigate the (tight) Gabor frames for $L_2(\mathbb{R})$ when relating window function to the refinable function of an MRA. We present a sufficient condition for guaranteeing frame property of Gabor systems when using the refinable function of an MRA as the window function, and give a construction of tight Gabor frames for $\ell_2(\mathbb{Z})$ using the square root of the refinable function of an MRA.

## 4.2 Discrete tight frame with Gabor and MRA structures

The discrete Gabor system we consider is generated by a finitely supported window sequence $\boldsymbol{g} \in \ell_2(\mathbb{Z})$, and it is composed by the translations of $\frac{1}{b} - 1$ atoms $\{\boldsymbol{g}_\ell\}_{\ell=0}^{\frac{1}{b}-1} \subset \ell_2(\mathbb{Z})$ defined by

$$\boldsymbol{g}_\ell(m) = \boldsymbol{g}(m)e^{-2\pi i b \ell m}, \quad m \in \mathbb{Z}. \tag{4.8}$$

Without loss of generality, we assume that $\boldsymbol{g}(m) = 0$, for all $m \notin [0, p-1] \cap \mathbb{Z}$. For such a finitely supported sequence $\boldsymbol{g}$, we define a refinable function (or distribution) $\phi$ by

$$\phi(t) = 2\sum_{m \in \mathbb{Z}} \boldsymbol{g}(m)\phi(2t - m), \quad t \in \mathbb{R}, \tag{4.9}$$

and a set of framelets $\Psi = \{\psi_\ell\}_{\ell=1}^{\frac{1}{b}-1}$ by

$$\psi_\ell(t) = 2\sum_{m \in \mathbb{Z}} \boldsymbol{g}_\ell(m)\phi(2t - m), \quad t \in \mathbb{R}. \tag{4.10}$$

Define an affine system $X(\Psi)$ by

$$X(\Psi) = \{\psi_{\ell,n,k}\}_{\substack{1 \le \ell \le 1/b \\ n,k \in \mathbb{Z}}} = \{2^{n/2}\psi_\ell(2^n \cdot -k)\}_{\substack{1 \le \ell \le 1/b \\ n,k \in \mathbb{Z}}}. \tag{4.11}$$

In the next result, we give a UEP-based sufficient condition on the window sequence $\boldsymbol{g}$ such that the affine system $X(\Psi)$ defined above forms an MRA-based tight wavelet frame for $L_2(\mathbb{R})$.

**Theorem 4.1.** *Consider a finitely supported sequence $\boldsymbol{g} \in \ell_2(\mathbb{Z})$. The function $\phi$ defined by (4.9) generates an MRA for $L_2(\mathbb{R})$ and the system $X(\Psi)$ defined by (4.10) and (4.11) forms a tight frame for $L_2(\mathbb{R})$, if the following conditions hold true:*

*(i) $\frac{1}{b} \geq p$;*

*(ii) $\sum_{n \in \mathbb{Z}} \boldsymbol{g}(n) = 1$;*

*(iii) $\sum_{n \in \Omega_j} |\boldsymbol{g}(n)|^2 = \frac{b}{2}$, where $j \in \mathbb{Z}/2\mathbb{Z}$ and $\Omega_j = (2\mathbb{Z} + j) \cap [0, p-1]$.*

*Proof.* For any $0 < m < 1 - p$, $\boldsymbol{g}(m) = 0$, and thus $\boldsymbol{g}_\ell(m) = 0$ for $\ell = 0, \ldots, \frac{1}{b} - 1$. Then, we have

$$\sum_{\ell=0}^{\frac{1}{b}-1} \sum_{n \in \Omega_j} \overline{\boldsymbol{g}_\ell(n)} \boldsymbol{g}_\ell(n+m) = 0,$$

for any $m \notin [-p+1, p-1]$. Thus, the UEP condition (2.9) holds true for any $m \notin [-p+1, p-1]$. Notice that

$$\sum_{\ell=0}^{\frac{1}{b}-1} \sum_{n \in \Omega_j} \overline{\boldsymbol{g}_\ell(n)} \boldsymbol{g}_\ell(n+m) = \sum_{n \in \Omega_j} \sum_{\ell=0}^{\frac{1}{b}-1} \overline{\boldsymbol{g}_\ell(n)} \boldsymbol{g}_\ell(n+m)$$

$$= \sum_{n \in \Omega_j} \overline{\boldsymbol{g}(n)} \boldsymbol{g}(n+m) \sum_{\ell=0}^{\frac{1}{b}-1} e^{-2\pi imb\ell}.$$

Then, for $1 \leq m \leq p-1$ or $-p+1 \leq m \leq -1$, we have

$$\sum_{\ell=0}^{\frac{1}{b}-1} \sum_{n \in \Omega_j} \overline{\boldsymbol{g}_\ell(n)} \boldsymbol{g}_\ell(n+m) = \sum_{n \in \Omega_j} \overline{\boldsymbol{g}(n)} \boldsymbol{g}(n+m) \sum_{\ell=0}^{\frac{1}{b}-1} e^{-2\pi imb\ell} = 0,$$

as $b \leq \frac{1}{p}$ stated in Condition (i). For $m = 0$, by Condition (iii), we have

$$\sum_{\ell=0}^{\frac{1}{b}-1} \sum_{n \in \Omega_j} \overline{\boldsymbol{g}_\ell(n)} \boldsymbol{g}_\ell(n+m) = \sum_{n \in \Omega_j} \overline{\boldsymbol{g}(n)} \boldsymbol{g}(n+m) \sum_{\ell=0}^{\frac{1}{b}-1} e^{-2\pi imb\ell} = \frac{1}{b} \sum_{n \in \Omega_j} |\boldsymbol{g}(n)|^2 = \frac{1}{2}.$$

Therefore, the UEP condition (2.9) holds for any integer $m$.

As shown in [52, Section 5.4], the finitely supported mask $\boldsymbol{g}$ will admit a refinable function in $L_2(\mathbb{R})$ with $\widehat{\phi}(0) = 1$ using (4.9), if it satisfies Condition (ii) and the

UEP condition (2.9). Furthermore, such a refinable function $\phi$ generates an MRA for $L_2(\mathbb{R})$ as well. Then, by Theorem 2.1, we have that the system $X(\Psi)$ defined by (4.10) and (4.11) forms a tight frame for $L_2(\mathbb{R})$. $\qquad\square$

It can be seen from Theorem 4.1 that the construction of MRA-based tight wavelet frame $X(\Psi)$ generated by $\Psi$ of the form (4.10) is done once we can construct the finitely supported window sequence $\boldsymbol{g} \in \ell_2(\mathbb{Z})$ satisfying Condition (i) Condition (ii) and Condition (iii). In the next result, we give closed-form solutions that satisfy these conditions.

**Proposition 4.2.** *A finitely supported sequence $\boldsymbol{g} \in \ell_2(\mathbb{Z})$ satisfies Conditions (i), (ii) and (iii) in Theorem 4.1 for some b, if and only if $\boldsymbol{g} = p^{-1}(\ldots, 0, 0, \underbrace{1, \ldots, 1}_{p}, 0, 0, \ldots)$ with some even positive integer p.*

*Proof.* If $\boldsymbol{g} = p^{-1}(\ldots, 0, 0, \underbrace{1, \ldots, 1}_{p}, 0, 0, \ldots)$ for some even positive integer $p$, it can be seen that Conditions (ii) and (iii) hold true when setting $\frac{1}{b} = p$.

Conversely, if Conditions (i), (ii) and (iii) in Theorem 4.1 hold true, we have

$$\sum_{m=0}^{p-1} |\boldsymbol{g}(m)|^2 = \sum_{j=0,1} \sum_{m \in \Omega_j} |\boldsymbol{g}(m)|^2 = b.$$

and

$$\sum_{m=0}^{p-1} |\boldsymbol{g}(m) - \frac{1}{p}|^2 = \sum_{m=0}^{p-1} \left( |\boldsymbol{g}(m)|^2 - \frac{1}{p}(\boldsymbol{g}(m) + \boldsymbol{g}^*(m)) \right) + \frac{1}{p^2} \cdot p = b - \frac{1}{p},$$

Then by Condition (i),

$$\sum_{m=0}^{p-1} |\boldsymbol{g}(m) - \frac{1}{p}|^2 = b - \frac{1}{p} \le 0,$$

Thus, we must have $b = \frac{1}{p}$, and $g(m) = \frac{1}{p}$ for any $m \in [0, p-1] \cap \mathbb{Z}$. Moreover, when $p$ is an odd number, the sequences $\boldsymbol{g}$ with the form above cannot satisfy Condition (iii). Therefore, $p$ can only be an even integer.

$\qquad\square$

Different with the tight Gabor frame constructed in Chapter 3, the discrete tight frame in this theorem has high-pass filters of zero DC offset. In fact, based on the first equality in the UEP condition (2.8) and the assumption that $\sum_n \boldsymbol{g}(n) = 1$, one can conclude $\sum_n \boldsymbol{g}_\ell(n) = 0$ for any $1 \leq \ell \leq \frac{1}{b} - 1$.

When the support of the mask $\boldsymbol{g}$ given in Proposition 4.2 is 2, the refinable function admitted by such a mask is the indicator function of the MRA associated with Haar wavelet basis. When the support of $\boldsymbol{g}$ is larger than 2, the associated refinable function is not the indicator function any more. The next proposition shows the smoothness of such refinable functions.

**Proposition 4.3.** *Consider a refinable function $\phi$ with $\widehat{\phi}(0) = 1$, defined by (4.9) using the mask $\boldsymbol{g} = 2^{-n}(1, 1, \ldots, 1, 1) \in \mathbb{R}^{2^n}$ for some integer $n \geq 2$. Then, $\phi \in C^{n-2}(\mathbb{R})$.*

*Proof.* The smoothness of $\phi$ is checked via checking the decay of $\widehat{\phi}$. As shown in [42], if $|\widehat{\phi}(\omega)| \leq c(1 + |\omega|)^{-1-\alpha-\epsilon}$ for some positive constant $c$ and $\epsilon$, then $\phi \in C^\alpha$. Since $\boldsymbol{g} = 2^{-n}(1, 1, \ldots, 1, 1)$, the Fourier series of $\boldsymbol{g}$ can be factorized as

$$\widehat{\boldsymbol{g}}_0(\omega) = \frac{1}{2^n} \prod_{k=0}^{n-1} (1 + e^{-i2^k \omega}).$$

By the definition of $\phi$ and $\widehat{\phi}(0) = 1$, we have

$$|\widehat{\phi}(\omega)| = |\prod_{j=1}^{+\infty} \widehat{\boldsymbol{g}}_0(2^{-j}\omega)| = \prod_{j=1}^{+\infty} \prod_{k=0}^{n-1} |\frac{1 + e^{-i2^{k-j}\omega}}{2}|.$$

Next, we show that the product $\prod_{j=1}^{+\infty} \prod_{k=0}^{n-1} |1 + \frac{e^{-i2^{k-j}\omega}-1}{2}|$ is absolutely convergent. Notice that $e^{-i\omega} - 1 = -2i \sin(\frac{\omega}{2}) e^{-i\frac{\omega}{2}}$ for any $\omega$. Then, we have

$$1 + |\frac{e^{-i2^{k-j}\omega} - 1}{2}| = 1 + |\sin(2^{k-j-1}\omega)| \leq 1 + |2^{k-j-1}\omega| \leq e^{|2^{k-j-1}\omega|},$$

and

$$\prod_{j=1}^{+\infty} \prod_{k=0}^{n-1} \left(1 + |\frac{e^{-i2^{k-j}\omega} - 1}{2}|\right) \leq \prod_{j=1}^{+\infty} \prod_{k=0}^{n-1} e^{|2^{k-j-1}\omega|} = \prod_{j=1}^{+\infty} e^{2^{n-1-j}|\omega|} = e^{2^{n-1}|\omega|},$$

Thus, $\prod_{j=1}^{+\infty} \prod_{k=0}^{n-1} |1 + \frac{e^{-i2^{k-j}\omega}-1}{2}|$ is absolutely convergent. Therefore,

$$|\widehat{\phi}(\omega)| = \prod_{j=1}^{+\infty}\prod_{k=0}^{n-1} |\frac{1 + e^{-i2^{k-j}\omega}}{2}| = \prod_{k=0}^{n-1}\prod_{j=1}^{+\infty} |\frac{1 + e^{-i2^{k-j}\omega}}{2}|.$$

By the fact that

$$\prod_{j=1}^{+\infty} |\frac{1+e^{-i2^{k-j}\omega}}{2}| = \lim_{m\to+\infty}\prod_{j=1}^{m} |\frac{1+e^{-i2^{k-j}\omega}}{2}| = \lim_{m\to+\infty} \frac{1-(e^{-i\frac{2^k}{2^m}\omega})^{2^m}}{2^m(1-e^{-i\frac{2^k}{2^m}\omega})}| = |\frac{1-e^{-i2^k\omega}}{i2^k\omega}|,$$

we have then

$$|\widehat{\phi}(\omega)| = \prod_{k=0}^{n-1} |\frac{1-e^{-i2^k\omega}}{i2^k\omega}| \le \prod_{k=0}^{n-1} \frac{c_k}{1+|2^k\omega|} \le \frac{c}{(1+|\omega|)^n},$$

for some constant $c$. Thus $\phi \in C^{n-2}$. $\square$

By Theorem 4.1, it can be seen that the number of framelets, i.e., $\frac{1}{b}-1$, is exactly $\operatorname{card}(\operatorname{supp}(\boldsymbol{g})) - 1$, i.e., one less than the cardinality of the support of $\boldsymbol{g}$. Once we have an MRA-based tight wavelet frame constructed via the UEP, a filter bank based implementation is available for $n$-level decomposition and reconstruction of discrete signals. Let $\star$ denote the usual convolution operator in $\ell_2(\mathbb{Z})$. Let $\downarrow_2$ denote the down-sampling operator defined by $(\boldsymbol{f}\downarrow_2)(m) = \boldsymbol{f}(2m), m \in \mathbb{Z}$, and $\uparrow_2$ denote the up-sampling operator, i.e. the adjoint operator of down-sampling operator. Then, given a signal $\boldsymbol{f} \in \ell_2(\mathbb{Z})$, the $n$-level wavelet decomposition can be recursively computed as follows: $\boldsymbol{c}_{0,0} = \boldsymbol{f}$, for $k = 1, \ldots n-1$,

$$\begin{cases} \boldsymbol{c}_{0,k} = \left(\sqrt{2}\cdot\overline{\boldsymbol{g}_0(-\cdot)} \star \boldsymbol{c}_{0,k-1}\right)\downarrow_2, \\ \boldsymbol{c}_{\ell,k} = \left(\sqrt{2}\cdot\overline{\boldsymbol{g}_\ell(-\cdot)} \star \boldsymbol{c}_{0,k-1}\right)\downarrow_2, \quad \ell = 1,...,r. \end{cases} \tag{4.12}$$

The reconstruction of $\boldsymbol{f}$ from the high-pass wavelet coefficients $(\{\boldsymbol{c}_{\ell,k}\}_{0\le k\le n-1, 1\le \ell\le r})$ and the low-pass coefficient $(\{\boldsymbol{c}_{0,n}\})$ is done in the same recursive way: for $k = n, n-1, ..., 1$,

$$\boldsymbol{c}_{0,k-1} = \sqrt{2}\sum_{\ell=0}^{r} \boldsymbol{g}_\ell \star (\boldsymbol{c}_{\ell,j}\uparrow_2). \tag{4.13}$$

It can be seen that such an $n$-level wavelet decomposition expands the signal over a discrete tight frame for $\ell_2(\mathbb{Z})$ defined by

$$\left\{\{\boldsymbol{\phi}_n(\cdot - 2^n j)\}_{j\in\mathbb{Z}}, \{\boldsymbol{\psi}_{1,k}(\cdot - 2^k j)\}_{1\leq k\leq n, j\in\mathbb{Z}}, \ldots, \{\boldsymbol{\psi}_{r,k}(\cdot - 2^k j)\}_{1\leq k\leq n, j\in\mathbb{Z}}\right\}, \quad (4.14)$$

where $\boldsymbol{\phi}_n, \boldsymbol{\psi}_{\ell,k}$ are sequences defined by

$$\widehat{\boldsymbol{\phi}_n}(\omega) = \sqrt{2}\prod_{m=0}^{n-1}\widehat{\boldsymbol{g}}_0(2^m\omega), \text{and} \quad \widehat{\boldsymbol{\psi}_{\ell,k}} = \sqrt{2}\widehat{\boldsymbol{g}}_\ell(2^{k-1}\omega)\prod_{m=0}^{k-1}\widehat{\boldsymbol{g}}_0(2^m\omega),$$

for $\ell = 1, \ldots, r, k = 1, \ldots, n$. The tight frame defined by (4.14) with the masks $\{\boldsymbol{g}_\ell\}_{\ell=0}^r$ of the form (4.8) indeed can be viewed as a discrete tight Gabor frame for $\ell_2(\mathbb{Z})$ with $n$-level multi-scale structure. When $n = 1$, the tight frame defined by (4.14) can be expressed as

$$\left\{\sqrt{2}\boldsymbol{g}_\ell(m - 2k) = \boldsymbol{g}(m - 2k)e^{-2\pi i b\ell m}\right\}_{0\leq\ell\leq\frac{1}{b}-1, k\in\mathbb{Z}},$$

which is exactly the tight Gabor frames for $\ell_2(\mathbb{Z})$ defined in (4.2) with $a = 2$.

**Example 4.4.** *When taking $p = 4$, we have $\boldsymbol{g}_0 = \boldsymbol{g} = (\frac{1}{4}, \frac{1}{4}, \frac{1}{4}, \frac{1}{4})$, and the other three Gabor atoms, $\boldsymbol{g}_1 = (\frac{1}{4}, -\frac{1}{4}i, -\frac{1}{4}, \frac{1}{4}i), \boldsymbol{g}_2 = (\frac{1}{4}, -\frac{1}{4}, \frac{1}{4}, -\frac{1}{4})$ and $\boldsymbol{g}_3 = (\frac{1}{4}, \frac{1}{4}i, -\frac{1}{4}, -\frac{1}{4}i)$. The refinable function $\phi$ with the mask $\boldsymbol{g}$ is a linear spline given by*

$$\phi(t) = \begin{cases} \frac{1}{2}t, & t \in [0, 1), \\[2mm] \frac{1}{2}, & t \in [1, 2), \\[2mm] \frac{1}{2}(3 - t), & t \in [2, 3), \\[2mm] 0, & \text{otherwise.} \end{cases}$$

*See Figure 4.1 for the plots of the refinable function $\phi$ and three framelets admitted by $\boldsymbol{g}_1, \boldsymbol{g}_2, \boldsymbol{g}_3$.*

**Example 4.5.** *When taking $p = 6$, we have $\boldsymbol{g} = (\frac{1}{6}, \frac{1}{6}, \frac{1}{6}, \frac{1}{6}, \frac{1}{6}, \frac{1}{6})$. The associated refinable function $\phi$ is continuous but is not a spline. See Figure 4.2 for the plots of the refinable function $\phi$ and five framelets.*

(a) Real $(\phi)$    (b) Imag $(\phi)$    (c) Real $(\psi_1)$    (d) Imag $(\psi_1)$

(e) Real $(\psi_2)$    (f) Image $(\psi_2)$    (g) Real $(\psi_3)$    (h) Image $(\psi_3)$

Figure 4.1: The real part and imaginary part of the refinable function and three framelets generated from $\boldsymbol{g} = (\frac{1}{4}, \frac{1}{4}, \frac{1}{4}, \frac{1}{4})$



(a) Real $(\phi)$    (b) Imag $(\phi)$    (c) Real $(\psi_1)$    (d) Imag $(\psi_1)$

(e) Real $(\psi_2)$    (f) Imag $(\psi_2)$    (g) Real $(\psi_3)$    (h) Imag $(\psi_3)$

(i) Real $(\psi_4)$    (j) Imag $(\psi_4)$    (k) Real $(\psi_5)$    (l) Imag $(\psi_5)$
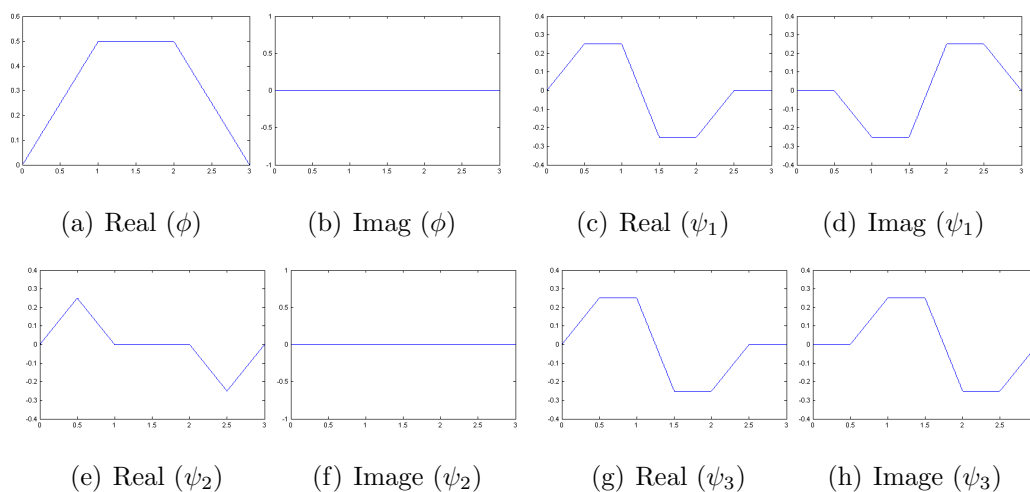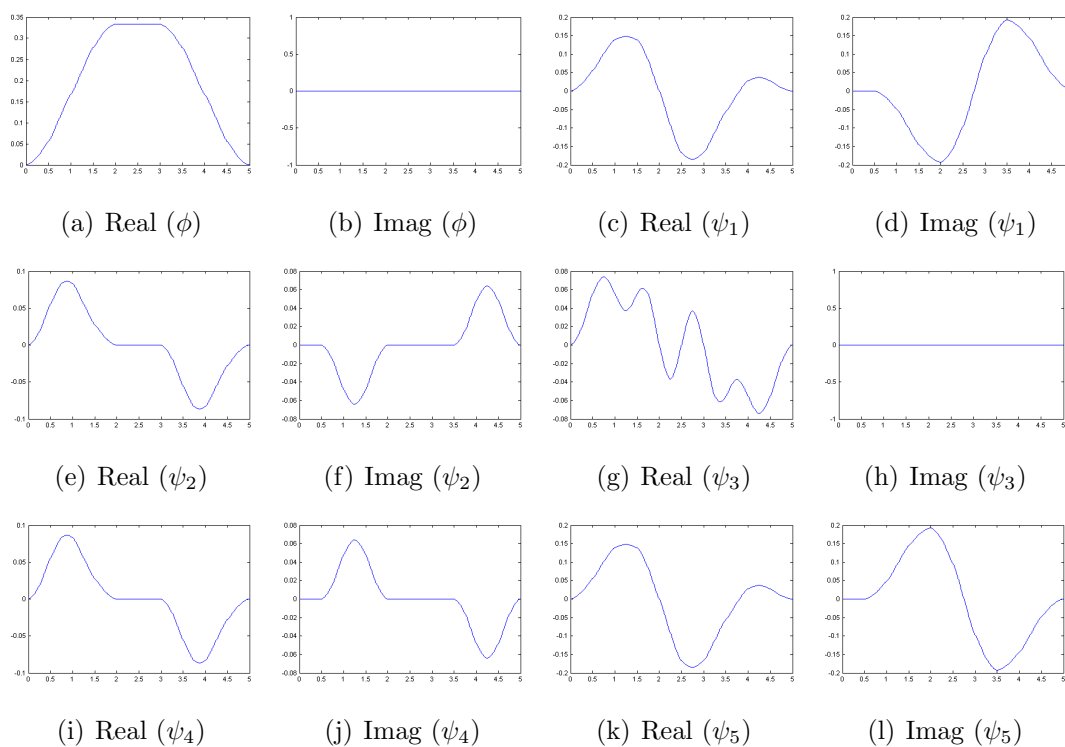
Figure 4.2: The real part and imaginary part of the refinable function and five framelets generated from $\boldsymbol{g}_0 = (\frac{1}{6}, \frac{1}{6}, \frac{1}{6}, \frac{1}{6}, \frac{1}{6}, \frac{1}{6})$

**Example 4.6.** *When taking $p = 8$, we have $\boldsymbol{g} = (\frac{1}{8}, \frac{1}{8}, \frac{1}{8}, \frac{1}{8}, \frac{1}{8}, \frac{1}{8}, \frac{1}{8}, \frac{1}{8})$. The corresponding refinable function is a quadratic spline given by*

$$\phi(t) = \begin{cases} \frac{1}{16}t^2, & t \in [0,1], \\[2mm] \frac{t}{8} - \frac{1}{16}, & t \in [1,2], \\[2mm] \frac{1}{16}(-t^2 + 6t - 5), & t \in [2,3], \\[2mm] \frac{1}{4}, & t \in [3,4], \\[2mm] \frac{1}{16}(-t^2 + 8t - 12), & t \in [4,5], \\[2mm] -\frac{t}{8} + \frac{13}{16}, & t \in [5,6], \\[2mm] \frac{1}{16}(t-7)^2, & t \in [6,7], \\[2mm] 0, & otherwise. \end{cases}$$

*See Figure 4.3 for the plots of the refinable function $\phi$ and seven framelets.*

Before ending this section, we would like to mention that the construction scheme presented in this section can also be used for constructing real-valued discrete tight frame formed by local cosine basis with MRA structure. Consider a local cosine basis with even support $p$:

$$\boldsymbol{g}_\ell(m) = \alpha_\ell \cos\left(\frac{\pi(2m+1)\ell}{2p}\right), \quad 0 \le m \le p - 1,$$

where $\alpha_0 = \frac{1}{p}$, and $\alpha_\ell = \frac{\sqrt{2}}{p}$ for $1 \le \ell \le p - 1$. By a direct calculation, the atoms of such a basis satisfy the UEP if being used as the refinement mask and wavelet masks. Thus, the system generated by these masks using (4.14) forms a tight frame for $\ell_2(\mathbb{Z})$. The refinable function admitted by $\boldsymbol{g}_0$ generated the same MRA as that of the previously constructed tight frames, but the resulting tight wavelet frames are different as the framelets are different. For example when taking $p = 4$, we have $\boldsymbol{g}_0 = (\frac{1}{4}, \frac{1}{4}, \frac{1}{4}, \frac{1}{4})$, $\boldsymbol{g}_1 = \frac{\sqrt{2}}{4}(\cos\frac{\pi}{8}, \cos\frac{3\pi}{8}, \cos\frac{5\pi}{8}, \cos\frac{7\pi}{8})$, $\boldsymbol{g}_2 = \frac{\sqrt{2}}{4}(\cos\frac{\pi}{4}, \cos\frac{3\pi}{4}, \cos\frac{5\pi}{4}, \cos\frac{7\pi}{4})$, $\boldsymbol{g}_3 = \frac{\sqrt{2}}{4}(\cos\frac{3\pi}{8}, \cos\frac{7\pi}{8}, \cos\frac{\pi}{8}, \cos\frac{5\pi}{8})$. See Figure 4.4 for the plots of the refinable function $\phi$ and three framelets.

(a) Real ($\phi$)          (b) Imag ($\phi$)          (c) Real ($\psi_1$)          (d) Imag ($\psi_1$)

(e) Real ($\psi_2$)          (f) Imag ($\psi_2$)          (g) Real ($\psi_3$)          (h) Imag ($\psi_3$)

(i) Real ($\psi_4$)          (j) Imag ($\psi_4$)          (k) Real ($\psi_5$)          (l) Imag ($\psi_5$)

(m) Real ($\psi_6$)          (n) Imag ($\psi_6$)          (o) Real ($\psi_7$)          (p) Imag ($\psi_7$)
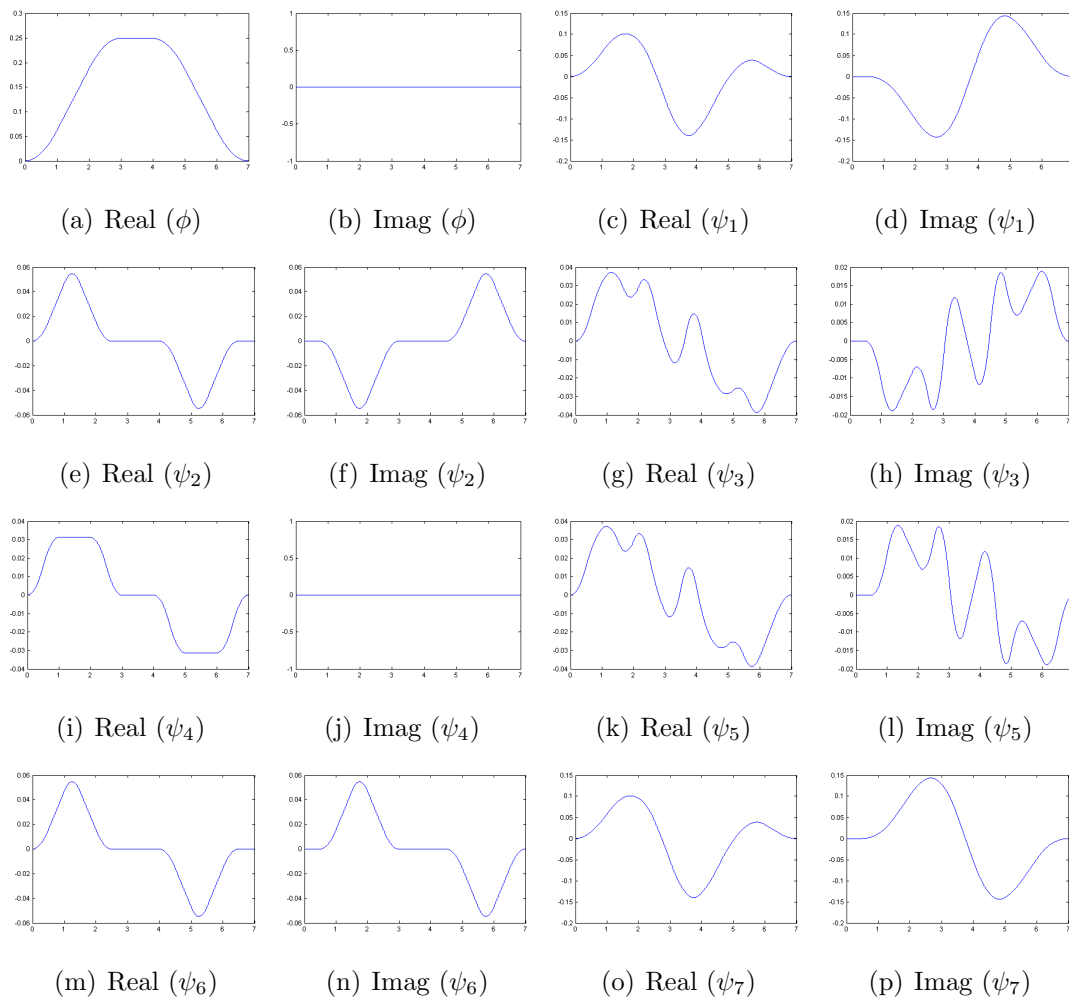
Figure 4.3: The real part and imaginary part of the refinable function and seven framelets generated from $\boldsymbol{g}_0 = (\frac{1}{8}, \frac{1}{8}, \frac{1}{8}, \frac{1}{8}, \frac{1}{8}, \frac{1}{8}, \frac{1}{8}, \frac{1}{8})$
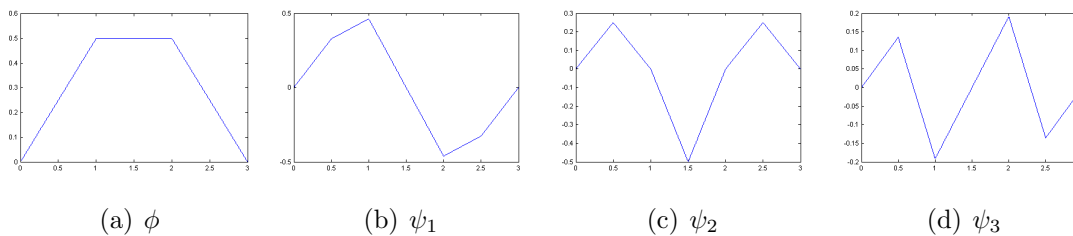


(a) $\phi$          (b) $\psi_1$          (c) $\psi_2$          (d) $\psi_3$

Figure 4.4: Wavelets generated from $\boldsymbol{g}_0 = (\frac{1}{4}, \frac{1}{4}, \frac{1}{4}, \frac{1}{4})$ and cosine basis

# 4.3 (Tight) Gabor frames induced from refinable functions

In the previous section, the discrete tight Gabor frames in the sequence domain are linked to the MRA-based tight wavelet frames in the continuum domain which brings MRA structure to discrete Gabor frames. Another interesting question is then can we link tight Gabor frames in the continuum domain to the MRA as well. In other words, can we link a refinable function to the window function of a tight Gabor frame?

Using the same sampling rate $a = 2$ and $b = \frac{1}{p}$ as discrete tight Gabor frames with MRA structure, we define a Gabor system on the lattices: $K = 2\mathbb{Z}$, $L = \frac{1}{p}\mathbb{Z}$:

$$(K, L)_g = \{g(t - 2k)e^{-\frac{2\pi i \ell x}{p}}, x \in \mathbb{R}\}_{t, \ell \in \mathbb{Z}}, \tag{4.15}$$

where $g \in L_2(\mathbb{R})$ is a compactly supported non-negative window function. In the next theorem, we give a sufficient condition on a refinable function so that the Gabor system defined as (4.15) will form a frame when $g = \phi$ and will form a tight frame when $g = \sqrt{2\phi/p}$.

**Theorem 4.7.** *Let $\phi \in L_2(\mathbb{R})$ with $\widehat{\phi}(0) = 1$ be a continuous refinable function supported on $[0, p-1]$. Suppose that $p \geq 4$ and $\phi(t) > 0$ for any $t \in (0, p-1)$. Let $\boldsymbol{g}_0$ denote its refinement mask. Then, the Gabor system $(K, L)_g$ with $g = \phi$ forms a frame for $L_2(\mathbb{R})$. Further, suppose the mask $\boldsymbol{g}_0$ satisfies*

$$\sum_{m \in \Lambda_j} \boldsymbol{g}_0(m) = \frac{1}{4}, \tag{4.16}$$

*where $j \in \mathbb{Z}/4\mathbb{Z}$ and $\Lambda_j = (4\mathbb{Z} + j) \cap [0, p-1]$. Then, the Gabor system $(K, L)_g$ with $g = \sqrt{2\phi/p}$ forms a tight frame for $L_2(\mathbb{R})$.*

*Proof.* The frame property of the Gabor system $(K, L)_\phi$ is proved by one sufficient condition presented in [29] which states that as long as the window function $\phi$ is

continuous on its support $[0, p-1]$, $\phi > 0$ on $(0, p-1)$, $b = \frac{1}{p} \leq \frac{1}{p-1}$ and $p \geq 4$, the system $(K, L)_\phi$ forms a frame for $L_2(\mathbb{R})$.

The proof of tight frame property of $(K, L)_{\sqrt{2\phi/p}}$ is based on Theorem 2.2. Since $b = \frac{1}{p} \leq \frac{1}{p-1}$, Condition (a) of Theorem 2.2 is satisfied. For any $j \in \mathbb{Z}$ and $r \in \mathbb{N}$,

$$\sum_{k \in \mathbb{Z}} \phi(\frac{j}{2^r} - 2k) = \sum_{k \in \mathbb{Z}} \sum_{m \in \mathbb{Z}} 2\boldsymbol{g}_0(m) \phi(\frac{j}{2^{r-1}} - 4k - m) = \sum_{k \in \mathbb{Z}} \sum_{m \in \mathbb{Z}} 2\boldsymbol{g}_0(m - 4k) \phi(\frac{j}{2^{r-1}} - m).$$

As both $\boldsymbol{g}_0$ and $\phi$ are compactly supported, one can then change the order of finite summations which gives

$$\sum_{k \in \mathbb{Z}} \phi(\frac{j}{2^r} - 2k) = \sum_{m \in \mathbb{Z}} \sum_{k \in \mathbb{Z}} 2g_0(m - 4k) \phi(\frac{j}{2^{r-1}} - m) = \frac{1}{2} \sum_{m \in \mathbb{Z}} \phi(\frac{j}{2^{r-1}} - m),$$

Herein, the last equality comes from (4.16). Moreover, by (4.16), we have $\sum_{k \in \mathbb{Z}} \boldsymbol{g}_0(m - 4k) = \sum_{k \in \mathbb{Z}} \boldsymbol{g}_0(m - 4k + 2) = \frac{1}{4}$, and thus $\sum_{k \in \mathbb{Z}} \boldsymbol{g}_0(m - 2k) = \frac{1}{2}$. By the same argument as above, we have

$$\sum_{m \in \mathbb{Z}} \phi(\frac{j}{2^{r-1}} - m) = \sum_{n \in \mathbb{Z}} \sum_{m \in \mathbb{Z}} 2\boldsymbol{g}_0(n - 2m) \phi(\frac{j}{2^{r-2}} - n) = \sum_{n \in \mathbb{Z}} \phi(\frac{j}{2^{r-2}} - n).$$

Repeat this process, one obtains

$$\sum_{m \in \mathbb{Z}} \phi(\frac{j}{2^{r-1}} - m) = \sum_{n \in \mathbb{Z}} \phi(\frac{j}{2^{r-2}} - n) = \cdots = \sum_{n \in \mathbb{Z}} \phi(j - n) = \sum_{n \in \mathbb{Z}} \phi(n).$$

Recall that we have

$$\widehat{\phi}(0) = \int_{-\infty}^{+\infty} \phi(t) dt = \sum_{n \in \mathbb{Z}} \phi(n),$$

when the function $\phi$ is a continuous refinable function (see more details in [37]). By the fact that $\widehat{\phi}(0) = 1$, we have then

$$\sum_{k \in \mathbb{Z}} \phi(\frac{j}{2^r} - 2k) = 1/2,$$

for any $j \in \mathbb{Z}$ and $r \in \mathbb{N}$. Since $\{\frac{j}{2^r}, j \in \mathbb{Z}, r \in \mathbb{N}\}$ is dense in $\mathbb{R}$ and the continuity of $\phi$ implies the continuity of $\sum_{k \in \mathbb{Z}} \phi(\cdot - 2k)$, it is established that for any $t \in \mathbb{R}$,

$$\sum_{k \in \mathbb{Z}} \phi(t - 2k) = 1/2,$$

(a) $p = 4$        (b) $p = 8$
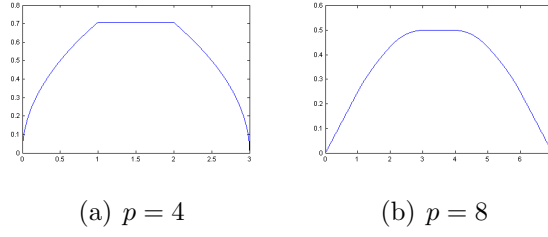
Figure 4.5: The square root of the refinable functions shown in Example 4.4 and Example 4.6, which are used as the window functions of tight Gabor frames.

which is exactly Condition (b) with $a = 2$ in Theorem 2.2. Thus, by Theorem 2.2, the Gabor system $(K, L)_g$ defined as (4.15) with $g = \sqrt{2\phi/p}$ forms a tight frame for $L_2(\mathbb{R})$. $\hfill\square$

**Example 4.8.** *Consider the masks in Example 4.4 and Example 4.6, i.e. $p = 4$, $\boldsymbol{g}_0 = (\frac{1}{4}, \frac{1}{4}, \frac{1}{4}, \frac{1}{4})$ and $p = 8$, $\boldsymbol{g}_0 = (\frac{1}{8}, \frac{1}{8}, \frac{1}{8}, \frac{1}{8}, \frac{1}{8}, \frac{1}{8}, \frac{1}{8}, \frac{1}{8})$. These masks and their refinable functions $\phi$ satisfy conditions in Theorem 4.7. Therefore, the Gabor system with window function $\sqrt{2\phi/p}$ is a tight frame for $L_2(\mathbb{R})$. For $p = 4$ and $p = 8$, $\sqrt{\phi}$ is shown in Figure 4.5.*

## 4.4 Conclusions

In this chapter, we studied the construction of discrete tight frames with Gabor and MRA structures. The basic idea is to connect the discrete tight Gabor frames to the MRA-based tight wavelet frames in continuum domain via UEP. A sufficient condition for constructing such discrete tight frames is presented, and we showed its closed-form solutions. The window sequence of the closed-form solutions takes the form $\frac{1}{p}(1, 1, \ldots, 1, 1)$, which generates the refinable function different from that associated with Haar wavelet for $p \geq 4$. In addition, we also introduced a class of tight Gabor frames for $L_2(\mathbb{R})$ whose window functions are induced from refinable functions of MRAs. Its efficiency in sparse representation will be shown in the experiment of image restoration in Chapter 5.

# Chapter 5

# Image recovery using multi-scale Gabor systems

## 5.1   Introduction

In recent years, by assuming images of interest can be sparsely approximated under a frame or tight frame, sparsity-prompting functional (e.g. $\ell_1$-norm) based regularization has been used in many image recovery tasks; see e.g. shift-invariant Daubechies wavelet system for image denoising [35], splines wavelet frame based image restoration methods [10, 16, 14] and curvelet based image recovery methods [104, 106]. Several approaches have been proposed for utilizing the sparse approximation of images, including synthesis approach, analysis approach and balanced approach. Interested readers are referred to [50, 102] for more details. There exist deep connections between wavelet frames based regularization method and the widely used total variation based regularization. Indeed, it is shown in [12] that the wavelet frame based analysis approach can be seen as sophisticated discretization of minimizations involving the total variation penalty.

Natural images are often composed of both cartoon and texture parts. Thus, a more efficient approach is viewing such images as the composite of multiple layers

with different characteristics. For example, a two-layer model is considered in [16] for image inpainting, in which one layer represents cartoon parts that are sparse in wavelet domain and the other layer represents texture parts that are sparse in local DCT domain. Different from spline wavelet frames, the discrete Gabor induced frames proposed in Chapter 3 have their origins from local time-frequency analysis. Thus, they can deal with both cartoon parts and texture parts by using window functions of varying supports.

Another way to handle the images including multi-scale features is to use the discrete tight frames with Gabor and MRA structures constructed in Chapter 4. By implementing wavelet transforms of multi-levels, one can use one single system to characterize different types of image features. Correspondingly, the usual analysis model ([16]) can be used as the regularization model.

## 5.2   Regularization models and numerical algorithms

A 2D image can be concatenated as a vector in $\mathbb{R}^N$, where $N$ is the total number of image pixels. Image recovery we consider in the experiment is about solving a linear inverse problem:

$$\boldsymbol{b} = \boldsymbol{A}\boldsymbol{f} + \boldsymbol{n}, \tag{5.1}$$

where $\boldsymbol{b} \in \mathbb{R}^N$ denotes the observed degraded image, $\boldsymbol{f} \in \mathbb{R}^N$ denotes the original image for recovery and $\boldsymbol{n} \in \mathbb{R}^N$ denotes noise. The operator $\boldsymbol{A} \in \mathbb{R}^{N \times N}$ is a measuring matrix that varies according to different image recovery problems. For image deblurring, $\boldsymbol{A}$ is a convolution operator with a low-pass filter. For image de-noising, $\boldsymbol{A}$ is an identity matrix. For image in-painting, $\boldsymbol{A}$ is a diagonal matrix whose diagonal element is 1 when the corresponding pixel value is available and 0 otherwise.

For an input image composed of both cartoon parts and texture parts, we propose a sparsity-based multi-layer composite model which is based on multiple discrete Gabor induced frames generated by window functions of different sizes. More

specifically, we assume that the input image is composed of multiple layers in which each layer can be sparsely approximated under a discrete Gabor induced frame with a different window size, which are constructed in Chapter 3. Suppose $\boldsymbol{W}_{Y_k}$ is the decomposition operator in the matrix form of a 2D Gabor induced frame $Y_k$ with window size $p_k$ and shift parameters $(a_k, b_k)$, and $\widetilde{\boldsymbol{W}_{Y_k}}$ is the reconstruction operator of its dual. Based on such a sparsity-based multi-layer composite model of images, we propose the following regularization model for solving (5.1):

$$\min_{\{\boldsymbol{u}_1,\ldots,\boldsymbol{u}_m\}\subset\mathbb{R}^N} \sum_{k=1}^m \lambda_k \|\boldsymbol{W}_{Y_k}\boldsymbol{u}_k\|_1, \quad \text{s.t.} \quad \|\boldsymbol{A}(\sum_{k=1}^m \boldsymbol{u}_k) - \boldsymbol{b}\|_2 \leq \epsilon, \qquad (5.2)$$

where $\epsilon$ denotes the tolerance determined by noise level and $\lambda_k$ denotes the pre-defined regularization parameter. The recovered image $\widetilde{\boldsymbol{u}}$ is then synthesized by $\boldsymbol{u}_k$'s via $\widetilde{\boldsymbol{u}} = \sum_{k=1}^m \boldsymbol{u}_k$.

Another way to handle images with multi-layer components is using the discrete tight frames with Gabor and MRA structures constructed in Chapter 4. Different from the above multi-layer composite model using several Gabor induced systems, in this approach only a single system is considered to deal with the scaling challenge, owing to the benifits of MRA structure. The decomposition operator of a 2D $n$-level discrete undecimated tight wavelet frame is represented by a matrix $\boldsymbol{W}$ and the reconstruction operator is its adjoint matrix $\boldsymbol{W}^*$. We apply the following sparsity-based regularization model, or referred to as the analysis model ([16]), for solving (5.1):

$$\min_{\boldsymbol{u}\in\mathbb{R}^N} \lambda\|\boldsymbol{W}\boldsymbol{u}\|_1, \quad \text{s.t.} \quad \|\boldsymbol{A}\boldsymbol{u} - \boldsymbol{b}\|_2 \leq \epsilon, \qquad (5.3)$$

where $\epsilon$ is the tolerance related to the noise level. The recovered image is given by the solution to this model.

By regarding the analysis model (5.3) as a special case of (5.2) with the number of systems $m = 1$, Models (5.2) and (5.3) can be combined and written as a more compact form like

$$\min_{\boldsymbol{u}\in\mathbb{R}^{mN}} \|\boldsymbol{W}\boldsymbol{u}\|_1, \quad \text{s.t.} \quad \|\widetilde{\boldsymbol{A}}\boldsymbol{u} - \boldsymbol{b}\|_2 \leq \epsilon, \qquad (5.4)$$

where $\boldsymbol{W} = \operatorname{diag}(\lambda_1 \boldsymbol{W}_{Y_1}, \ldots, \lambda_m \boldsymbol{W}_{Y_m})$, $\widetilde{\boldsymbol{A}} = [\boldsymbol{A}, \boldsymbol{A}, \ldots, \boldsymbol{A}] \in \mathbb{R}^{N \times mN}$ and $\boldsymbol{u} = [\boldsymbol{u}_1^\top, \ldots, \boldsymbol{u}_m^\top]^\top \in \mathbb{R}^{mN}$.

The minimization problem (5.4) is an $\ell_1$-norm related convex problem which has been extensively studied in recent years. It can be efficiently solved by the split Bregman iteration or equivalently the ADMM method via the following iteration scheme:

$$
\begin{cases}
(\widetilde{\boldsymbol{A}}^\top \widetilde{\boldsymbol{A}} + \mu \boldsymbol{W}^* \boldsymbol{W}) \boldsymbol{u}^{k+1} = \widetilde{\boldsymbol{A}}^\top (\boldsymbol{b} - \boldsymbol{c}^k) + \mu \boldsymbol{W}^* (\boldsymbol{d}^k - \boldsymbol{h}^k) \\
\boldsymbol{d}^{k+1} = \mathcal{H}_{\frac{1}{\mu}} (\boldsymbol{W} \boldsymbol{u}^{k+1} + \boldsymbol{h}^k), \\
\boldsymbol{h}^{k+1} = \boldsymbol{h}^k + \boldsymbol{W} \boldsymbol{u}^{k+1} - \boldsymbol{d}^{k+1}, \\
\boldsymbol{c}^{k+1} = \boldsymbol{c}^k + \widetilde{\boldsymbol{A}} \boldsymbol{u}^{k+1} - \boldsymbol{b},
\end{cases}
\tag{5.5}
$$

where $\mathcal{H}_\delta(w) = [t_\delta(w_1), t_\delta(w_2), \ldots]^\top$ is the soft thresholding operator, with $t_\delta(w_i) = \frac{w_i}{|w_i|} \max\{0, |w_i| - \delta\}$ if $w_i \neq 0$ and $t_\delta(0) = 0$. Interested readers are referred to [16] for more details. In our implementation using discrete Gabor induced frames, the conjugate gradient method is called for solving the linear system in the first step of the iteration. In the implementation using discrete tight frame with Gabor and MRA structures, note that $\boldsymbol{W}^* \boldsymbol{W} = \boldsymbol{I}$. If $\boldsymbol{A}$ is a convolution matrix, the linear system in the first step of the iteration can be solved via the fast Fourier transform if the periodic boundary condition is considered. If $\boldsymbol{A}$ is an identity matrix or diagonal matrix, the linear system can be solved via directly inverting $\boldsymbol{A}^\top \boldsymbol{A} + \mu \boldsymbol{I}$.

It is noted that although $\boldsymbol{W}$ is a complex-valued operator, all intermediate variables $\boldsymbol{u}^{k+1}, \boldsymbol{c}^{k+1}$ are real-valued in both implementations. The reason is that the filters corresponding to the proposed Gabor induced frames or tight frames with Gabor and MRA structures always appear as conjugate pairs. In other words, the coefficients also appear as conjugate pairs. In addition, for any conjugate pair of coefficients, the thresholding operator $t_\delta$ either set both to 0 or keep them remaining as a conjugate pair. Thus, all intermediate variables are real-valued.

## 5.3   Image recovery and experimental evaluation

In this section, we apply multi-scale discrete Gabor induced frames based regularization model (5.2) and discrete tight frames with Gabor and MRA structures based regularization model (5.3) to solve two typical image recovery problems: image denoising and image deconvolution.

The implementation of the regularization method (5.2) is done as follows. The multi-scale discrete Gabor induced frames are composed of two systems constructed in Section 3.4.2 with two different scales. One is the discrete Gabor induced frame of the form (3.18) modified from the tight Gabor frame in Example 3.6 using the B-spline of order 4 with the nodes $\{0, 2, 4, 6, 8\}$. Two shift parameters of the lattices are $a = 2$ and $b = 1$. The other system is the large-scale version of the first one, whose window function is obtained by sampling the same B-spline function of order 4 but with the nodes $\{0, 4, 8, \ldots, 16\}$. Two shift parameters of the lattices are $a = 4$ and $b = 1$. The filter size of the filter banks associated with these two systems are $p = 7$ and $p = 15$ respectively.

In the implementation of the regularization model (5.3), the system for sparsifying images is the undecimated version of discrete tight frames with Gabor and MRA structures constructed from Theorem 4.1 and Proposition 4.2 in Section 4.2. Tests are taken with transforms in different settings, which include (1) two-level tight wavelet frame with filter size $p = 4$; and (2) one-level tight wavelet frame with $p = 8$. By writing the model as the compact form (5.4), both regularization models based on discrete Gabor induced frames and tight wavelet frames, are solved via the iteration scheme (5.5).

To illustrate the benefit of constructed discrete Gabor induced frames and tight wavelet frames with Gabor structure for sparsity-based image recovery, the results are compared to that from several other $\ell_1$ norm based regularization methods using different systems for sparsifying images. The first one is the popular TV based image restoration method (see e.g. [112]), in which the total variation of the image

(a) Barbara      (b) Bowl      (c) Cameraman      (e) Lena
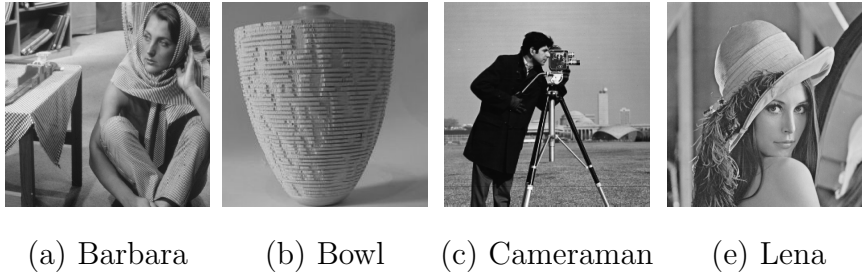
Figure 5.1: Visualization of four tested images

is regularized. The next one is wavelet frame sparsified method from [16]. For image deblurring, the analysis model (5.3) is used and the linear spline tight wavelet frame [99] is applied as the sparsifying system. For image denoising, two systems (local DCT and linear spline tight wavelet frame) and a multi-layer composite model of images modified from (5.2) are considered. The last one is using the same regularization model (5.3) but the sparsifying system is the dual-tree complex wavelet (DT-CWT) [101] whose associated filter bank has up to six orientations. In the implementation of DT-CWT, near Symmetric $(13, 19)$ tap filters are chosen in the lowest level and Q-Shift $(10, 10)$ tap filters are chosen in two higher levels to gain the optimal performance. The parameters involved in these methods are rigorously tuned up to achieve the best average performance over tested images. The performance of image recovery is measured in terms of the PSNR value given by

$$\text{PSNR} = -20 \log_{10} \frac{\|\boldsymbol{f} - \widetilde{\boldsymbol{u}}\|}{255N},$$

where $N$ denotes the total number of image pixels, $\boldsymbol{f}$ and $\widetilde{\boldsymbol{u}}$ denote the truth and the result.

In the experiments of image deconvolution, the tested images, shown in Figure 5.1, are firstly convoluted with a blur kernel and then added with Gaussian white noise. The standard deviation of noise is $\sigma = 3$ and four types of blur kernel are tested: (1) disk kernel of radius 3 pixels, (2) linear motion blur kernel of length 15 pixels and of orientation $30°$, (3) Gaussian kernel of size $15 \times 15$ pixels and standard derivation 2, and (4) averaging kernel of size $9 \times 9$ pixels. Through the experiments, the parameter of (5.5) for solving multi-scale Gabor induced frame

based regularization model is uniformly set for all images as follows: $\lambda_1 = \lambda_2 = \frac{\sigma^2}{5} + 3\sigma - 1$ and $\mu = \frac{\sigma}{10}$. The parameters of (5.5) for solving the regularization models using tight frames with Gabor and MRA structures are uniformly set as follows: (1) for two-level tight frame with $p = 4$, set $\lambda = 4$ and $\mu = \frac{1}{80}$; (2) for one-level tight frame with $p = 8$, set $\lambda = 1$ and $\mu = 0.2$. See Table 5.1 for the summary of PSNR values of results deblurred by different methods. It can be seen that the performance of the proposed multi-scale discrete Gabor induced frames based method outperform other methods for comparison. And tight wavelet frame based method is also competitive with other approaches, especially when the filter size is large enough. The improvement on the PSNR value is also consistent with the improvement on visual quality; for a visual illustration of deconvolution results by different methods, one may check Figure 5.2.

In the experiments of image denoising, the tested images are synthesized by adding Gaussian white noise with standard deviation $\sigma = 20$ on five tested images shown in Figure 5.3. The parameters of denoising using discrete Gabor induced frames are uniformly set for all images by the empirical formulation: $\lambda_1 = \frac{\sigma^2}{80} - \frac{\sigma}{5} + 13$; $\lambda_2 = -\frac{\sigma^2}{400} + \frac{7\sigma}{5} - 10$ and $\mu = \frac{1}{2}\sigma$. The parameters of denoising using tight frames with Gabor and MRA structures are uniformly set for all images: (1) for two-level tight frame with $p = 4$, set $\lambda = 765$ and $\mu = \frac{4}{3*255^2}$; (2) for one-level tight frame with $p = 8$, set $\lambda = \frac{765}{2}$ and $\mu = \frac{16}{3*255^2}$. See Table 5.2 for the summary of the PSNR values of the results denoised by different methods. Similarly as the deconvolution problem, the denoising results of both proposed approaches are competitive compared to those of other methods. Especially, the discrete multi-scale Gabor induced frames provide very good performance. And see Figure 5.3 for a visualization of the denoised images.

Table 5.1: PSNR values of deblurred results for blurred images with noise level $\sigma = 3$

| image | kernel | TV | linear spline framelet | DT-CWT | multi-scale Gabor frame | 2-level frames w/ $p = 4$ | 1-level frame w/ $p = 8$ |
|---|---|---|---|---|---|---|---|
| Barbara512 | disk | 24.77 | 25.17 | 25.15 | 25.65 | 25.12 | 25.48 |
|  | motion | 24.64 | 24.97 | 25.00 | 25.70 | 25.00 | 25.49 |
|  | gaussian | 24.13 | 24.14 | 24.19 | 24.21 | 24.18 | 24.18 |
|  | average | 23.99 | 24.03 | 24.07 | 24.27 | 24.05 | 24.10 |
| Bowl256 | disk | 28.73 | 28.92 | 28.99 | 29.35 | 29.10 | 29.13 |
|  | motion | 28.88 | 29.08 | 29.15 | 29.67 | 29.46 | 29.36 |
|  | gaussian | 27.96 | 27.82 | 28.32 | 28.66 | 28.04 | 28.46 |
|  | average | 28.73 | 28.84 | 28.94 | 29.25 | 29.12 | 29.21 |
| Cameraman256 | disk | 26.31 | 26.83 | 26.22 | 27.01 | 27.08 | 26.73 |
|  | motion | 26.18 | 27.14 | 26.35 | 26.93 | 27.07 | 26.72 |
|  | gaussian | 24.96 | 24.84 | 24.73 | 25.04 | 25.06 | 24.94 |
|  | average | 25.08 | 25.12 | 25.00 | 25.55 | 25.41 | 25.30 |
| Lena512 | disk | 32.05 | 32.17 | 32.25 | 32.53 | 32.03 | 32.06 |
|  | motion | 30.86 | 30.49 | 31.21 | 31.43 | 30.80 | 30.45 |
|  | gaussian | 31.34 | 31.26 | 31.59 | 31.74 | 31.52 | 31.55 |
|  | average | 30.10 | 29.96 | 30.21 | 30.36 | 29.91 | 30.06 |

Table 5.2: PSNR values of denoised results for noisy images with noise level $\sigma = 20$

| image | TV | linear spline framelet | DT-CWT | multi-scale Gabor frame | 2-level tight frames w/ $p = 4$ | 1-level tight frame w/ $p = 8$ |
|---|---|---|---|---|---|---|
| Barbara512 | 26.84 | 29.25 | 28.90 | 30.39 | 28.07 | 29.38 |
| Bowl256 | 29.24 | 30.15 | 29.43 | 30.58 | 30.06 | 30.40 |
| Cameraman256 | 28.83 | 29.00 | 28.94 | 29.26 | 29.41 | 29.29 |
| Lena512 | 30.71 | 31.10 | 31.49 | 31.74 | 31.03 | 31.39 |

(a) original image      (b) blurred image      (c) TV

(d) framelet      (e) DT-CWT      (f) Gabor induced frame

(g) two-level, $p = 4$      (h) one-level, $p = 8$
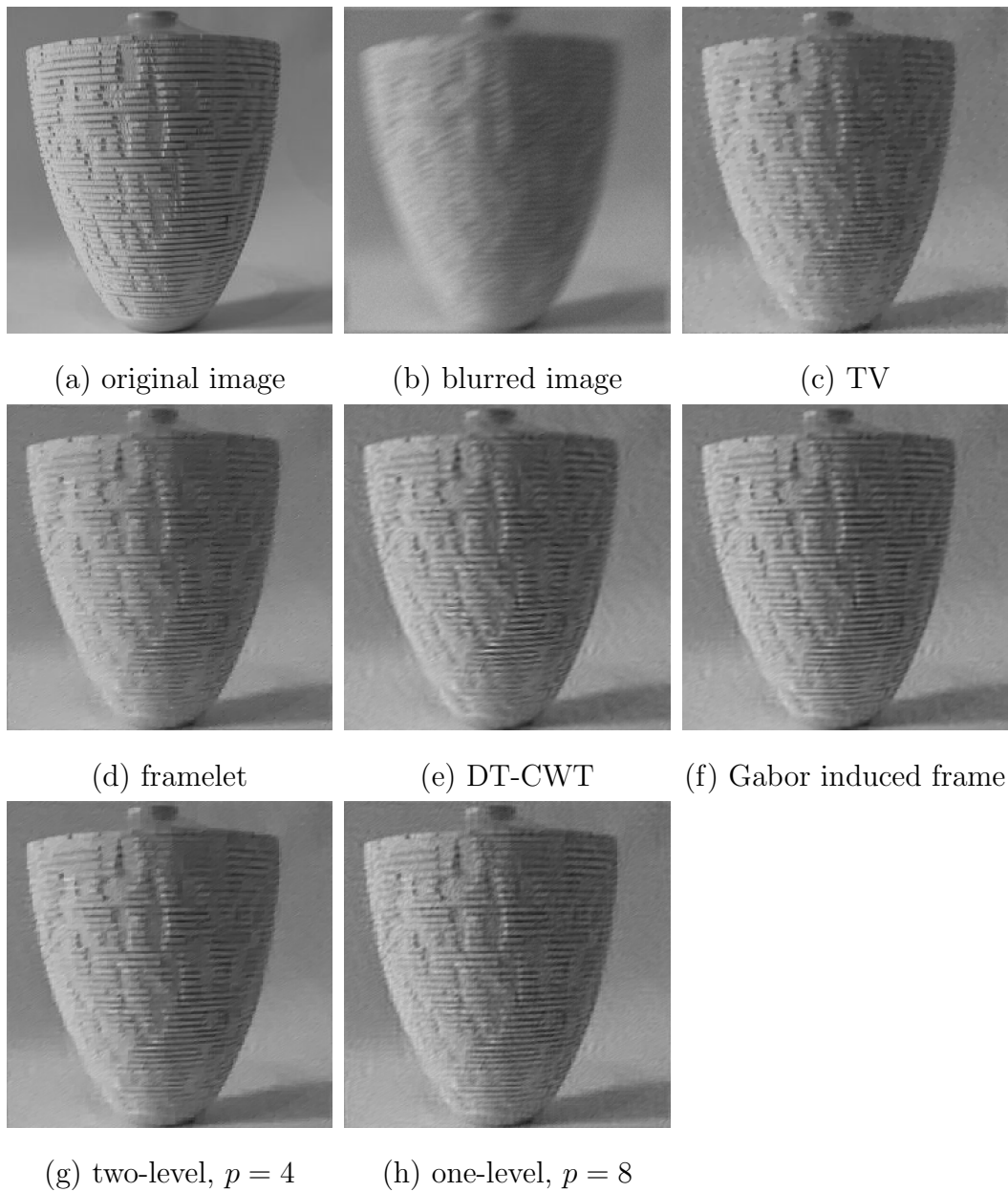
Figure 5.2: Visual illustration of image deconvolution. (a) True image; (b) image blurred by motion kernel and added by noise with noise level $\sigma = 3$; (c)-(j) deblurred results by different methods.

(a) original image (b) noisy image (c) TV

(d) framelet & local DCT (e) DT-CWT (f) Gabor induced frame

(g) two-level, $p = 4$ (h) one-level, $p = 8$
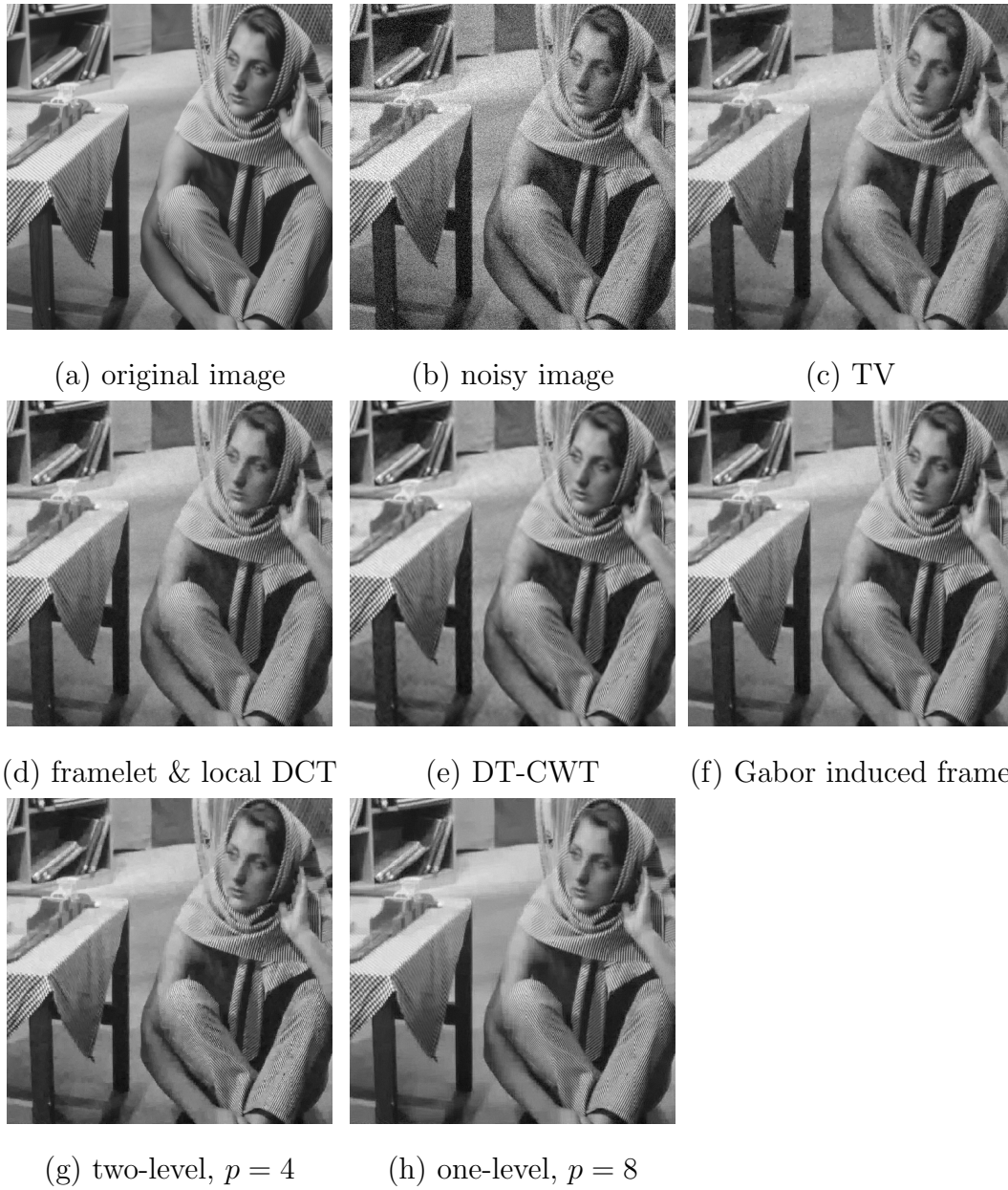
Figure 5.3: Visual illustration of image denoising. (a) True image; (b) noisy image with noise level $\sigma = 20$; (c)-(j) denoised results by four different methods.

## 5.4    Conclusions

In this chapter, we tested the efficiency of the constructed discrete Gabor induced frames and tight frames with Gabor and MRA structures for finite signals from the need of sparse image modeling. As shown in the experiments, compared to the existing wavelet frames often seen in many sparsity-based image recovery methods, the discrete Gabor induced frames constructed in Chapter 3 and tight frames with Gabor and MRA structures constructed in Chapter 4 have their advantages on orientation selectivity and on the flexibilities of modelling both image edges and local textures. Especially, the discrete Gabor induced frames, which possess the flexibility in desinging window functions with different decay, provide noticeably better results than other methods.

# Chapter 6

# $\ell_1$ regularizers with different loss functions for sparse recovery

## 6.1   Introduction

Recall that the problem of signal recovery usually models the observation as the output of applying a linear operator $\boldsymbol{A}$ to image of interest:

$$\boldsymbol{b} = \boldsymbol{A}\boldsymbol{f} + \boldsymbol{n}, \tag{6.1}$$

where $\boldsymbol{b} \in \mathbb{C}^M$ denotes the observed data, $\boldsymbol{f} \in \mathbb{C}^N$ denotes the truth to be esti-mated, and $\boldsymbol{n} \in \mathbb{C}^M$ denotes the measurement noise. In the last few chapters, we are devoted to finding proper systems to meet the needs of sparsity-induced image recovery, i.e. the underlying image can be sparsely represented under the given sys-tem. Based on the sparsity assumption, $\ell_1$-norm regularizer has been widely used as the convex relaxation of $\ell_0$-norm regularizer for sparse recovery. In this chapter, we will investigate the stability and robustness of $\ell_1$-norm related regularization mod-els. For convenience, we assume that the truth $\boldsymbol{f}$ itself is sparse or approximately sparse. In fact, sometimes the analysis based on such assumption is equivalent to that based on the assumption $\boldsymbol{f}$ is sparse under some transform. For example, con-sider the problem of image deconvolution or denoising, where $\boldsymbol{A}$ is a convolution

matrix or identity matrix. And assume $\boldsymbol{W}$ is the analysis operator of a tight frame defined by the filter bank. By the commutativity of $\boldsymbol{W}$ and $\boldsymbol{A}$,

$$\lambda\|\boldsymbol{Ax} - \boldsymbol{b}\|_2^2 + \|\boldsymbol{Wx}\|_1 = \lambda\|\boldsymbol{WAx} - \boldsymbol{Wb}\|_2^2 + \|\boldsymbol{Wx}\|_1 = \lambda\|\boldsymbol{AWx} - \boldsymbol{Wb}\|_2^2 + \|\boldsymbol{Wx}\|_1.$$

Therefore, in order to estimate $\|\widetilde{\boldsymbol{x}} - \boldsymbol{f}\|_2$, where $\widetilde{\boldsymbol{x}}$ is a solution to

$$\min_{\boldsymbol{x}} \lambda\|\boldsymbol{Ax} - \boldsymbol{b}\|_2^2 + \|\boldsymbol{Wx}\|_1,$$

one only need to estimate $\|\widetilde{\boldsymbol{y}} - \boldsymbol{Wf}\|_2 = \|\widetilde{\boldsymbol{x}} - \boldsymbol{f}\|_2$, where $\widetilde{\boldsymbol{y}} = \boldsymbol{W}\widetilde{\boldsymbol{x}}$ is a solution to

$$\min_{\boldsymbol{y}} \lambda\|\boldsymbol{Ay} - \boldsymbol{Wb}\|_2^2 + \|\boldsymbol{y}\|_1.$$

By assuming $\boldsymbol{f}$ is sparse, i.e. most elements of $\boldsymbol{f}$ are zero or close to zero, typical $\ell_1$-norm regularizer based optimization models for sparse recovery can be either a constrained model:

$$\min_{\boldsymbol{x}} \|\boldsymbol{x}\|_1, \quad \text{subject to} \quad \mathcal{L}(\boldsymbol{b} - \boldsymbol{Ax}) \leq \delta, \tag{6.2}$$

or an unconstrained model:

$$\min_{\boldsymbol{x}} \lambda\mathcal{L}(\boldsymbol{b} - \boldsymbol{Ax}) + \|\boldsymbol{x}\|_1, \tag{6.3}$$

where $\mathcal{L}$ is a loss function, $\delta$ and $\lambda$ are both pre-defined parameters. Usually the loss function $\mathcal{L}$ is set according to the statistical property of measurement noise $\boldsymbol{n}$. For example, $\mathcal{L}(\cdot) = \|\cdot\|_2^2$ is preferred, when noise $\boldsymbol{n}$ is the additive Gaussian white noise (see e.g. [100, 4, 61, 25]). When noise is impulse noise or there exists significant amount of outliers, the $\ell_1$-norm based loss function $\mathcal{L}(\cdot) = \|\cdot\|_1$ is preferred ([66, 67, 90]). In recent years, many efficient algorithms have been developed to solve these non-smooth $\ell_1$-norm relating optimization problems; see e.g. [62, 55, 41, 5, 115, 15, 94, 114]. In this chapter, we aim at studying sufficient conditions on the measurement matrix $\boldsymbol{A}$ for guaranteeing a robust and stable recovery of signal via solving (6.3) with different loss functions $\mathcal{L}$, as well as how to set optimal value of the regularization parameter $\lambda$.

### 6.1.1 Robust and stable recovery

We consider a robust and stable recovery of sparse signals in terms of the following three aspects.

1. *Noise-robustness.* The stability to noise refers to how much the noise $\boldsymbol{n}$ in (6.1) is magnified in the solution.

2. *Approximation-stability.* Often a signal $\boldsymbol{f}$ is only approximately sparse with most entries close to zero. The stability to sparse approximation refers to how much the following best $s$-sparse approximation error is magnified in the solution:

$$\sigma_s(\boldsymbol{f}) = \inf_{\boldsymbol{y}\in\Sigma_s} \|\boldsymbol{f} - \boldsymbol{y}\|_1,$$

where $\Sigma_s$ is the collection of all signals with at most $s$ non-zero entries.

3. *$\epsilon$-optimality-stability.* As the model (6.3) is usually solved via some iterative method, only an approximate solution $\widetilde{\boldsymbol{f}}$ to (6.3) will be available which satisfies

$$\lambda\mathcal{L}(\boldsymbol{b} - \boldsymbol{A}\widetilde{\boldsymbol{f}}) + \|\widetilde{\boldsymbol{f}}\|_1 \leq \min_{\boldsymbol{x}}(\lambda\mathcal{L}(\boldsymbol{b} - \boldsymbol{A}\boldsymbol{x}) + \|\boldsymbol{x}\|_1) + \epsilon,$$

for some constant $\epsilon$. The stability to the $\epsilon$-optimality refers to how much $\epsilon$ is magnified in the solution.

Therefore, we give the following definition of a robust and stable recovery of sparse signals by model (6.3).

**Definition 6.1** (Robust and Stable Sparse Recovery). Consider a noisy measurement $\boldsymbol{b} = \boldsymbol{A}\boldsymbol{f} + \boldsymbol{n}$ of signal $\boldsymbol{f}$. We say that the model (6.3) admits a robust and stable sparse recovery of $\boldsymbol{f}$ under $p$-norm if there exists some $\lambda > 0$ such that for any $\widetilde{\boldsymbol{f}}$ satisfying $\epsilon$-optimality condition:

$$\lambda\mathcal{L}(\boldsymbol{b} - \boldsymbol{A}\widetilde{\boldsymbol{f}}) + \|\widetilde{\boldsymbol{f}}\|_1 \leq \min_{\boldsymbol{x}}(\lambda\mathcal{L}(\boldsymbol{b} - \boldsymbol{A}\boldsymbol{x}) + \|\boldsymbol{x}\|_1) + \epsilon,$$

we have

$$\|\widetilde{\boldsymbol{f}} - \boldsymbol{f}\|_p \leq c_1\|\boldsymbol{n}\|_p + c_2 s^{1/p-1}\sigma_s(\boldsymbol{f}) + c_3\epsilon.$$

Here, $\|\cdot\|_p$ denotes the $p$-norm of a vector space with $p \geq 1$, and $c_1, c_2, c_3$ are all constants that are independent of the sparsity degree $s$, as well as the dimensions of $\boldsymbol{f}$ and $\boldsymbol{b}$.

## 6.1.2   Literature review

Before going to our results, we give a brief review of existing works about the robust and stable recovery via related $\ell_1$-norm regularizer based models in this part.

In the noise-free case where $\boldsymbol{n} = 0$ in (6.1), the $\ell_1$-norm regularizer based model for sparse recovery becomes $\ell_1$ minimization with equality constraints:

$$\min_{\boldsymbol{x}} \|\boldsymbol{x}\|_1, \qquad \text{subject to } \boldsymbol{Ax} = \boldsymbol{b}, \tag{6.4}$$

which is also known as basis pursuit problem ([26]). One necessary and sufficient condition of exact sparse recovery is imposed on the null space of $\boldsymbol{A}$. Suppose the truth $\boldsymbol{f}$ is $s$-sparse. It is shown in [59] that the truth $\boldsymbol{f}$ is the unique solution to (6.4) if and only if the null space property (2.10) of order $s$ holds for some constant $\beta \in (0, 1)$. When $\boldsymbol{f}$ is approximately $s$-sparse, it is shown in [59] that

$$\|\widetilde{\boldsymbol{f}} - \boldsymbol{f}\|_1 \leq \frac{1 + \beta}{1 - \beta}\left(\|\widetilde{\boldsymbol{f}}\|_1 - \|\boldsymbol{f}\|_1 + 2\sigma_s(\boldsymbol{f})\right)$$

for any $\boldsymbol{A}\widetilde{\boldsymbol{f}} = \boldsymbol{A}\boldsymbol{f}$ if and only if $\boldsymbol{A}$ satisfies the null space property of order $s$ with constant $0 < \beta < 1$. It implies that the null space property is a sufficient condition for stable sparse recovery when using (6.4). Besides the null-space property, many other sufficient conditions are proposed for exact sparse recovery using (6.4). For example, the so-called *mutual coherence* is used in [46, 49] for exact recovery of $\boldsymbol{f}$, which states that $\boldsymbol{f}$ can be exactly recovered by solving (6.4) if $\mu(\boldsymbol{A}) < \frac{1}{2\|\boldsymbol{f}\|_0 - 1}$, where

$$\mu(\boldsymbol{A}) = \max_{j \neq k} \frac{|\langle \boldsymbol{A}_j, \boldsymbol{A}_k \rangle|}{\|\boldsymbol{A}_k\|_2 \|\boldsymbol{A}_j\|_2}.$$

By restricting the maximum radius of the intersection of unit $\ell_1$ ball and $\ker(\boldsymbol{A})$ to be $c/\sqrt{s}$ for some constant c, the so-called *width property*, i.e., there exists a

constant $c > 0$ such that

$$\|\boldsymbol{f}\|_2 \leq \frac{c}{\sqrt{s}}\|\boldsymbol{x}\|_1, \quad \text{for any } \boldsymbol{x} \in \ker \boldsymbol{A},$$

is proposed in [70] to guarantee an exact recovery of $\boldsymbol{f}$ via (6.4), as well as the approximation-stable recovery of $\boldsymbol{f}$ when $\boldsymbol{f}$ is approximately sparse.

In the presence of noise such that $\boldsymbol{b} = \boldsymbol{A}\boldsymbol{f} + \boldsymbol{n}$ with non-zero noise $\boldsymbol{n}$, both $\ell_1$-norm and $\ell_2$-norm have been used as the loss function, and most of the researchers consider the constrained optimization model (6.2), with $\mathcal{L}$ being either $\|\cdot\|_2$ or $\|\cdot\|_1$. For the $\ell_2$-norm loss function based model, which reads

$$\min_{\boldsymbol{x}} \|\boldsymbol{x}\|_1 \quad \text{subject to } \|\boldsymbol{b} - \boldsymbol{A}\boldsymbol{x}\|_2 \leq \delta, \tag{6.5}$$

the *robust null-space property* defined in Definition 2.2 is introduced in [59, 57, 107] to ensure an approximation stable and noise robust recovery. It is shown in [59, 57, 107] that if $\boldsymbol{A}$ satisfies the robust null-space property (2.10), then any minimizer $\widetilde{\boldsymbol{f}}$ of (6.5) satisfies

$$\|\widetilde{\boldsymbol{f}} - \boldsymbol{f}\|_2 \leq \frac{c_1}{\sqrt{s}}\sigma_s(\boldsymbol{f}) + c_2\delta, \tag{6.6}$$

where $c_1, c_2$ are two positive constants. The same result can also be obtained if the matrix $\boldsymbol{A}$ satisfies the robust width property ([70]). Another well-known sufficient condition for guaranteeing the stable and robust sparse recovery is the so-called *restricted isometry property* first introduced in [24]. A matrix $\boldsymbol{A}$ is said to satisfy the $s$-th order restricted isometry property with constant $\gamma_s$ if for any $s$-sparse vector $\boldsymbol{x}$,

$$(1 - \gamma_s)\|\boldsymbol{x}\|_2^2 \leq \|A\boldsymbol{x}\|_2^2 \leq (1 + \gamma_s)\|\boldsymbol{x}\|_2^2,$$

where $\gamma_s$ is a positive constant called restricted isometry constant. More details can be found in [23, 19, 58, 56, 17].

For the $\ell_1$-norm loss function based model which reads

$$\min_{\boldsymbol{x}} \|\boldsymbol{x}\|_1 \quad \text{subject to} \quad \|\boldsymbol{b} - \boldsymbol{A}\boldsymbol{x}\|_1 \leq \delta, \tag{6.7}$$

it is shown in [107] that when $\boldsymbol{A}$ satisfies the robust null-space property (2.11), the model (6.7) will admit a robust and stable recovery of sparse signals such that for any minimizer $\widetilde{\boldsymbol{f}}$ of (6.7),

$$\|\widetilde{\boldsymbol{f}} - \boldsymbol{f}\|_1 \leq c_1 \sigma_s(\boldsymbol{f}) + c_2 \delta. \tag{6.8}$$

Furthermore, in the context of super-resolution of sparse signals, it is shown in [21] that as long as the matrix $\boldsymbol{A}$ satisfy the null-space property, the constrained model (6.7) will admit a stable and robust recovery of sparse signals in the form of (6.8).

The $\ell_1$-norm regularizer based unconstrained model with the square of $\ell_2$-norm loss function has been known as the *lasso* estimator ([109]). The model usually reads

$$\min_{\boldsymbol{x}} \lambda \|\boldsymbol{b} - \boldsymbol{A}\boldsymbol{x}\|_2^2 + \|\boldsymbol{x}\|_1, \tag{6.9}$$

where $\lambda$ is some pre-defined positive regularization parameter. As a statistical regression tool, (6.9) has been extensively studied in the literature; see e.g. [84, 118, 116, 85, 22]. The error analysis of (6.9) in statistical regression is rather different from that of signal recovery, as it focuses on the estimation error in terms of $\|\boldsymbol{A}\boldsymbol{f} - \boldsymbol{A}\widetilde{\boldsymbol{f}}\|$, where $\widetilde{\boldsymbol{f}}$ denotes one minimizer of (6.9). In the context of sparse model, it is shown in [22] that when the parameter $\boldsymbol{f}$ is a $s$-sparse vector, the term $\|\boldsymbol{A}\boldsymbol{f} - \boldsymbol{A}\widetilde{\boldsymbol{f}}\|_2$ is well bounded with high probability provided that $s$ is sufficiently small.

From the viewpoint of sparse recovery, the $\ell_1$-norm loss function based unconstrained model,

$$\min_{\boldsymbol{x}} \lambda \|\boldsymbol{b} - \boldsymbol{A}\boldsymbol{x}\|_1 + \|\boldsymbol{x}\|_1, \tag{6.10}$$

is discussed in [68]. A sufficient condition on stable and robust sparse recovery using (6.10) is proposed in [68], which assumes that there exist constants $D > 0$ and $0 < \beta < 1$ such that

$$\|\boldsymbol{x}_T\|_1 + \|\boldsymbol{x}\|_1 - \|\boldsymbol{x}_{T^c}\|_1 \leq D\|A\boldsymbol{x}\|_1 + \beta\|\boldsymbol{x}\|_1$$

holds for any $\boldsymbol{x}$ and any set $T$ with $|T| \leq s$, if $\lambda$ is suitably chosen.

## 6.2 Robustness and Stability of $\ell_2^2$-$\ell_1$ and $\ell_1$-$\ell_1$ models

As aforementioned, two most often used loss functions $\mathcal{L}$ are $\mathcal{L}(\cdot) = \|\cdot\|_2^2$ and $\mathcal{L}(\cdot) = \|\cdot\|_1$. We call the model (6.9) with $\|\cdot\|_2^2$ based loss function the $\ell_2^2$-$\ell_1$ model:

$$\min_{\boldsymbol{x}} \lambda \|\boldsymbol{b} - \boldsymbol{A}\boldsymbol{x}\|_2^2 + \|\boldsymbol{x}\|_1, \tag{6.11}$$

and call the model (6.10) with $\|\cdot\|_1$ based loss function the $\ell_1$-$\ell_1$ model:

$$\min_{\boldsymbol{x}} \lambda \|\boldsymbol{b} - \boldsymbol{A}\boldsymbol{x}\|_1 + \|\boldsymbol{x}\|_1. \tag{6.12}$$

In this section, we would like to investigate the sufficient conditions on $\boldsymbol{A}$ so that the models (6.11) and (6.12) can admit robust and stable recovery of sparse signals in terms of Definition 6.1, as well as how to set the regularization parameter $\lambda$ accordingly.

Assume $N \geq 2s$. For $\ell_2^2$-$\ell_1$ model (6.11), we have the following result.

**Theorem 6.1.** *Let $\widetilde{\boldsymbol{f}}$ denote any vector that satisfies the $\epsilon$-optimality condition:*

$$\lambda \|\boldsymbol{b} - \boldsymbol{A}\widetilde{\boldsymbol{f}}\|_2^2 + \|\widetilde{\boldsymbol{f}}\|_1 \leq \min_{\boldsymbol{x}}(\lambda \|\boldsymbol{b} - \boldsymbol{A}\boldsymbol{x}\|_2^2 + \|\boldsymbol{x}\|_1) + \epsilon. \tag{6.13}$$

*Suppose that the matrix $\boldsymbol{A}$ satisfies the robust null-space property of order $s$ with constants $D_1 > 0$ and $\beta_1 \in (0,1)$. Then for $\lambda = \frac{\sqrt{s}}{\|\boldsymbol{n}\|_2}$, we have*

$$\|\boldsymbol{f} - \widetilde{\boldsymbol{f}}\|_2 \leq \frac{c_1}{\sqrt{s}}\sigma_s(\boldsymbol{f}) + c_2\|\boldsymbol{n}\|_2 + c_3\epsilon, \tag{6.14}$$

*where $c_1 = \frac{\frac{7}{2}D_1 + \frac{5}{2}}{(1-\beta_1)^2}$, $c_2 = \frac{8D_1^2 + 16D_1 + \frac{5}{4}}{(1-\beta_1)^2}$ and $c_3 = \frac{4D_1 + 2}{(1-\beta_1)^2}$.*

Before giving the proof of Theorem 6.1, the following lemma is introduced.

**Lemma 6.2.** *For any $\boldsymbol{d} \in \mathbb{C}^N$ and any index subset $T \subset \{1, ..., N\}$ of size $|T| = s$,*

$$\|\boldsymbol{d}\|_2 \leq \|\boldsymbol{d}_T\|_2 + \|\boldsymbol{d}_{T_1}\|_2 + \frac{1}{\sqrt{s}}\|\boldsymbol{d}_{T^c}\|_1. \tag{6.15}$$

*where $T_1$ is the index set of the $s$ largest elements of $|\boldsymbol{d}|$ in $T^c$.*

*Proof.* For the given vector $\boldsymbol{d} \in \mathbb{C}^N$ and the index set $T$ of $|T| = s$, we divide $T^c$ into sets of size $s$ in order of decreasing magnitude of $\boldsymbol{d}_{T^c}$, denoted by $T_1, T_2, \ldots$. That is, define $T_1$ to be the index set of the $s$ largest elements of $|\boldsymbol{d}|$ in $T^c$. Let $T_2$ be the index set of the $s$ largest elements of $|\boldsymbol{d}|$ in $(T \cup T_1)^c$, and so on. Based on the definition of $\{T_1, T_2, \ldots\}$, $|\boldsymbol{d}_{T_j}(m)| \leq \frac{1}{s}\|\boldsymbol{d}_{T_{j-1}}\|_1$ for any $m$ and $j \geq 2$. Then $\sum_m |\boldsymbol{d}_{T_j}(m)|^2 \leq s \cdot \frac{\|\boldsymbol{d}_{T_{j-1}}\|_1^2}{s^2}$, i.e.

$$\|\boldsymbol{d}_{T_j}\|_2 \leq s^{-1/2}\|\boldsymbol{d}_{T_{j-1}}\|_1, \quad j \geq 2.$$

Therefore, we have the following inequality about $\|\boldsymbol{d}\|_2$:

$$\begin{aligned}
\|\boldsymbol{d}\|_2 &\leq \|\boldsymbol{d}_T\|_2 + \|\boldsymbol{d}_{T_1}\|_2 + \sum_{j \geq 2} \|\boldsymbol{d}_{T_j}\|_2 \\
&\leq \|\boldsymbol{d}_T\|_2 + \|\boldsymbol{d}_{T_1}\|_2 + \frac{1}{\sqrt{s}} \sum_{j \geq 1} \|\boldsymbol{d}_{T_j}\|_1 \\
&\leq \|\boldsymbol{d}_T\|_2 + \|\boldsymbol{d}_{T_1}\|_2 + \frac{1}{\sqrt{s}}\|\boldsymbol{d}_{T^c}\|_1.
\end{aligned}$$

The proof is done. $\qquad\qquad\qquad\qquad\qquad\qquad\qquad\qquad\qquad\qquad\quad\square$

*proof of Theorem 6.1.* Let $\boldsymbol{h} = \widetilde{\boldsymbol{f}} - \boldsymbol{f}$. By the condition on $\widetilde{\boldsymbol{f}}$,

$$\begin{aligned}
\lambda\|\boldsymbol{b} - \boldsymbol{A}\widetilde{\boldsymbol{f}}\|_2^2 + \|\widetilde{\boldsymbol{f}}\|_1 &\leq \min_{\boldsymbol{x}}(\lambda\|\boldsymbol{b} - \boldsymbol{A}\boldsymbol{x}\|_2^2 + \|\boldsymbol{x}\|_1) + \epsilon \\
&\leq \lambda\|\boldsymbol{b} - \boldsymbol{A}\boldsymbol{f}\|_2^2 + \|\boldsymbol{f}\|_1 + \epsilon \\
&= \lambda\|\boldsymbol{n}\|_2^2 + \|\boldsymbol{f}\|_1 + \epsilon. \qquad\qquad (6.16)
\end{aligned}$$

Expanding $\|\boldsymbol{b} - \boldsymbol{A}\widetilde{\boldsymbol{f}}\|_2^2$ as

$$\begin{aligned}
&\|\boldsymbol{b} - \boldsymbol{A}\widetilde{\boldsymbol{f}}\|_2^2 \\
=&\|\boldsymbol{b} - \boldsymbol{A}\boldsymbol{f}\|_2^2 + \|\boldsymbol{A}\widetilde{\boldsymbol{f}} - \boldsymbol{A}\boldsymbol{f}\|_2^2 - \langle \boldsymbol{b} - \boldsymbol{A}\boldsymbol{f}, \boldsymbol{A}\widetilde{\boldsymbol{f}} - \boldsymbol{A}\boldsymbol{f} \rangle - \langle \boldsymbol{A}\widetilde{\boldsymbol{f}} - \boldsymbol{A}\boldsymbol{f}, \boldsymbol{b} - \boldsymbol{A}\boldsymbol{f} \rangle \\
=&\|\boldsymbol{n}\|_2^2 + \|\boldsymbol{A}\boldsymbol{h}\|_2^2 - \langle \boldsymbol{n}, \boldsymbol{A}\boldsymbol{h} \rangle - \langle \boldsymbol{A}\boldsymbol{h}, \boldsymbol{n} \rangle,
\end{aligned}$$

we have then

$$\begin{aligned}
\|\boldsymbol{A}\boldsymbol{h}\|_2^2 &\leq \frac{1}{\lambda}(\|\boldsymbol{f}\|_1 - \|\widetilde{\boldsymbol{f}}\|_1) + \langle \boldsymbol{n}, \boldsymbol{A}\boldsymbol{h} \rangle + \langle \boldsymbol{A}\boldsymbol{h}, \boldsymbol{n} \rangle + \frac{\epsilon}{\lambda} \\
&\leq \frac{1}{\lambda}\|\boldsymbol{h}\|_1 + 2\|\boldsymbol{n}\|_2\|\boldsymbol{A}\boldsymbol{h}\|_2 + \frac{\epsilon}{\lambda}.
\end{aligned} \qquad (6.17)$$

For $\boldsymbol{f} \in \mathbb{C}^N$, we divide it into the sets of size $s$ in the order of decreasing magnitude, denoted by $T, T_1, T_2, \ldots$. That is, $T$ is the index set of $s$ largest elements of $|\boldsymbol{f}|$, then define $T_1$ be the index set of $s$ largest elements of $|\boldsymbol{f}|$ in $T^c$, and so on. Then obviously $\sigma_s(\boldsymbol{f}) = \|\boldsymbol{f}_{T^c}\|_1$. Use (6.16) and notice that $\|\boldsymbol{f}\|_1 = \|\boldsymbol{f}_T\|_1 + \|\boldsymbol{f}_{T^c}\|_1$,

$$\|\boldsymbol{f}\|_1 + \lambda\|\boldsymbol{n}\|_2^2 + \epsilon \geq \|\widetilde{\boldsymbol{f}}\|_1 \geq \|\boldsymbol{f}_T\|_1 - \|\boldsymbol{h}_T\|_1 - \|\boldsymbol{f}_{T^c}\|_1 + \|\boldsymbol{h}_{T^c}\|_1.$$

Thus,

$$\|\boldsymbol{h}_{T^c}\|_1 \leq 2\|\boldsymbol{f}_{T^c}\|_1 + \|\boldsymbol{h}_T\|_1 + \lambda\|\boldsymbol{n}\|_2^2 + \epsilon. \tag{6.18}$$

Together with the robust null-space property and notice that $\|\boldsymbol{h}_T\|_1 \leq \sqrt{s}\|\boldsymbol{h}_T\|_2$, we have

$$\|\boldsymbol{h}_T\|_2 \leq D_1\|\boldsymbol{A}\boldsymbol{h}\|_2 + \frac{\beta_1}{\sqrt{s}}\left(2\|\boldsymbol{f}_{T^c}\|_1 + \|\boldsymbol{h}_T\|_1 + \lambda\|\boldsymbol{n}\|_2^2 + \epsilon\right)$$

$$\leq \beta_1\|\boldsymbol{h}_T\|_2 + D_1\|\boldsymbol{A}\boldsymbol{h}\|_2 + \frac{\beta_1}{\sqrt{s}}\left(2\|\boldsymbol{f}_{T^c}\|_1 + \lambda\|\boldsymbol{n}\|_2^2 + \epsilon\right),$$

which implies

$$\|\boldsymbol{h}_T\|_2 \leq \frac{1}{1-\beta_1}\left(\frac{2\beta_1}{\sqrt{s}}\|\boldsymbol{f}_{T^c}\|_1 + \frac{\beta_1}{\sqrt{s}} \cdot (\lambda\|\boldsymbol{n}\|_2^2 + \epsilon) + D_1\|\boldsymbol{A}\boldsymbol{h}\|_2\right). \tag{6.19}$$

Then combining (6.18) and (6.19), we have

$$\|\boldsymbol{h}_{T^c}\|_1 \leq 2\|\boldsymbol{f}_{T^c}\|_1 + \lambda\|\boldsymbol{n}\|_2^2 + \epsilon + \sqrt{s}\|\boldsymbol{h}_T\|_2$$
$$\leq \frac{2}{1-\beta_1}\|\boldsymbol{f}_{T^c}\|_1 + \frac{1}{1-\beta_1}(\lambda\|\boldsymbol{n}\|_2^2 + \epsilon) + \frac{D_1}{1-\beta_1}\sqrt{s}\|\boldsymbol{A}\boldsymbol{h}\|_2. \tag{6.20}$$

Thus,

$$\|\boldsymbol{h}\|_1 = \|\boldsymbol{h}_T\|_1 + \|\boldsymbol{h}_{T^c}\|_1$$
$$\leq \alpha(2\|\boldsymbol{f}_{T^c}\|_1 + \lambda\|\boldsymbol{n}\|_2^2 + \epsilon) + \frac{2D_1}{1-\beta_1}\sqrt{s}\|\boldsymbol{A}\boldsymbol{h}\|_2, \tag{6.21}$$

where $\alpha = \frac{1+\beta_1}{1-\beta_1}$. By (6.17), we have

$$\|\boldsymbol{A}\boldsymbol{h}\|_2^2 \leq \frac{1}{\lambda}\|\boldsymbol{h}\|_1 + 2\|\boldsymbol{n}\|_2\|\boldsymbol{A}\boldsymbol{h}\|_2 + \frac{\epsilon}{\lambda}$$
$$\leq \alpha\left(\frac{2}{\lambda}\|\boldsymbol{f}_{T^c}\|_1 + \|\boldsymbol{n}\|_2^2 + \frac{\epsilon}{\lambda}\right) + \frac{2D_1\sqrt{s}}{\lambda(1-\beta_1)}\|\boldsymbol{A}\boldsymbol{h}\|_2 + 2\|\boldsymbol{n}\|_2\|\boldsymbol{A}\boldsymbol{h}\|_2 + \frac{\epsilon}{\lambda}$$
$$= \frac{2\alpha}{\lambda}\|\boldsymbol{f}_{T^c}\|_1 + \alpha\|\boldsymbol{n}\|_2^2 + \left(\frac{2D_1\sqrt{s}}{\lambda(1-\beta_1)} + 2\|\boldsymbol{n}\|_2\right)\|\boldsymbol{A}\boldsymbol{h}\|_2 + \frac{2\epsilon}{\lambda(1-\beta_1)}.$$

Thus, we have the following inequality on $\|\boldsymbol{Ah}\|_2$:

$$
\begin{aligned}
\|\boldsymbol{Ah}\|_2 &\le (\frac{2D_1\sqrt{s}}{\lambda(1-\beta_1)} + 2\|\boldsymbol{n}\|_2) + \sqrt{\alpha}\sqrt{\frac{2\|\boldsymbol{f}_{T^c}\|_1}{\lambda} + \|\boldsymbol{n}\|_2^2 + \frac{2\epsilon}{\lambda(1+\beta_1)}} \\
&\le (\frac{2D_1\sqrt{s}}{\lambda(1-\beta_1)} + 2\|\boldsymbol{n}\|_2) + \sqrt{\alpha}\left(2\sqrt{\frac{\|\boldsymbol{f}_{T^c}\|_1}{2\lambda}} + \|\boldsymbol{n}\|_2 + 2\sqrt{\frac{\epsilon}{2\lambda(1+\beta_1)}}\right) \\
&\le \frac{2D_1\sqrt{s}}{\lambda(1-\beta_1)} + (2+\sqrt{\alpha})\|\boldsymbol{n}\|_2 + \sqrt{\alpha}\left(\frac{\sqrt{s}}{2\lambda} + \frac{\|\boldsymbol{f}_{T^c}\|_1}{\sqrt{s}}\right) + (\frac{1}{2\lambda} + \frac{\epsilon}{1-\beta_1}).
\end{aligned}
\tag{6.22}
$$

The remaining step is to give an upper bound of $\|\boldsymbol{h}\|_2$. By robust null-space property,

$$
\|\boldsymbol{h}_{T_1}\|_2 \le D_1\|\boldsymbol{Ah}\|_2 + \frac{\beta_1}{\sqrt{s}}\|\boldsymbol{h}_{T_1^c}\|_1.
$$

By (6.21), we have then

$$
\begin{aligned}
\|\boldsymbol{h}_{T_1}\|_2 &\le D_1\|\boldsymbol{Ah}\|_2 + \frac{\beta_1}{\sqrt{s}}\|\boldsymbol{h}_{T_1^c}\|_1 \\
&\le D_1\|\boldsymbol{Ah}\|_2 + \frac{\beta_1}{\sqrt{s}}\|\boldsymbol{h}\|_1 \\
&\le \alpha D_1\|\boldsymbol{Ah}\|_2 + \frac{\alpha\beta_1}{\sqrt{s}}\left(2\|\boldsymbol{f}_{T^c}\|_1 + \lambda\|\boldsymbol{n}\|_2^2 + \epsilon\right).
\end{aligned}
\tag{6.23}
$$

By the inequality provided in Lemma 6.2:

$$
\|\boldsymbol{h}\|_2 \le \|\boldsymbol{h}_T\|_2 + \|\boldsymbol{h}_{T_1}\|_2 + \frac{1}{\sqrt{s}}\|\boldsymbol{h}_{T^c}\|_1,
$$

together with (6.19), (6.20) and (6.23), we have

$$
\|\boldsymbol{h}\|_2 \le \frac{1}{1-\beta_1}\left[D_1(3+\beta_1)\|\boldsymbol{Ah}\|_2 + \frac{(1+\beta_1)^2}{\sqrt{s}}(2\|\boldsymbol{f}_{T^c}\|_1 + \lambda\|\boldsymbol{n}\|_2^2 + \epsilon)\right].
\tag{6.24}
$$

Recall that $\lambda = \frac{\sqrt{s}}{\|\boldsymbol{n}\|_2}$. Combining the above inequality with (6.22) gives

$$
\|\boldsymbol{h}\|_2 \le \frac{c_1}{\sqrt{s}}\|\boldsymbol{f}_{T^c}\|_1 + c_2\|\boldsymbol{n}\|_2 + c_3\epsilon,
\tag{6.25}
$$

where

$$
\begin{cases}
c_1 = \frac{D_1(3+\beta_1)(1+\beta_1)^{1/2}}{(1-\beta_1)^{3/2}} + 2\frac{(1+\beta_1)^2}{1-\beta_1} \le \frac{\frac{7}{2}D_1+\frac{5}{2}}{(1-\beta_1)^2}, \\
c_2 = D_1\frac{3+\beta_1}{1-\beta_1}\left(\frac{2D_1}{1-\beta_1} + \frac{3}{2}\sqrt{\frac{1+\beta_1}{1-\beta_1}} + 2 + \frac{1}{2\sqrt{s}}\right) + \frac{(1+\beta_1)^2}{1-\beta_1} \le \frac{8D_1^2+16D_1+\frac{5}{4}}{(1-\beta_1)^2}, \\
c_3 = \frac{D_1(3+\beta_1)}{1-\beta_1}\frac{1}{1-\beta_1} + \frac{(1+\beta_1)^2}{\sqrt{s}(1-\beta_1)} \le \frac{4D_1+2}{(1-\beta_1)^2}.
\end{cases}
\tag{6.26}
$$

The proof is done. $\qquad\square$

This theorem shows that the robust null-space property is sufficient for the robust and stable recovery of $\ell_2^2$-$\ell_1$ model, given a suitable choice of $\lambda$ related to the noise level. For $\ell_1$-$\ell_1$ model (6.12), we have

**Theorem 6.3.** *Let $\widetilde{\boldsymbol{f}}$ denote any vector that satisfies the $\epsilon$-optimality condition:*

$$\lambda\|\boldsymbol{b} - \boldsymbol{A}\widetilde{\boldsymbol{f}}\|_1 + \|\widetilde{\boldsymbol{f}}\|_1 \leq \min_{\boldsymbol{x}}(\lambda\|\boldsymbol{b} - \boldsymbol{A}\boldsymbol{x}\|_1 + \|\boldsymbol{x}\|_1) + \epsilon. \tag{6.27}$$

*Define $\gamma = \inf_{\boldsymbol{A}\boldsymbol{R}\boldsymbol{A}=\boldsymbol{A}} \|\boldsymbol{R}\|_1$. Suppose that $\boldsymbol{A}$ satisfies the null space property of order $s$ with constant $\beta \in (0,1)$. Then for $\lambda = \frac{2\gamma}{1+\beta}$, we have*

$$\|\boldsymbol{f} - \widetilde{\boldsymbol{f}}\|_1 \leq c_1\sigma_s(\boldsymbol{f}) + c_2\|\boldsymbol{n}\|_1 + c_3\tau, \tag{6.28}$$

*where $c_1 = \frac{2+2\beta}{1-\beta}$, $c_2 = \frac{4\gamma}{1-\beta}$, and $c_3 = \frac{1+\beta}{1-\beta}$.*

*Proof.* Denote $\boldsymbol{h} = \widetilde{\boldsymbol{f}} - \boldsymbol{f}$. For any $\boldsymbol{R}$ satisfying $\boldsymbol{A} = \boldsymbol{A}\boldsymbol{R}\boldsymbol{A}$, decompose $\boldsymbol{h}$ as $\boldsymbol{h} = \boldsymbol{h}^R + \boldsymbol{h}^N$, where $\boldsymbol{h}^R = \boldsymbol{R}\boldsymbol{A}\boldsymbol{h}$ and $\boldsymbol{h}^N = \boldsymbol{h} - \boldsymbol{h}^R$. Obviously, $\boldsymbol{h}^N \in \ker \boldsymbol{A}$. Take $T$ to be the index set of the $s$ largest components in $|\boldsymbol{f}|$, then $\sigma_s(\boldsymbol{f}) = \|\boldsymbol{f}_{T^c}\|_1$. $\widetilde{\boldsymbol{f}}$ satisfies (6.27), which implies that

$$\|\widetilde{\boldsymbol{f}}\|_1 + \lambda\|\boldsymbol{A}\widetilde{\boldsymbol{f}} - \boldsymbol{b}\|_1 \leq \min_{\boldsymbol{x}}(\|\boldsymbol{x}\|_1 + \lambda\|\boldsymbol{A}\boldsymbol{x} - \boldsymbol{b}\|_1) + \epsilon$$

$$\leq \|\boldsymbol{f}\|_1 + \lambda\|\boldsymbol{A}\boldsymbol{f} - \boldsymbol{b}\|_1 + \epsilon.$$

Since $\widetilde{\boldsymbol{f}} = \boldsymbol{f} + \boldsymbol{h} = \boldsymbol{f} + \boldsymbol{h}^N + \boldsymbol{h}^R$,

$$\|\widetilde{\boldsymbol{f}}\|_1 + \lambda\|\boldsymbol{A}\widetilde{\boldsymbol{f}} - \boldsymbol{b}\|_1$$
$$=\|\boldsymbol{f} + \boldsymbol{h}^N + \boldsymbol{h}^R\|_1 + \lambda\|\boldsymbol{A}\widetilde{\boldsymbol{f}} - \boldsymbol{b}\|_1$$
$$\geq\|\boldsymbol{f}_T\|_1 - \|(\boldsymbol{h}^N)_T\|_1 + \|(\boldsymbol{h}^N)_{T^c}\|_1 - \|\boldsymbol{f}_{T^c}\|_1 - \|\boldsymbol{h}^R\|_1 + \lambda\|\boldsymbol{A}\widetilde{\boldsymbol{f}} - \boldsymbol{b}\|_1.$$

Therefore,

$$2\|\boldsymbol{f}_{T^c}\|_1 + \lambda\left(\|\boldsymbol{A}\boldsymbol{f} - \boldsymbol{b}\|_1 - \|\boldsymbol{A}\widetilde{\boldsymbol{f}} - \boldsymbol{b}\|_1\right) + \|\boldsymbol{h}^R\|_1 + \epsilon \geq \|(\boldsymbol{h}^N)_{T^c}\|_1 - \|(\boldsymbol{h}^N)_T\|_1$$

$$\geq (1 - \beta)\|(\boldsymbol{h}^N)_{T^c}\|_1.$$

Here, the last inequality is by the null space property and the fact that $\boldsymbol{h}^N \in \ker \boldsymbol{A}$. Therefore,

$$\frac{1}{1-\beta}\left(2\|\boldsymbol{f}_{T^c}\|_1 + \lambda\left(\|\boldsymbol{Af}-\boldsymbol{b}\|_1 - \|\boldsymbol{A}\widetilde{\boldsymbol{f}}-\boldsymbol{b}\|_1\right) + \|\boldsymbol{h}^R\|_1 + \epsilon\right) \geq \|(\boldsymbol{h}^N)_{T^c}\|_1.$$
(6.29)

By using the null space property,

$$\frac{\beta}{1-\beta}\left(2\|\boldsymbol{f}_{T^c}\|_1 + \lambda\left(\|\boldsymbol{Af}-\boldsymbol{b}\|_1 - \|\boldsymbol{A}\widetilde{\boldsymbol{f}}-\boldsymbol{b}\|_1\right) + \|\boldsymbol{h}^R\|_1 + \epsilon\right) \geq \|(\boldsymbol{h}^N)_{T}\|_1. \quad (6.30)$$

Then by adding (6.29) and (6.30) together, we obtain

$$\frac{1+\beta}{1-\beta}\left(2\|\boldsymbol{f}_{T^c}\|_1 + \lambda\left(\|\boldsymbol{Af}-\boldsymbol{b}\|_1 - \|\boldsymbol{A}\widetilde{\boldsymbol{f}}-\boldsymbol{b}\|_1\right) + \|\boldsymbol{h}^R\|_1 + \epsilon\right) \geq \|\boldsymbol{h}^N\|_1.$$

Adding $\|h^R\|_1$ on both sides leads to

$$\frac{1+\beta}{1-\beta}\left(2\|\boldsymbol{f}_{T^c}\|_1 + \lambda\left(\|\boldsymbol{Af}-\boldsymbol{b}\|_1 - \|\boldsymbol{A}\widetilde{\boldsymbol{f}}-\boldsymbol{b}\|_1\right) + \epsilon\right) + \frac{2}{1-\beta}\|\boldsymbol{h}^R\|_1 \geq \|\boldsymbol{h}\|_1.$$

Since

$$\|\boldsymbol{h}^R\|_1 = \|\boldsymbol{RAh}\|_1 \leq \|\boldsymbol{R}\|_1\|\boldsymbol{A}(\boldsymbol{f}-\widetilde{\boldsymbol{f}})\|_1 \leq \|\boldsymbol{R}\|_1\left(\|\boldsymbol{Af}-\boldsymbol{b}\|_1 + \|\boldsymbol{A}\widetilde{\boldsymbol{f}}-\boldsymbol{b}\|_1\right),$$

and $\|\boldsymbol{Af}-\boldsymbol{b}\|_1 = \|\boldsymbol{n}\|_1$, we get

$$\|\boldsymbol{h}\|_1 \leq c_1\|\boldsymbol{f}_{T^c}\|_1 + c_2'\|\boldsymbol{n}\|_1 + c_3\epsilon + \frac{1}{1-\beta}\left(2\|\boldsymbol{R}\|_1 - \lambda(1+\beta)\right)\|\boldsymbol{A}\widetilde{\boldsymbol{f}}-\boldsymbol{b}\|_1,$$

where $c_1 = \frac{2+2\beta}{1-\beta}$, $c_2' = \frac{1}{1-\beta}\left(2\|\boldsymbol{R}\|_1 + \lambda(1+\beta)\right)$ and $c_3 = \frac{1+\beta}{1-\beta}$. Note that the above process holds for all $\boldsymbol{R}$ satisfying $\boldsymbol{ARA} = \boldsymbol{A}$ and $\gamma = \inf_{\boldsymbol{ARA}=\boldsymbol{A}} \|\boldsymbol{R}\|_1$. Therefore,

$$\|\boldsymbol{h}\|_1 \leq c_1\|\boldsymbol{f}_{T^c}\|_1 + c_2\|\boldsymbol{n}\|_1 + c_3\epsilon + \frac{1}{1-\beta}\left(2\gamma - \lambda(1+\beta)\right)\|\boldsymbol{A}\widetilde{\boldsymbol{f}}-\boldsymbol{b}\|_1,$$

where $c_2 = \frac{1}{1-\beta}\left(2\gamma + \lambda(1+\beta)\right)$. If $\lambda = \frac{2\gamma}{1+\beta}$,

$$\|\boldsymbol{h}\|_1 \leq c_1\|\boldsymbol{f}_{T^c}\|_1 + c_2\|\boldsymbol{n}\|_1 + c_3\epsilon, \quad (6.31)$$

with $c_2 = \frac{4\gamma}{1+\beta}$. $\qquad\qquad\square$

It can be seen that the $\ell_1$-$\ell_1$ model (6.12) only requires the null space property to guarantee a stable and robust recovery of sparse signals, while the $\ell_2^2$-$\ell_1$ model (6.11) requires a seemingly stronger condition. At this point, the natural question is whether there indeed exists a gap between (6.12) and (6.11) on the requirement for the stable and robust sparse recovery. The following example gives a positive answer.

**Proposition 6.4.** *For arbitrary $0 < \beta < 1$, suppose that $M, N$ and $s$ satisfy $N/2 \geq M \geq 2C(\beta/3)s\log^4(N)$. Then, there exists a matrix $\boldsymbol{A} \in \mathbb{R}^{M \times N}$ that satisfies the null-space property of order $s$ with constant $\beta$, but the $\ell_2^2$-$\ell_1$ model (6.11) with $\boldsymbol{A}$ cannot guarantee neither robust nor stable recovery.*

Before proving the result about the gap between the null-space property and the robust and stable sparse recovery of $\ell_2^2$-$\ell_1$ model (6.11), we introduce the following lemma from [9].

**Lemma 6.5.** *([9]) For any given $\beta < 1$, there exists $C(\beta)$ such that when $M, N, s$ satisfy $N/2 \geq M \geq C(\beta)s\log^4(N)$, then there exists a matrix $\boldsymbol{R} \in \mathbb{R}^{M \times N}$ that has the null-space property of order $s$ with constant $\beta$ and $(1, \ldots, 1)^\top \in \ker \boldsymbol{R}$.*

To prove Proposition 6.4, we first construct a matrix $\boldsymbol{A}$ satisfying the null-space property. With the constructed $\boldsymbol{A}$, we then give particular examples of original signal $\boldsymbol{f}$ and observation $\boldsymbol{b}$. And in these examples, the robust or stable recovery as defined in Definition 6.1 cannot be obtained. The idea of such construction is inspired by [9], which provides an example about the gap between the null-space property (NSP) and restricted isometry property-null space property (RIP-NSP).

*Proof of Proposition 6.4.* Since $N/2 \geq M \geq 2C(\beta/3)s\log^4(N)$ implies $(N - s)/2 \geq (M - s) \geq C(\beta/3)s\log^4(N - s)$, one can find $\boldsymbol{B} \in \mathbb{R}^{(m-s) \times (N-s)}$ satisfying the null-space property of order $s$ with constant $\beta/3$ and $\boldsymbol{e} = (\underbrace{1, ..., 1}_{N-s})^\top \in \ker \boldsymbol{B}$. Define

$$N_{\boldsymbol{e}} = \{\boldsymbol{x} \in \ker \boldsymbol{B} : \boldsymbol{x} \perp \boldsymbol{e}\},$$

$$N_e' = \{(\underbrace{0, ..., 0}_{s}, \boldsymbol{x}) : \boldsymbol{x} \in N_e\},$$

and

$$\bar{N} = N_e' \oplus \mathrm{span}(\boldsymbol{d}),$$

where $\boldsymbol{d} = (\frac{N-s}{2}\gamma, \underbrace{0, ..., 0}_{s-1}, \underbrace{-1, ..., -1}_{N-s})$. Then set $\boldsymbol{\phi} = (\frac{2}{\gamma}, \underbrace{0, ..., 0}_{s-1}, \underbrace{1, ..., 1}_{N-s})$, $\alpha = \|\boldsymbol{\phi}\|_2$ and $\boldsymbol{\phi}_1 = \frac{1}{\alpha}\boldsymbol{\phi}$. Easily, one may verify $\boldsymbol{\phi}_1 \perp \bar{N}$. Therefore, there exists an orthonormal basis of $\bar{N}^\perp$ including $\boldsymbol{\phi}_1$. Let $\boldsymbol{A}$ be the matrix whose rows are this orthogonal basis and $\boldsymbol{\phi}_1$ is its first row.

Claim: $\boldsymbol{A}$ satisfies the null space property of order $s$ with constant $\beta$.

To prove this assertion, we follow the similar steps as that in [9]. Without loss of generality, consider $\boldsymbol{h} \in \ker \boldsymbol{A}$, that can be represented by $\boldsymbol{h} = \boldsymbol{g} + \boldsymbol{d}$, where $\boldsymbol{g} \in \bar{N}_e'$. Take $T = \{1, 2, ..., s\}$, and arbitrary $I \subset \{1, ..., N\}$, with $|I| \leq s$. Then

$$\|\boldsymbol{h}_T\|_1 = \|\boldsymbol{d}_T\|_1 = \frac{N-s}{2}\beta,$$

and

$$\|\boldsymbol{h}_{T^c}\|_1 \geq -\sum_{j \in T^c} \boldsymbol{h}_{T^c}(j) = N - s,$$

since $\boldsymbol{g}_{T^c} \perp e$. Therefore, $\|\boldsymbol{h}_T\|_1 \leq \frac{\beta}{2}\|\boldsymbol{h}_{T^c}\|_1$. Then,

$$
\begin{aligned}
\|\boldsymbol{h}_I\|_1 &= \|\boldsymbol{h}_{I \cap T}\|_1 + \|\boldsymbol{h}_{I \cap T^c}\|_1 \\
&\leq \|\boldsymbol{h}_T\|_1 + \|\boldsymbol{h}_{I \cap T^c}\|_1 \\
&\leq \frac{\beta}{2}\|\boldsymbol{h}_{T^c}\|_1 + \|\boldsymbol{h}_{I \cap T^c}\|_1 \\
&= \frac{\beta}{2}\|\boldsymbol{h}_{I^c \cap T^c}\|_1 + (1 + \frac{\beta}{2})\|\boldsymbol{h}_{I \cap T^c}\|_1.
\end{aligned}
$$

Note that $\boldsymbol{h}_{T^c} \in \ker \boldsymbol{B}$. Therefore,

$$
\begin{aligned}
\|\boldsymbol{h}_I\|_1 &\leq \frac{\beta}{2}\|\boldsymbol{h}_{I^c \cap T^c}\|_1 + (1 + \frac{\beta}{2})\|\boldsymbol{h}_{I \cap T^c}\|_1 \\
&\leq (\frac{\beta}{2} + \frac{\beta+2}{2}\frac{\beta}{3})\|\boldsymbol{h}_{I^c \cap T^c}\|_1 \\
&< \beta\|\boldsymbol{h}_{I^c \cap T^c}\|_1 \\
&\leq \beta\|\boldsymbol{h}_{I^c}\|_1.
\end{aligned}
$$

Thus, we have shown that $\boldsymbol{A}$ has the null-space property with constant $\beta$.

Next, we give two particular examples which violate the robust and stable recovery. Firstly, for robustness, consider the $s$ sparse signal $\boldsymbol{f} = \boldsymbol{d} + \boldsymbol{\phi} = (\frac{N-s}{2}\beta + \frac{2}{\beta}, 0, ..., 0)$, observation $\boldsymbol{b} = 0$ and noise $\boldsymbol{n} = -\boldsymbol{A}\boldsymbol{f}$. Then $\widetilde{\boldsymbol{f}} = 0$ is the exact solution to the $\ell_2^2$-$\ell_1$ model (6.11), and $\|\widetilde{\boldsymbol{f}} - \boldsymbol{f}\|_2 = \frac{N-s}{2}\beta + \frac{2}{\beta}$. Since $\boldsymbol{d} \in \ker \boldsymbol{A}$, $\boldsymbol{A}\boldsymbol{f} = \boldsymbol{A}\boldsymbol{\phi} = (\|\boldsymbol{\phi}\|_2, 0, ..., 0)^\top$. Then $\|\boldsymbol{n}\|_2 = \|\boldsymbol{A}\boldsymbol{f}\|_2 = \sqrt{\frac{4}{\beta^2} + N - s}$. Therefore, $\|\widetilde{\boldsymbol{f}} - \boldsymbol{f}\|_2 / \|\boldsymbol{n}\|_2 \approx c\sqrt{N - s}$, where $c$ is a constant. This contradicts with the requirement of robust recovery that $\|\widetilde{\boldsymbol{f}} - \boldsymbol{f}\|_2 \le c_1 \|\boldsymbol{n}\|_2$, for some constant $c_1$.

Secondly, for stability, consider the true signal $\boldsymbol{f} = \boldsymbol{d} \in \ker \boldsymbol{A}$, as well as the observation and noise $\boldsymbol{b} = \boldsymbol{n} = 0$. Then $\widetilde{\boldsymbol{f}} = 0$ is the exact solution to the $\ell_2^2$-$\ell_1$ model (6.11). However, in this example, $\|\widetilde{\boldsymbol{f}} - \boldsymbol{f}\|_2 = \|\boldsymbol{d}\|_2 = \sqrt{\frac{(N-s)^2}{4}\beta^2 + N - s}$, and $\sigma_s(\boldsymbol{f}) \le \|\boldsymbol{f}_{T^c}\|_1 = N - s$, where $T = \{1, ..., s\}$. This violates the requirement of stable recovery that $\|\widetilde{\boldsymbol{f}} - \boldsymbol{f}\|_2 \le \frac{c}{\sqrt{s}}\sigma_s(\boldsymbol{f})$, for some constant $c$ independent of $s$. $\qquad\square$

## 6.3 Experiments

In this section, we evaluate the effciency of the $\ell_2^2$-$\ell_1$ and $\ell_1$-$\ell_1$ models when solving the super-resolution problem. The details of the problem formulation are as follows. To recover an $N$ dimensional signal $\boldsymbol{f}$, the information $\boldsymbol{b}$ we observe is $M = 2f_c + 1$ lowest Fourier transform coefficients of the truth $\boldsymbol{f}$, added with measurement noise $\boldsymbol{n}$, i.e.

$$\boldsymbol{b} = \boldsymbol{A}\boldsymbol{f} + \boldsymbol{n}. \tag{6.32}$$

That means the measurement matrix $\boldsymbol{A}$ is part of the discrete Fourier matrix $\boldsymbol{F} \in \mathbb{C}^{N \times N}$ by selecting its $M$ rows corresponding to the low frequencies. Usually the information available is far less than the signal dimension, i.e. $M << N$. By the assumption that the true signal $\boldsymbol{f} \in \mathbb{C}^N$ has certain sparsity, i.e. it has at most $s$ nonzero elements with $s << N$, one may implement the $\ell_2^2$-$\ell_1$ model (6.11) or the $\ell_1$-$\ell_1$ model (6.12) to solve the linear inverse problem (6.32).

## 6.3.1  Numerical algorithms

To solve the proposed models, we apply the alternating direction method (ADM) derived from their dual problems, or referred to as dual-based ADM ([114]).

Firstly, we consider the $\ell_2^2$-$\ell_1$ model. The dual problem of (6.11) is

$$\max_{\boldsymbol{y}\in\mathbb{C}^M} \mathbf{Re}(\boldsymbol{b}^*\boldsymbol{y}) - \frac{1}{4\lambda}\|\boldsymbol{y}\|_2^2 \quad \text{subject to} \quad \boldsymbol{A}^*\boldsymbol{y} \in B_1^\infty, \tag{6.33}$$

where $B_1^\infty = \{\boldsymbol{z} \in \mathbb{C}^N : \|\boldsymbol{z}\|_\infty \leq 1\}$. Since $\boldsymbol{A}$ is a partial Fourier matrix, the rows of $\boldsymbol{A} \in \mathbb{C}^{M\times N}$ are orthogonal, i.e. $\boldsymbol{A}\boldsymbol{A}^* = \boldsymbol{I}$. Then it can be solved via the following schemes:

$$\begin{cases} \boldsymbol{y}^{k+1} = \alpha\boldsymbol{A}\boldsymbol{z}^k - \beta(\boldsymbol{A}\boldsymbol{x}^k - \boldsymbol{b}) \\ \boldsymbol{z}^{k+1} = \mathcal{P}_{B_1^\infty}(\boldsymbol{A}^*\boldsymbol{y}^{k+1} + \boldsymbol{x}^k/\mu) \\ \boldsymbol{x}^{k+1} = \boldsymbol{x}^k + \gamma\mu(\boldsymbol{A}^*\boldsymbol{y}^{k+1} - \boldsymbol{z}^{k+1}), \end{cases} \tag{6.34}$$

where $\alpha = \frac{\mu}{\mu+\frac{1}{2\lambda}}$, $\beta = \frac{1}{\mu+\frac{1}{\lambda}}$. Herein $\mu > 0$ is an intermediate penalty parameter, $\gamma \in (0, (\sqrt{5}+1)/2)$ is the steplength attached to the update of $\lambda$, and $\mathcal{P}_S$ is the projection operator onto a set $S$. The solution $\widetilde{\boldsymbol{f}}$ is given by $\boldsymbol{x}^k$ at some step $k$ when the stopping criterion is satisfied. For more details of the algorithm and the convergence analysis, one may check [114].

For the $\ell_1$-$\ell_1$ model (6.12), it is equivalent to the constraint $\ell_1$ regularized minimization with the introduction of auxiliary variable $\boldsymbol{r}$:

$$\min_{\substack{\boldsymbol{x}\in\mathbb{C}^N \\ \boldsymbol{r}\in\mathbb{C}^M}} \frac{1}{\lambda}\|\boldsymbol{x}\|_1 + \|\boldsymbol{r}\|_1 \quad \text{subject to} \quad \boldsymbol{A}\boldsymbol{x} + \boldsymbol{r} = \boldsymbol{b}.$$

Therefore it can also be formulated as a basis pursuit problem by raising up the dimensions of $\boldsymbol{x}$ and $\boldsymbol{A}$:

$$\min_{\bar{\boldsymbol{x}}\in\mathbb{C}^{M+N}} \|\bar{\boldsymbol{x}}\|_1 \quad \text{subject to} \quad \bar{\boldsymbol{A}}\bar{\boldsymbol{x}} = \bar{\boldsymbol{b}}, \tag{6.35}$$

where $\bar{\boldsymbol{A}} = \frac{[\boldsymbol{A} \; \frac{1}{\lambda}\boldsymbol{I}]}{\sqrt{1+\frac{1}{\lambda^2}}}$, $\bar{\boldsymbol{b}} = \frac{\boldsymbol{b}}{\lambda\sqrt{1+\frac{1}{\lambda^2}}}$ and $\bar{\boldsymbol{x}} = \begin{bmatrix} \frac{\boldsymbol{x}}{\lambda} \\ \boldsymbol{r} \end{bmatrix}$. Note that $\bar{\boldsymbol{A}}\bar{\boldsymbol{A}}^* = \boldsymbol{I}$, if $\boldsymbol{A}\boldsymbol{A}^* = \boldsymbol{I}$.

In fact, the basis pursuit problem can also be solved via the dual-based ADM. The

dual problem of basis pursuit model (6.35) is given by

$$\max_{\boldsymbol{y} \in \mathbb{C}^M} \mathbf{Re}(\bar{\boldsymbol{b}}^* \boldsymbol{y}) \quad \text{subject to} \quad \bar{\boldsymbol{A}}^* \boldsymbol{y} \in B_2^\infty,$$

where $B_2^\infty = \{\boldsymbol{z} \in \mathbb{C}^{M+N} : \|\boldsymbol{z}\|_\infty \leq 1\}$. This problem is a special case of (6.33) with $\frac{1}{\lambda} = 0$. Therefore, it can be solved by the same scheme as (6.34) by setting $\frac{1}{\lambda} = 0$ and replacing $\boldsymbol{A}$, $\boldsymbol{b}$ and $\boldsymbol{x}$ by $\bar{\boldsymbol{A}}$, $\bar{\boldsymbol{b}}$ and $\bar{\boldsymbol{x}}$. For more details, interested readers are referred to [114].

### 6.3.2 Experimental evaluation

In the experiment, we take the dimension of original signal $\boldsymbol{x}$ as $N = 1000$ and the sparsity $s = 40$. We are targeted at recovering the following two types of sparse signals: 1) the support is chosen at random and the values of nonzeros are randomly generated from the standard normal distribution; 2) the support satisfies the sufficient separation condition, i.e. for some constant $c > 0$,

$$\min_{j,j' \in \text{supp}(\boldsymbol{x}), j \neq j'} |j - j'| \geq c,$$

and the values on the support are randomly generated from the standard normal distribution. In particular, the minimum separation constant $c = 19$ in our experiment. As in the linear model (6.32), the observation $\boldsymbol{b}$ is the $M = 2f_c + 1$ lowest Fourier coefficients of $\boldsymbol{x}$ with $f_c = 150$, added by Gaussian white noise $\boldsymbol{n}$. The standard deviation of Gaussian noise is set as $\sigma = 0.002$, $0.005$ or $0.02$, respectively. The signal to noise ratio (SNR) of $\boldsymbol{b}$ is measured by

$$\text{SNR} = 20 \log_{10}(\|\boldsymbol{b} - \mathbf{E}(\boldsymbol{b})\|_2 / \|\boldsymbol{n}\|_2),$$

where $\mathbf{E}(\boldsymbol{b})$ is the mean of $\boldsymbol{b}$. For each type of signal support and each noise level $\sigma$, we randomly generate 10 tested signals $\boldsymbol{x}$ and corresponding observations $\boldsymbol{b}$. The mean of SNRs of the 10 simulated data $\boldsymbol{b}$ is shown in Table 6.1. To solve $\boldsymbol{x}$ from $\boldsymbol{b}$ using the $\ell_2^2$-$\ell_1$ and $\ell_1$-$\ell_1$ models, we apply the YALL1 solver [114] that implements

Table 6.1: Results of experiments

| $\sigma$ | supp | SNR | $\ell_2^2$-$\ell_1$ | | $\ell_1$-$\ell_1$ | |
|---|---|---|---|---|---|---|
| | | | RelErr2 | RelErr1 | RelErr2 | RelErr1 |
| 0.002 | suff seprt | 39.3819 | 0.0066 | 0.0067 | 0.0060 | 0.0071 |
| | rand | 39.3326 | 0.1978 | 0.1284 | 0.1940 | 0.1283 |
| 0.005 | suff seprt | 31.4272 | 0.0187 | 0.0236 | 0.0236 | 0.0352 |
| | rand | 31.3776 | 0.2112 | 0.1622 | 0.2186 | 0.1822 |
| 0.02 | suff seprt | 19.4401 | 0.1064 | 0.2104 | 0.1195 | 0.2265 |
| | rand | 19.3895 | 0.2786 | 0.3561 | 0.2849 | 0.3688 |

the dual-based ADM described in the last section. The suitable values of parameter $\lambda$ in the two models for different noise levels are shown in Table 6.1.

The performance of each model can be evaluated by the relative error (RelErr) of the solution $\widetilde{\boldsymbol{f}}$ to the truth $\boldsymbol{f}$ in $\ell_2$ norm, i.e.

$$\text{RelErr2} = \frac{\|\boldsymbol{f} - \widetilde{\boldsymbol{f}}\|_2}{\|\boldsymbol{f}\|_2},$$

and the relative error in $\ell_1$ norm, i.e.

$$\text{RelErr1} = \frac{\|\boldsymbol{f} - \widetilde{\boldsymbol{f}}\|_1}{\|\boldsymbol{f}\|_1}.$$

To reveal the average performance of the two models on 10 randomly generated test signals, the mean of the resulted relative errors are illustrated in Table 6.1.

From the results, we find that when the original signal satisfies certain sufficient separation condition, the results will be much better than the case that the support is randomly chosen. And although the observation is simulated by Gaussian noise, the $\ell_1$-$\ell_1$ model is competitive with the $\ell_2^2$-$\ell_1$ model.

## 6.4   Conclusions

In this chapter, we investigate the conditions to ensure a robust and stable recovery of sparse signals via two $\ell_1$-norm regularizer based unconstrained models with

square of $\ell_2$-norm and $\ell_1$-norm based loss functions. The results stated in Theorem 6.1, Theorem 6.3 and Proposition 6.4 not only tell us sufficient conditions for a robust and stable recovery via the $\ell_2^2$-$\ell_1$ and $\ell_1$-$\ell_1$ models, but also show that the $\ell_1$-norm based loss function requires a weaker condition for robust and stable sparse recovery than the square of $\ell_2$-norm based loss function. In addition, how to set the regularization parameter for achieving robust and stable recovery is also provided in our analysis. The experimental results reveal that the efficiency of $\ell_1$-$\ell_1$ model (6.12) is competitive with that of $\ell_2^2$-$\ell_1$ model (6.11), even if the additive noise is of Gaussian type.

# Bibliography

[1] M. Aharon, M. Elad, and A. Bruckstein, *K-SVD: An algorithm for designing overcomplete dictionaries for sparse representation*, Signal Processing, IEEE Transactions on, 54 (2006), pp. 4311–4322.

[2] R. Balian, *Un principe d'incertitude fort en théorie du signal ou en mécanique quantique*, CR Acad. Sci. Paris, 292 (1981), pp. 1357–1361.

[3] G. Battle, *Heisenberg proof of the Balian-Low theorem*, Letters in Mathematical Physics, 15 (1988), pp. 175–177.

[4] A. Beck and M. Teboulle, *Fast gradient-based algorithms for constrained total variation image denoising and deblurring problems*, Image Processing, IEEE Transactions on, 18 (2009), pp. 2419–2434.

[5] ——, *A fast iterative shrinkage-thresholding algorithm for linear inverse problems*, SIAM Journal on Imaging Sciences, 2 (2009), pp. 183–202.

[6] H. Bölcskei and F. Hlawatsch, *Discrete Zak transforms, polyphase transforms, and applications*, Signal Processing, IEEE Transactions on, 45 (1997), pp. 851–866.

[7] F. Bunea, A. B. Tsybakov, and M. Wegkamp, *Aggregation and sparsity via $\ell_1$ penalized least squares*, in Learning theory, Springer, 2006, pp. 379–391.

[8] ——, *Sparsity oracle inequalities for the Lasso*, Electronic Journal of Statistics, 1 (2007), pp. 169–194.

[9] J. Cahill, X. Chen, and R. Wang, *The gap between the null space property and the restricted isometry property*, arXiv preprint arXiv:1506.03040, (2015).

[10] J.-F. Cai, R. H. Chan, and Z. Shen, *A framelet-based image inpainting algorithm*, Applied and Computational Harmonic Analysis, 24 (2008), pp. 131–149.

[11] ——, *Simultaneous cartoon and texture inpainting*, Inverse Problem and Imaging, 4 (2010), pp. 379–395.

[12] J.-F. Cai, B. Dong, S. Osher, and Z. Shen, *Image restoration: total variation, wavelet frames, and beyond*, Journal of the American Mathematical Society, 25 (2012), pp. 1033–1089.

[13] J.-F. Cai, H. Ji, C. Liu, and Z. Shen, *Blind motion deblurring from a single image using sparse approximation*, in Computer Vision and Pattern Recognition, 2009. CVPR 2009. IEEE Conference on, IEEE, 2009, pp. 104–111.

[14] ——, *Framelet-based blind image deblurring from a single image*, Image Processing, IEEE Transactions on, 21 (2012), pp. 562–572.

[15] J.-F. Cai, S. Osher, and Z. Shen, *Linearized Bregman iterations for frame-based image deblurring*, SIAM Journal on Imaging Sciences, 2 (2009), pp. 226–252.

[16] ——, *Split Bregman methods and frame based image restoration*, Multiscale modeling & simulation, 8 (2009), pp. 337–369.

[17] T. T. CAI, L. WANG, AND G. XU, *Shifting inequality and recovery of sparse signals*, Signal Processing, IEEE Transactions on, 58 (2010), pp. 1300–1308.

[18] T. T. CAI AND A. ZHANG, *Sparse representation of a polytope and recovery of sparse signals and low-rank matrices*, Information Theory, IEEE Transactions on, 60 (2014), pp. 122–132.

[19] E. J. CANDÈS, *The restricted isometry property and its implications for compressed sensing*, Comptes Rendus Mathematique, 346 (2008), pp. 589–592.

[20] E. J. CANDÈS AND D. L. DONOHO, *New tight frames of curvelets and optimal representations of objects with piecewise $C^2$ singularities*, Communications on pure and applied mathematics, 57 (2004), pp. 219–266.

[21] E. J. CANDÈS AND C. FERNANDEZ-GRANDA, *Towards a mathematical theory of super-resolution*, Communications on Pure and Applied Mathematics, 67 (2014), pp. 906–956.

[22] E. J. CANDÈS AND Y. PLAN, *Near-ideal model selection by $\ell_1$ minimization*, The Annals of Statistics, 37 (2009), pp. 2145–2177.

[23] E. J. CANDÈS, J. K. ROMBERG, AND T. TAO, *Stable signal recovery from incomplete and inaccurate measurements*, Communications on Pure and Applied mathematics, 59 (2006), pp. 1207–1223.

[24] E. J. CANDÈS AND T. TAO, *Decoding by linear programming*, Information Theory, IEEE Transactions on, 51 (2005), pp. 4203–4215.

[25] A. CHAMBOLLE, *An algorithm for total variation minimization and applications*, Journal of Mathematical imaging and vision, 20 (2004), pp. 89–97.

[26] S. S. CHEN, D. L. DONOHO, AND M. A. SAUNDERS, *Atomic decomposition by basis pursuit*, SIAM Journal on Scientific Computing, 20 (1998), pp. 33–61.

[27] O. Christensen, *An introduction to frames and Riesz bases*, Birkhäuser Boston, 2002.

[28] ——, *Pairs of dual Gabor frame generators with compact support and desired frequency localization*, Applied and Computational Harmonic Analysis, 20 (2006), pp. 403–410.

[29] ——, *Frames and bases: An introductory course*, Springer Science & Business Media, 2008.

[30] O. Christensen and S. S. Goh, *Fourier-like frames on locally compact abelian groups*, Journal of Approximation Theory, 192 (2015), pp. 82–101.

[31] O. Christensen and R. Y. Kim, *On dual gabor frame pairs generated by polynomials*, Journal of Fourier Analysis and Applications, 16 (2010), pp. 1–16.

[32] C. K. Chui, W. He, and J. Stöckler, *Compactly supported tight and sibling frames with maximum vanishing moments*, Applied and Computational Harmonic Analysis, 13 (2002), pp. 224–262.

[33] A. Cohen, W. Dahmen, and R. DeVore, *Compressed sensing and best k-term approximation*, Journal of the American Mathematical Society, 22 (2009), pp. 211–231.

[34] A. Cohen, I. Daubechies, and J.-C. Feauveau, *Biorthogonal bases of compactly supported wavelets*, Communications on Pure and Applied Mathematics, 45 (1992), pp. 485–560.

[35] R. Coifman and D. Donoho, *Translation-invariant de-noising*, in Wavelet and Statistics, vol. 103 of Springer Lecture Notes in Statistics, Springer-Verlag., 1994, pp. 125–150.

[36] Z. Cvetković and M. Vetterli, *Tight Weyl-Heisenberg frame in $\ell^2(Z)$*, Signal Processing, IEEE Transactions on, 46 (1998), pp. 1256–1260.

[37] W. D. V. DE WET, *On the analysis of refinable functions with respect to mask factorisation, regularity and corresponding subdivision convergence*, PhD thesis, Stellenbosch: University of Stellenbosch, 2007.

[38] I. DAUBECHIES, *Orthonormal bases of compactly supported wavelets*, Communications on Pure and Applied Mathematics, 41 (1988), pp. 909–996.

[39] ——, *The wavelet transform, time-frequency localization and signal analysis*, Information Theory, IEEE Transactions on, 36 (1990), pp. 961–1005.

[40] ——, *Ten Lectures on Wavelets*, SIAM, 1992.

[41] I. DAUBECHIES, M. DEFRISE, AND C. DE MOL, *An iterative thresholding algorithm for linear inverse problems with a sparsity constraint*, Communications on Pure and Applied Mathematics, 57 (2004), pp. 1413–1457.

[42] I. DAUBECHIES, B. HAN, A. RON, AND Z. SHEN, *Framelets: MRA-based constructions of wavelet frames*, Applied and Computational Harmonic Analysis, 14 (2003), pp. 1–46.

[43] I. DAUBECHIES, H. J. LANDAU, AND Z. LANDAU, *Gabor time-frequency lattices and the Wexler-Raz identity*, Journal of Fourier Analysis and Applications, 4 (1994), pp. 437–478.

[44] J. G. DAUGMAN, *Two-dimensional spectral analysis of cortical receptive field profile*, Vision research, 20 (1980), pp. 847–856.

[45] C. DE BOOR, *B (asic)-spline basics*, Mathematics Research Center, University of Wisconsin-Madison, 1986.

[46] D. L. DONOHO AND X. HUO, *Uncertainty principles and ideal atomic decomposition*, Information Theory, IEEE Transactions on, 47 (2001), pp. 2845–2862.

[47] R. J. DUFFIN AND A. C. SCHAEFFER, *A class of nonharmonic fourier series*, Transactions of the American Mathematical Society, 72 (1952), pp. 341–366.

[48] M. ELAD AND M. AHARON, *Image denoising via sparse and redundant representations over learned dictionaries*, Image Processing, IEEE Transactions on, 15 (2006), pp. 3736–3745.

[49] M. ELAD AND A. M. BRUCKSTEIN, *A generalized uncertainty principle and sparse representation in pairs of bases*, Information Theory, IEEE Transactions on, 48 (2002), pp. 2558–2567.

[50] M. ELAD, P. MILANFAR, AND R. RUBINSTEIN, *Analysis versus synthesis in signal priors*, Inverse problems, 23 (2007).

[51] J. FAN AND R. LI, *Variable selection via nonconcave penalized likelihood and its oracle properties*, Journal of the American statistical Association, 96 (2001), pp. 1348–1360.

[52] Z. FAN, A. HEINECKE, AND Z. SHEN, *Duality for frames*, Journal of Fourier Analysis and Applications, 22 (2016), pp. 71–136.

[53] Z. FAN, H. JI, AND Z. SHEN, *Dual gramian analysis: duality principle and unitary extension principle*, Mathematics of Computation, 85 (2016), pp. 239–270.

[54] H. G. FEICHTINGER, W. KOZEK, AND F. LUEF, *Gabor analysis over finite Abelian groups*, Applied and Computational Harmonic Analysis, 26 (2009), pp. 230–248.

[55] M. A. FIGUEIREDO, R. D. NOWAK, AND S. J. WRIGHT, *Gradient projection for sparse reconstruction: Application to compressed sensing and other inverse problems*, Selected Topics in Signal Processing, IEEE Journal of, 1 (2007), pp. 586–597.

[56] S. FOUCART, *A note on guaranteed sparse recovery via $\ell_1$-minimization*, Applied and Computational Harmonic Analysis, 29 (2010), pp. 97–103.

[57] ——, *Stability and robustness of $\ell_1$-minimizations with Weibull matrices and redundant dictionaries*, Linear Algebra and its Applications, 441 (2014), pp. 4–21.

[58] S. FOUCART AND M.-J. LAI, *Sparsest solutions of underdetermined linear systems via $\ell_q$-minimization for $0 < q \leq 1$*, Applied and Computational Harmonic Analysis, 26 (2009), pp. 395–407.

[59] S. FOUCART AND H. RAUHUT, *A mathematical introduction to compressive sensing*, Springer, 2013.

[60] D. GABOR, *Theory of communication*, Electrical Engineers-Part III: Radio and Communication Engineering, Journal of the Institution of, 93 (1946), pp. 429–457.

[61] P. GETREUER, *Rudin-Osher-Fatemi total variation denoising using split bregman*, Image Processing On Line, 10 (2012).

[62] E. T. HALE, W. YIN, AND Y. ZHANG, *A fixed-point continuation method for $\ell_1$-regularized minimization with applications to compressed sensing*, CAAM TR07-07, Rice University, 43 (2007), p. 44.

[63] A. JANSSEN, *Duality and biorthogonality for Weyl-Heisenberg frames*, Journal of Fourier Analysis and applications, 1 (1994), pp. 403–436.

[64] ——, *Signal analytic proofs of two basic results on lattice expansions*, Applied and Computational Harmonic Analysis, 1 (1994), pp. 350–354.

[65] ——, *From continuous to discrete Weyl-Heisenberg frames through sampling*, Journal of Fourier Analysis and Applications, 3 (1997), pp. 583–596.

[66] H. JI, Z. SHEN, AND Y. XU, *Wavelet frame based scene reconstruction from range data*, Journal of Computational Physics, 229 (2010), pp. 2093–2108.

[67] ——, *Wavelet frame based image restoration with missing/damaged pixels*, East Asia Journal on Applied Mathematics, 1 (2011), pp. 108–131.

[68] A. JUDITSKY, F. K. KARZAN, AND A. NEMIROVSKI, *On a unified view of nullspace-type conditions for recoveries associated with general sparsity structures*, Linear Algebra and its Applications, 441 (2014), pp. 124–151.

[69] A. JUDITSKY AND A. NEMIROVSKI, *Functional aggregation for nonparametric regression*, The Annals of Statistics, (2000), pp. 681–712.

[70] B. S. KASHIN AND V. N. TEMLYAKOV, *A remark on compressed sensing*, Mathematical notes, 82 (2007), pp. 748–755.

[71] G. KUTYNIOK AND D. LABATE, *Construction of Regular and Irregular Shearlet Frames*, Journal of Wavelet Theory and Applications, 1 (2007), pp. 1–10.

[72] T. LE, R. CHARTRAND, AND T. J. ASAKI, *A variational approach to reconstructing images corrupted by Poisson noise*, Journal of mathematical imaging and vision, 27 (2007), pp. 257–263.

[73] E. LE PENNEC AND S. MALLAT, *Sparse geometric image representations with bandelets*, Image Processing, IEEE Transactions on, 14 (2005), pp. 423–438.

[74] T. S. LEE, *Image representation using 2D Gabor wavelets*, Pattern Analysis and Machine Intelligence, IEEE Transactions on, 18 (1996), pp. 959–971.

[75] J. LI, Z. SHEN, R. YIN, AND X. ZHANG, *A reweighted $\ell^2$ method for image restoration with Poisson and mixed Poisson-Gaussian noise*, UCLA Computational and Applied Mathematics Reports, (2012), pp. 12–84.

[76] S. LI, *On general frame decompositions*, Numerical functional analysis and optimization, 16 (1995), pp. 1181–1191.

[77] ——, *Discrete multi-Gabor expansions*, Information Theory, IEEE Transactions on, 45 (1999), pp. 1954–1958.

[78] Y. R. Li, L. Shen, and B. W. Suter, *Adaptive inpainting algorithm based on DCT induced wavelet regularization*, Image Processing, IEEE Transactions on, 22 (2013), pp. 752–763.

[79] J. Lopez and D. Han, *Discrete Gabor frames in $\ell^2(Z^d)$*, Proceedings of the American Mathematical Society, 141 (2013), pp. 3839–3851.

[80] F. Low, *Complete sets of wave packets*, A passion for physics–essays in honor of Geoofrey Chew, World Scientific, Singapore, (1985), pp. 17–22.

[81] Y. Lu and J. M. Morris, *Some results on discrete Gabor transforms for finite periodic sequences*, Signal Processing, IEEE Transactions on, 46 (1998), pp. 1703–1708.

[82] J. Mairal, F. Bach, J. Ponce, and G. Sapiro, *Online dictionary learning for sparse coding*, in Proceedings of the 26th Annual International Conference on Machine Learning, ACM, 2009, pp. 689–696.

[83] S. Mallat, *Multiresolution approximations and wavelet orthonormal bases of $L^2(R)$*, Transactions of the American Mathematical Society, 315 (1989), pp. 69–87.

[84] N. Meinshausen and P. Bühlmann, *High-dimensional graphs and variable selection with the lasso*, The Annals of Statistics, (2006), pp. 1436–1462.

[85] N. Meinshausen and B. Yu, *Lasso-type recovery of sparse representations for high-dimensional data*, The Annals of Statistics, (2009), pp. 246–270.

[86] Y. Meyer, *Principle d'incertitude, bases hilbertiennes et algèbres d' opérateurs*, Séminaire Bourbaki, 662 (1986).

[87] Y. Meyer and D. H. Salinger, *Wavelets and operators*, vol. 1, Cambridge university press, 1995.

[88] J. M. MORRIS AND Y. LU, *Discrete gabor expansion of discrete-time signals in $\ell^2(Z)$ via frame theory*, Signal Processing, 40 (1994), pp. 155–181.

[89] B. K. NATARAJAN, *Sparse approximate solutions to linear systems*, SIAM Journal on Computing, 24 (1995), pp. 227–234.

[90] M. NIKOLOVA, *A variational approach to remove outliers and impulse noise*, Journal of Mathematical Imaging and Vision, 20 (2004), pp. 99–120.

[91] R. S. ORR, *Derivation of the finite discrete Gabor transform by periodization and sampling*, Signal processing, 34 (1993), pp. 85–97.

[92] S. QIAN AND D. CHEN, *Discrete Gabor transform*, Signal Processing, IEEE Transactions on, 41 (1993), pp. 2429–2438.

[93] S. QIU, *Discrete Gabor transforms: the Gabor-Gram matrix approach*, Journal of Fourier Analysis and Applications, 4 (1998), pp. 1–17.

[94] P. RODRIGUEZ AND B. WOHLBERG, *An efficient algorithm for sparse representations with $\ell^p$ data fidelity term*, in IEEE Andean Tech. Conf, 2008.

[95] A. RON AND Z. SHEN, *Frames and stable bases for subspaces of $L^2(\mathbb{R}^d)$: the duality principle of Weyl-Heisenberg sets*, in Proceedings of the Lanczos Centenary Conference Raleigh, SIAM Pub., 1993, pp. 422–425.

[96] ——, *Frames and stable bases for shift-invariant subspaces of $L_2(\mathbb{R}^d)$*, Canadian Journal of Mathematics, 47 (1995), pp. 1051–1094.

[97] ——, *Affine system in $L_2(\mathbb{R}^d)$: the analysis of the analysis operator*, Journal of Functional Analysis, 148 (1997).

[98] ——, *Affine systems in $L_2(\mathbb{R}^d)$ II: Dual systems*, Journal of Fourier Analysis and applications, 3 (1997), pp. 617–637.

[99] ——, *Weyl-Heisenberg Frames and Riesz Bases in $L^2(\mathbb{R}^d)$*, Duke Mathematical Journal, 89 (1997), pp. 237–282.

[100] L. I. RUDIN, S. OSHER, AND E. FATEMI, *Nonlinear total variation based noise removal algorithms*, Physica D: Nonlinear Phenomena, 60 (1992), pp. 259–268.

[101] I. W. SELESNICK, R. G. BARANIUK, AND N. G. KINGSBURY, *The dual-tree complex wavelet transform*, Signal Processing Magazine, IEEE, 22 (2005), pp. 123–151.

[102] Z. SHEN, *Wavelet frames and image restorations*, in Proceedings of the International Congress of Mathematicians, vol. 4, 2010, pp. 2834–2863.

[103] P. L. SØNDERGAARD, *Gabor frames by sampling and periodization*, Advances in Computational Mathematics, 27 (2007), pp. 355–373.

[104] J.-L. STARCK, E. J. CANDÈS, AND D. L. DONOHO, *The curvelet transform for image denoising*, Image Processing, IEEE Transactions on, 11 (2002), pp. 670–684.

[105] J.-L. STARCK, M. ELAD, AND D. L. DONOHO, *Image decomposition via the combination of sparse representations and a variational approach*, Image Processing, IEEE Transactions on, 14 (2005), pp. 1570–1582.

[106] J.-L. STARCK, M. K. NGUYEN, AND F. MURTAGH, *Wavelets and curvelets for image deconvolution: a combined approach*, Signal Processing, 83 (2003), pp. 2279–2283.

[107] Q. SUN, *Sparse approximation property and stable recovery of sparse signals from noisy measurements*, Signal Processing, IEEE Transactions on, 59 (2011), pp. 5086–5090.

[108] ——, *Recovery of sparsest signals via $\ell q$-minimization*, Applied and Computational Harmonic Analysis, 32 (2012), pp. 329–341.

[109] R. TIBSHIRANI, *Regression shrinkage and selection via the lasso*, Journal of the Royal Statistical Society. Series B (Methodological), (1996), pp. 267–288.

[110] M. VETTERLI AND C. HERLEY, *Wavelets and filter banks: Theory and design*, Signal Processing, IEEE Transactions on, 40 (1992), pp. 2207–2232.

[111] D. F. WALNUT, *Continuity properties of the gabor frame operator*, Journal of mathematical analysis and applications, 165 (1992), pp. 479–504.

[112] Y. WANG, J. YANG, W. YIN, AND Y. ZHANG, *A new alternating minimization algorithm for total variation image reconstruction*, SIAM Journal on Imaging Sciences, 1 (2008), pp. 248–272.

[113] J. WEXLER AND S. RAZ, *Discrete gabor expansions*, Signal processing, 21 (1990), pp. 207–220.

[114] J. YANG AND Y. ZHANG, *Alternating direction algorithms for $\ell_1$-problems in compressive sensing*, SIAM Journal on Scientific Computing, 33 (2011), pp. 250–278.

[115] W. YIN, S. OSHER, D. GOLDFARB, AND J. DARBON, *Bregman iterative algorithms for $\ell_1$-minimization with applications to compressed sensing*, SIAM Journal on Imaging Sciences, 1 (2008), pp. 143–168.

[116] C.-H. ZHANG AND J. HUANG, *The sparsity and bias of the Lasso selection in high-dimensional linear regression*, The Annals of Statistics, (2008), pp. 1567–1594.

[117] T. ZHANG, *Multi-stage convex relaxation for learning with sparse regularization*, in Advances in Neural Information Processing Systems, 2009, pp. 1929–1936.

[118] P. ZHAO AND B. YU, *On model selection consistency of Lasso*, The Journal of Machine Learning Research, 7 (2006), pp. 2541–2563.